

# **Synthesis and Evaluation of Hexahomotrioxacalix[3]arene-based Fluorescent Chemosensors via Click Chemistry**



**September 2017**

**Department of Advanced Technology Fusion,  
Graduate School of Science and Engineering,  
Saga University, Japan**

**Wu Chong**

# **Synthesis and Evaluation of Hexahomotrioxacalix[3]arene-based Fluorescent Chemosensors via Click Chemistry**



**A dissertation presented to the Graduate School of  
Science and Engineering of Saga University in partial  
fulfillment of the requirements for the degree of  
Doctor of Philosophy**

**September 2017**

By

**Wu Chong**

Supervisor:

**Professor Dr. Takehiko Yamato**

**CERTIFICATE OF APPROVAL**  
**Ph.D Dissertation**

This is to certify that the Ph.D Dissertation of

**Wu Chong**

has been approved by the Examining Committee for the dissertation  
requirement for the Doctor of Philosophy degree in Chemistry at the  
September, 2017 graduation.

Dissertation committee: \_\_\_\_\_

Supervisor: Prof. Takehiko Yamato

\_\_\_\_\_  
Member, Prof. Tsugio Kitamura

\_\_\_\_\_  
Member, Prof. Takeshi Hanamoto

\_\_\_\_\_  
Member, Prof. Michinori Takeshita

## ACKNOWLEDGEMENTS

Firstly, I would like to express my deepest gratitude to my supervisor, Professor *Takehiko Yamato*, for his invaluable guidance, limitless helping and understanding. His profound knowledge, constructive advices inspired me during the whole doctor course.

I would like to express great appreciate to professor *Tsugio Kitamura*, professor *Mishinori Takeshita*, and professor *Takeshi Hanamoto* and the rest of my thesis committee for their kind cooperation and suggestions. I also wish to convey my sincere thanks to professor *Xi Zeng*, professor *Lan Mu* and other professors at Guizhou University, China, due to their inspiriting discussions and constant encouragement. Furthermore, I must acknowledge to Prof. *Carl Redshaw* and Dr. *Mark R. J. Elsegood* (United Kingdom) for single-crystal X-ray analysis and valuable suggestions during my research.

I also would like to express my deep gratitude to all of the members in Yamato Lab., especially to Dr. *Hirotsugu Tomiyasu*, Dr. *Zannatul Kowser*, Dr. *Xue-Kai Jiang*, Dr. *Jiang-Lin Zhao*, *Tahmina Akter*, *Chuan-Zeng Wang*, *Yusuke Ikejiri*, *Hisashi Ichiyanagi*, *Yuki Noda*, *Rie Kihara* and *Kouya Sakaguti*, who made my research work more enjoyable. Special thanks are given to the staffs and faculty in the International Division of Saga University for their acting concerns.

Finally, I would like to express my deeply appreciation to my parents *Xue-Xin Wu* and *Shi-Lian Song*, my wife *Juan-Juan Yao*, my son *Yi-Ning Wu*, my brother *Xi Wu*, for their endless encouragement, understanding and sacrifice. Without their careful assistance, it would not have been possible to complete my doctoral study. I would like to dedicate this thesis to my family.

Wu Chong

September, 2017, Saga University, Japan

## ABSTRACT

Hexahomotrioxacalix[3]arene as the new generation of supramolecular host molecules, it can provide a suitable binding environment for species that require trigonal-planar, tetrahedral or octahedral coordination. Based on this excellent structure characteristic, homooxacalix[3]arenes have been used as ideal molecular platforms for the development of chemosensors in the molecular recognition of chemical and biological targets. In this dissertation, we explored the application of hexahomotrioxacalix[3]arene to develop novel fluorescent chemosensors.

Firstly, a novel quinoline-functionalized homooxacalix[3]arene was synthesized via Click chemistry and its chemosensing properties with various metal ions were investigated. The designed chemosensor exhibited a high selectivity and antidisturbance for  $\text{Fe}^{3+}$  among environmentally and biologically relevant metal ions, leading to a prominent off-on-type fluorescent signaling behavior. Further study demonstrates the detection limit on fluorescence response of the sensor to  $\text{Fe}^{3+}$  is down to  $10^{-7}$  M range.

Secondly, a upper rim pyrene-functionalized hexahomotrioxacalix[3]arene, which can be utilized as a highly selective and sensitive fluorescent chemosensor to  $\text{Hg}^{2+}$  with a detection limit in nM level. Interestingly, the quenched fluorescence emission can be successfully revived upon the addition of water. In this process, the heavy atom effect and blocking thereof were demonstrated within the same system by the use of a  $C_3$ -symmetric homooxacalix[3]arene scaffold.

Finally, a new type of chemosensor-based approach to the detection of 2,4,6-trinitrophenol (TNP) is described. Two hexahomotrioxacalix[3]arene based chemosensors were synthesized through click chemistry, which exhibited high binding affinity and selectivity toward TNP as evidenced by UV-vis and fluorescence spectroscopy studies.  $^1\text{H}$  NMR titration analysis verified that  $\text{CH}\cdots\text{O}$  hydrogen bonding is demonstrated as the mode of interaction, which possibly facilitates effective charge-transfer.

In summary, it is believed that the excellent recognition properties of these receptors in this present thesis would help to expand the application of the hexahomotrioxacalix[3]arene skeleton in the design and synthesis of novel fluorescent chemosensors.

# TABLE OF CONTENTS

<b>ACKNOWLEDGMENTS</b> .....	i
<b>ABSTRACT</b> .....	ii
<b>TABLE OF CONTENTS</b> .....	iii

## Chapter 1

### Recent Development of Fluorescence Chemosensors Based on Calixarene Derivatives

1.1 General Introduction of Calixarene.....	2
1.2 General Introduction of Fluorescent Chemosensor.....	6
1.2.1 Photoinduced Electron Transfer (PET) .....	6
1.2.2 Photoinduced Charge Transfer (PCT) .....	7
1.2.3 Excimer Formation.....	9
1.2.4 Fluorescence Resonance Energy Transfer (FRET).....	9
1.3 Calixarene-based Fluorescent Chemosensors.....	11
1.3.1 PET Chemosensors.....	11
1.3.2 PCT Chemosensors.....	14
1.3.3 Excimer Chemosensors.....	16
1.3.4 FRET Chemosensors.....	19
1.3.5 Other Chemosensors.....	21
1.4 Conclusions.....	27
1.5 References.....	27

## Chapter 2

### Click Synthesis of Quinoline-functionalized Homooxalix[3]arene as Turn-on Fluorescence Chemosensor for Fe<sup>3+</sup>

2.1 Introduction.....	36
-----------------------	----

2.2 Results and Discussion	37
2.2.1 Synthesis and Characterization of Chemosensor L	37
2.2.2 Chemosensing Properties of L for $\text{Fe}^{3+}$	38
2.2.3 Sensing Mechanism of L for $\text{Fe}^{3+}$	43
2.3 Conclusions	45
2.4 Experimental Section	46
2.4.1 General	46
2.4.2 General Procedure for Synthesis of Sensor L	46
2.4.3 General Procedure for the UV-vis and Fluorescence Titrations	47
2.5 References	47

### **Chapter 3**

#### **A Novel Fluorescence “On–Off–On” Chemosensor for $\text{Hg}^{2+}$ via a Water-assistant Blocking Heavy Atom Effect**

3.1 Introduction	52
3.2 Results and Discussion	53
3.2.1 Synthesis and Characterization	53
3.2.2 Chemosensing Properties of L	54
3.3 Conclusions	66
3.4 Experimental Section	66
3.4.1 General	67
3.4.2 Materials	67
3.4.3 General Procedure for the UV-vis and Fluorescence Titrations	69
3.5 References	69

### **Chapter 4**

#### **Click-modified Hexahomotrioxacalix[3]arenes as Fluorometric and Colorimetric Dual-modal Chemosensors for 2,4,6-Trinitrophenol**

4.1 Introduction	73
------------------	----

4.2 Results and Discussion.....	74
4.2.1 Syntheses of Fluorescent Chemosensors 1 and 2.....	74
4.2.2 Fluorescence and UV-vis Spectroscopy Studies.....	76
4.2.3 Proton NMR Titration Analysis.....	85
4.3 Conclusions.....	87
4.4 Experimental Section.....	87
4.4.1 General.....	87
4.4.2 General Procedure for Synthesis of Chemosensors 1 and 2 .....	88
4.4.3 General Procedure for the UV-vis and Fluorescence Titrations .....	89
4.5 References.....	89
<b>Summary.....</b>	<b>93</b>
<b>Publications.....</b>	<b>96</b>



## **Chapter 1**

# **Recent Development of Fluorescence Chemosensors Based on Calixarene Derivatives**

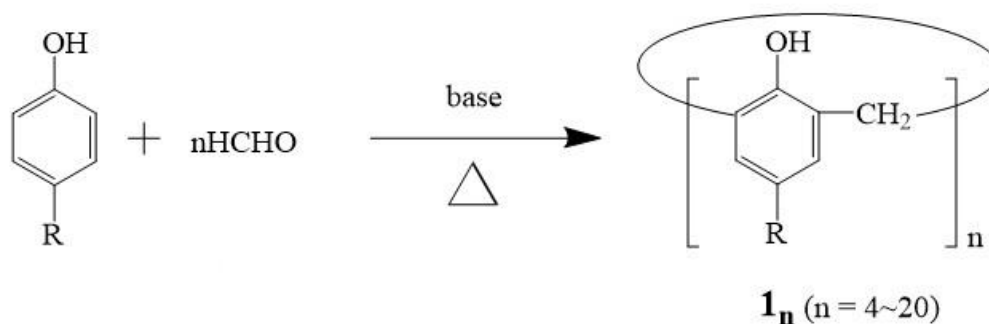
*In this chapter a shortly review focus on the development of fluorescence chemosensors based on calixarene derivatives.*

## 1.1 General Introduction of Calixarene

Molecular recognition plays a crucial role in biological systems and is fundamental for many applications in biological, medical, environmental, and chemical sciences.<sup>1</sup> There is considerable interest in developing efficient artificial receptors for molecular recognition and sensing. In the last decades, there has been significant progress in exploring artificial receptors for molecular recognition.<sup>2</sup> However, the design and synthesis of artificial receptors possesses high binding affinity, selectivity, and sensitivity to a targeted analyte is still a great challenge.

Supramolecular chemistry has provided solutions in the search for molecular structures that can serve as building blocks for the production of various receptors for charged species or neutral molecules. A relatively new class of synthetic macrocyclic building blocks has emerged among molecular receptors of numerous types, capable of binding specific substrates with high efficiency and selectivity.<sup>3</sup> Calixarenes<sup>4</sup> have been actively studied and utilized as the third generation of host compounds in addition to the well-known crown ethers<sup>5</sup> and cyclodextrins.<sup>6</sup> They are a class of supramolecular building blocks or platforms offer not only boundless possibilities for chemical modification, but also make them extremely useful in the study of molecular recognition and supramolecular processes.

Calixarenes **1n** can be synthesized by the base-catalyzed condensation of *para*-substituted phenols with formaldehyde (Scheme 1). By selecting appropriate reaction conditions, analogues of a given number of phenolic units can be selective synthesized;<sup>7</sup> even those having as many as 20-phenol units have been obtained (calix[20]arene).<sup>8</sup> Thus, it is possible to control the cavity size according to the desired purposes. Furthermore, since a calix[n]arene is constructed from alternating phenol and methylene groups, chemical modification of the parent entity can be readily achieved by relying on the traditional phenol chemistry. Thus, various functional groups can be introduced by etherification or esterification at the phenolic hydroxy groups and electrophilic substitution at the *para*-positions of the phenol nuclei.<sup>9</sup>



**Scheme 1.** Synthesis of Calix[n]arenes.

The name of calixarenes was suggested to Gutsche by inspection of the CPK molecular model of the cyclic tetramers (Figure 1), which shows a cuplike structure resembling a Greek vase (calix in Latin and Greek) when all four aryl groups are oriented in the same direction. Calixarene nomenclature is based on the number of phenolic units in the ring, thus, calix[4]arene and calix[6]arene have 4 and 6 benzene rings, respectively.<sup>10</sup> Two regions can be distinguished in calixarenes (Figure 1), namely, the phenolic OH groups region and the *para* position of the aromatic rings, which are respectively called the *lower rim* and the *upper rim*, implying that the calixarene structure is drawn with the OH groups pointing downward (*endo*) and the *para*-substituents pointing upward (*exo*).<sup>11</sup>

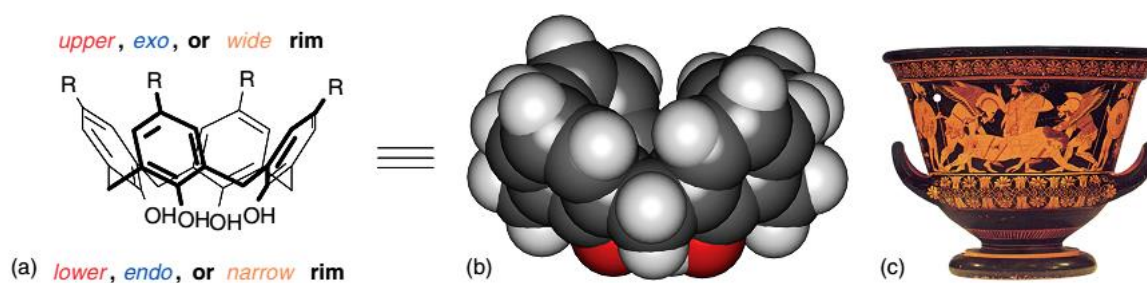


**Figure 1.** (a) The 3D representation of calix[4]arenes with an indication of the nomenclatures used to identify the two rims, (b) the CPK model, and (c) the *Greek vase* that inspired their name.

Calixarene possess characteristic conformational features unlike other host molecules such as crown ethers and cyclodextrins. In particular, the phenol units of calix[4]arene **14** can rotate via the hydroxy group, going through the macrocyclic ring comprised of the phenol and methylene units in solution (Figure 2a). However, rotation of the individual phenol unit of **14** can be blocked by introducing a substituent bulkier than a propyl group to the hydroxy

group, and then four conformers can be isolated as stable isomers under the usual conditions (Figure 2b). This indicates that the molecular framework of calixarenes can be fabricated to be flexible or rigid, depending on the particular requirements for the host. This adds complexity to the conformational analysis of calix[4]arene derivatives but widens the functions of the host molecules due to the varying structures.<sup>12</sup>

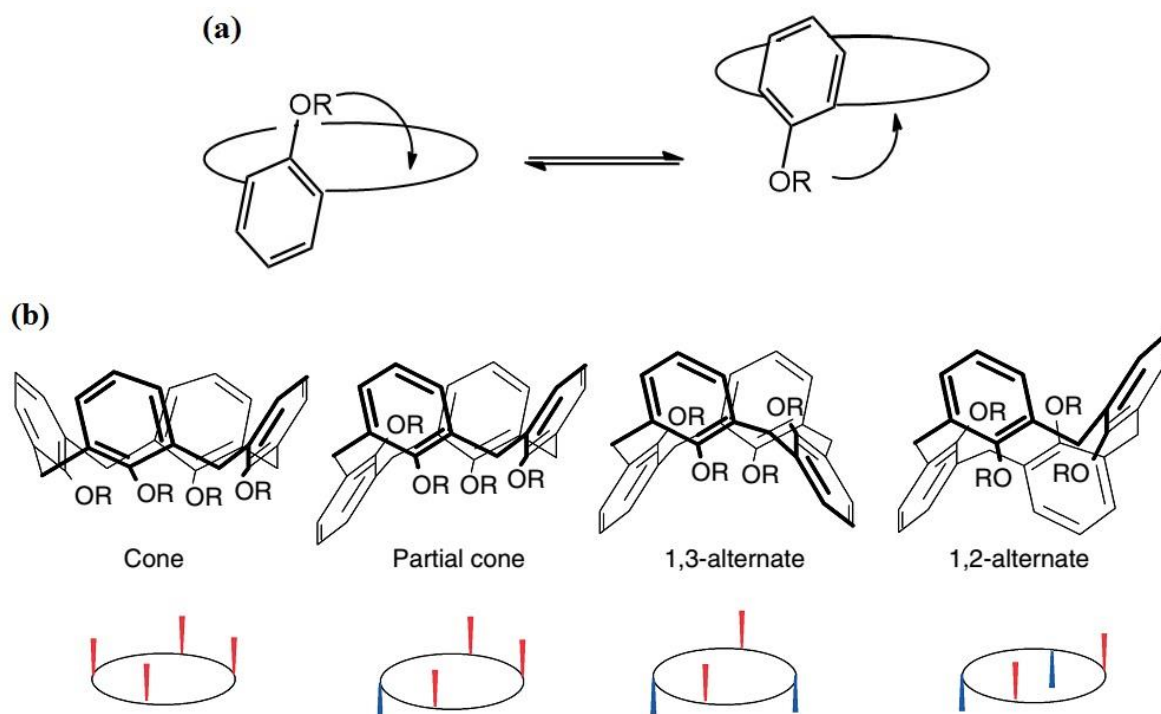


**Figure 2.** (a) Rotation of phenol ring of calixarene, (b) The four conformers of calix[4]arene **14** (cone, partial cone, 1,3-alternate and 1,2-alternate).

It may be noted that, beyond the carbon bridges skeleton, calixarene-like macrocycles containing sulfur atoms as bridges (thiacalixarenes) were also synthesized.<sup>13</sup> They were then quickly followed by others containing oxygens (oxacalixarenes),<sup>14</sup> nitrogen (azacalixarenes),<sup>15</sup> or other heteroatoms (heteracalixarenes).<sup>16</sup> A further addition came with the advent of macrocycles containing more than one bridging atom (homocalixarenes, homooxacalixarenes, or homoheteracalixarenes).<sup>17</sup> Beyond the benzenoid rings, several others aromatic and heteroaromatics rings, such as naphthalene, pyrrole, pyridine, etc., were also used to construct macrocycles that bear resemblance to calixarenes giving rise to heteracalixaromatics, such as calixpyrroles, calixpyridines, calixnaphthalenes, etc (Figure 3).<sup>18</sup> These macrocycles extended the application of calixarenes in molecular recognition.

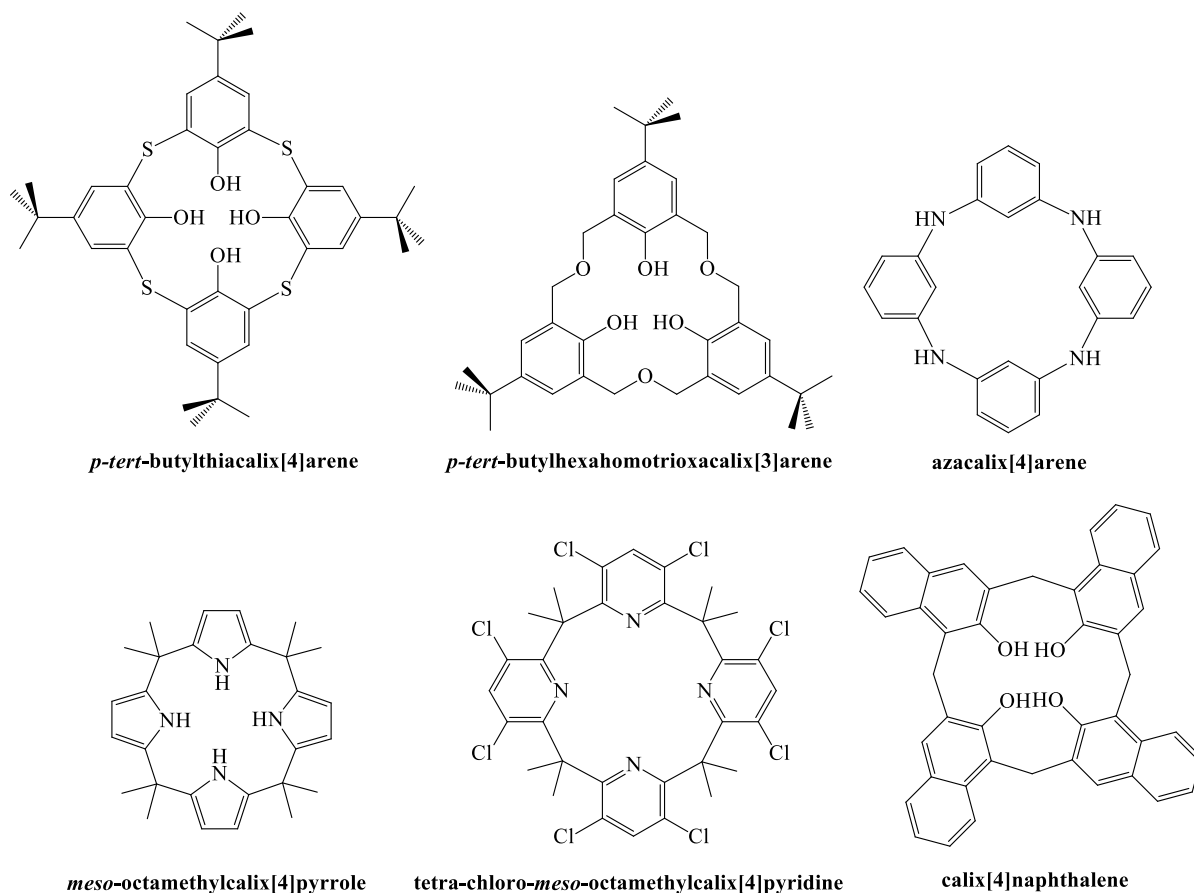


**Figure 3.** Examples for heterocalixarenes and heterocalixaromatics.

In comparison to the structural characteristics of the calixarene family, the homooxacalix[3]arene have received great attention for the following reasons: (i) homooxacalix[3]arene has a cavity composed of an 18-membered ring, which is comparable with that of calix[4]arene composed of a 16-membered ring; (ii) the rate of ring inversion for homooxacalix[3]arene should be much faster than that for calix[4]arene because of the flexibility of the ethereal linkages; (iii) there are only two possible conformations (cone and partial-cone), in contrast to four possible conformations in calix[4]arene, so that the conformational isomerism is much more simplified; (iv) ethereal ring oxygens may act cooperatively with phenolic oxygens upon the binding of metal ions; and (v) the basic structure has  $C_3$  symmetry which is expected to be particularly useful for the design of receptors for alkylammonium cations.<sup>19</sup>

## 1.2 General Introduction of Fluorescent Chemosensor

In recent years, the development of methods to recognize and sense biologically and environmentally important species has emerged as a significant target in the field of chemical sensors.<sup>20</sup> Several methods, such as high-performance liquid chromatography, mass spectrometry, atomic absorption spectroscopy, inductively coupled plasma atomic emission spectrometry, electrochemical sensing, etc., have been developed to analyze the targets concerned.<sup>21</sup> However, these methods suffer from extensive and time-consuming procedures that involve the use of sophisticated instrumentation. Fluorogenic methods in conjunction with suitable sensors are preferable approaches for the measurement of these analytes because fluorimetry is rapidly performed, is nondestructive, is highly sensitive, is suitable for high-throughput screening applications, and can afford real information on the localization and quantity of the targets of interest.<sup>22</sup> Basically, a fluorescent chemosensor consists of two significant units i.e. an ionophore (guest recognition unit) and a fluorophore (optical signaling unit, Figure 4). The ionophore is required for selective binding of the substrate, while the fluorophore provides the means of signaling this binding, whether by fluorescence enhancement or inhibition. Mechanisms which control the response of a fluorophore to substrate binding include photoinduced electron transfer (PET), photoinduced charge transfer (PCT), excimer/exciple formation or extinction, and Fluorescence resonance energy transfer (FRET).<sup>23</sup>

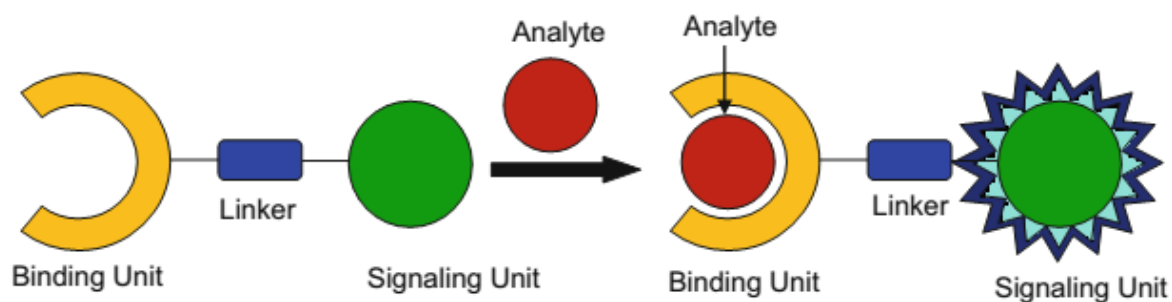


**Figure 4.** Generalized representation of a chemosensor.

### 1.2.1 Photoinduced Electron Transfer (PET)

Figure 5 illustrates how a cation can control the photoinduced electron transfer (PET) in a fluorescent chemosensor in which the cation receptor is an electron donor and the fluorophore plays the role of an acceptor. Upon excitation of the fluorophore, an electron of the highest occupied molecular orbital (HOMO) is promoted to the lowest unoccupied molecular orbital (LUMO), which enables PET from the HOMO of the donor (belonging to the free cation receptor) to that of the fluorophore, causing fluorescence quenching of the latter. Upon cation binding, the redox potential of the donor is raised so that the relevant HOMO becomes lower in energy than that of the fluorophore; consequently, PET is not possible any more and fluorescence quenching is suppressed. In other words, fluorescence intensity is enhanced upon cation binding. In most of PET sensors, the cation receptor involves aliphatic or aromatic amines acting as quenchers. Indeed, it has long been discovered that PET can take place from amino groups to aromatic hydrocarbons, thus causing fluorescence quenching of the latter.<sup>24</sup>

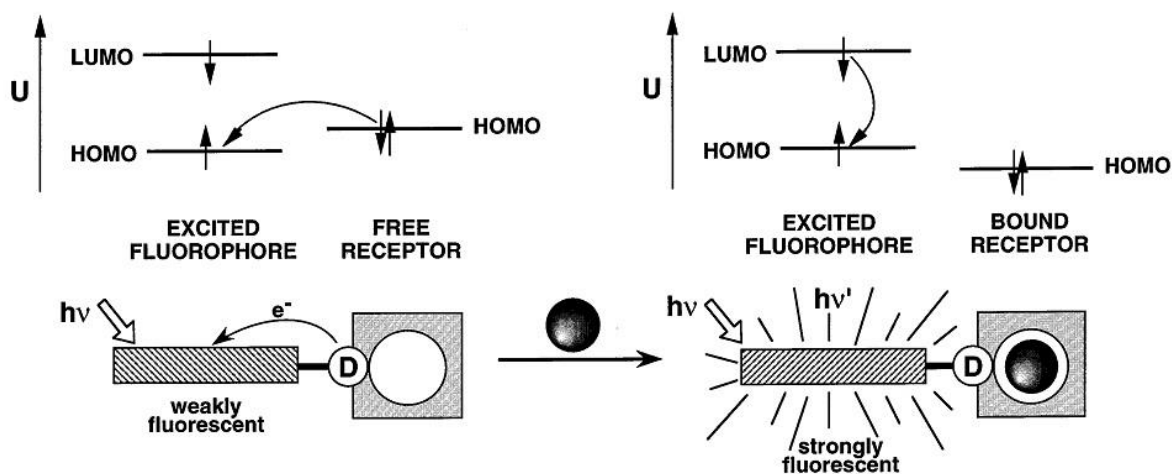


**Figure 5.** Principle of cation recognition by fluorescent PET sensors.

### 1.2.2 Photoinduced Charge Transfer (PCT)

When a fluorophore contains an electron-donating group (e.g. amino group) conjugated to an electron-withdrawing group, it undergoes intramolecular charge transfer from the donor to the acceptor upon excitation by light. This charge transfer may occur over long distances and be associated with major dipole moment changes, making the process particularly

sensitive to the microenvironment of the fluorophore. It can thus be anticipated that cations in close interaction with the donor or the acceptor moiety will change the photophysical properties of the fluorophore because the complexed cation affects the efficiency of intramolecular charge transfer.<sup>25</sup>

When a cation complexation of an electron donor group within a fluorophore, the electron-donating character of the donor group will be reduced. The resulting reduction of conjugation causes a blue shift of the absorption spectrum together with a decrease of the molar absorptivity. In contrast, metal ion binding to the acceptor group enhances its electron-withdrawing character, and the absorption spectrum is thus red-shifted with an increase in molar absorptivity (Figure 6).<sup>26</sup> The fluorescence spectra should be shifted in the same direction as the absorption spectra, and in addition to these shifts, changes in the quantum yields and lifetimes can be observed. All these photophysical effects are obviously dependent on the charge and the size of the cation, and therefore, some selectivity is expected.<sup>27</sup>

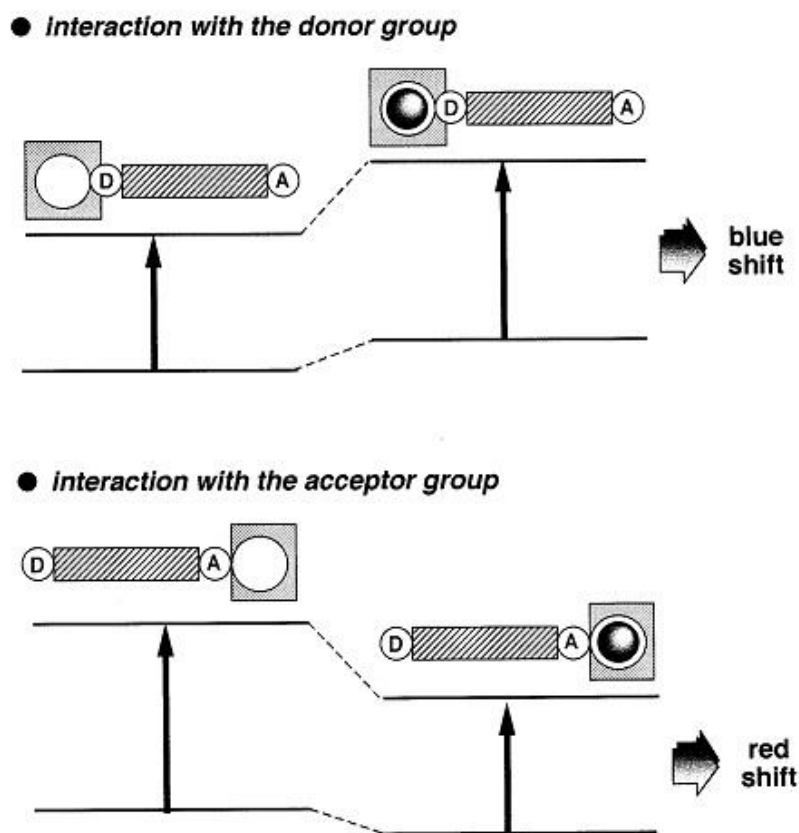


**Figure 6.** Principle of cation recognition by fluorescent PCT sensors.

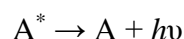
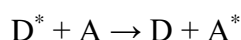
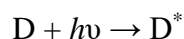


### 1.2.3 Excimer Formation

Where aromatic rings are involved in weak interactions (such as  $\pi$ -stacking) which bring them within van der Waals contact distances, electronic excitation of one ring can cause an enhanced interaction with its neighbor, leading to what is termed an excited-state dimer or “excimer”.<sup>28</sup> In other words, an excimer is a complex formed by the interaction of an excited fluorophore with another fluorophore in its ground state. Excimer emission typically provides a broad fluorescence band without vibrational structure, with the maximum shifted, in the case of most aromatic molecules,<sup>29</sup> by about  $6000\text{ cm}^{-1}$  to lower energies compared to that of the uncomplexed (“monomer”) fluorophore emission. An excimer may also form from an excited monomer if the interaction develops within the lifetime of the latter. Thus, it is expected that excimers are more likely to be produced by relatively long-lived monomer excited states.<sup>30</sup> Rates of fluorophore diffusion, especially in viscous solvents, are therefore another limit on excimer formation.<sup>31</sup> Importantly, the separation and relative orientation of multiple fluorophore units attached to ligands can be controlled by metal ion coordination, so that recognition of a cation can be monitored by the monomer:excimer fluorescence intensity ratio.<sup>32</sup>

### 1.2.4 Fluorescence Resonance Energy Transfer (FRET)

In the process of FRET, initially a donor fluorophore (D) absorbs the energy due to the excitation of incident light and transfer the excitation energy to a nearby chromophore, the acceptor (A).



[Where  $h$  is the Planck’s constant and  $\nu$  is the frequency of the radiation]

Figure 7 illustrates the transitions involved between the donor emission and acceptor absorbance in FRET system. In presence of suitable acceptor, the donor fluorophore can transfer its excited state energy directly to the acceptor without emitting a photon. This returns the donor to its electronic ground state, and emission may then occur from the acceptor center. Energy transfer manifests itself through decrease or quenching of the donor

fluorescence and a reduction of excited state lifetime accompanied also by an increase in acceptor fluorescence intensity.<sup>33</sup>

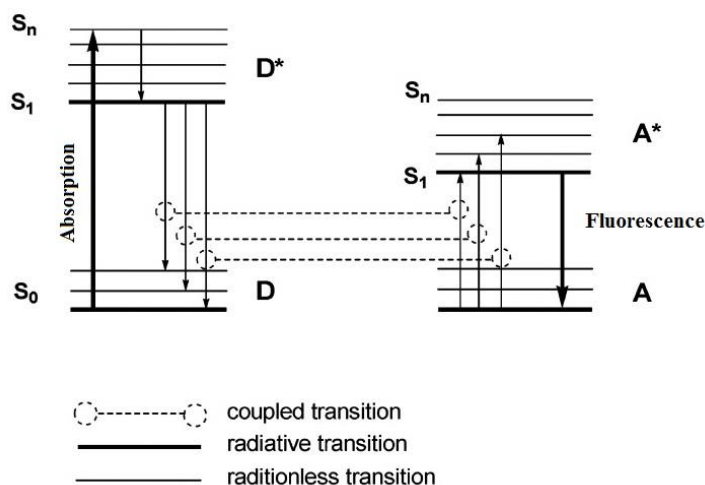


**Figure 7.** Fluorescence resonance energy transfer system.

There are few criteria that must be satisfied in order for FRET to occur. These are: (i) the fluorescence emission spectrum of the donor molecule must overlap the absorption or excitation spectrum of the acceptor chromophore (Figure 8). The degree of overlap is referred to as spectral overlap integral ( $J$ ). (ii) The two fluorophore (donor and acceptor) must be in the close proximity to one another (typically 1 to 10 nanometer). (iii) The transition dipole orientations of the donor and acceptor must be approximately parallel to each other. (iv) The fluorescence lifetime of the donor molecule must be of sufficient duration to allow the FRET to occur.<sup>34</sup>

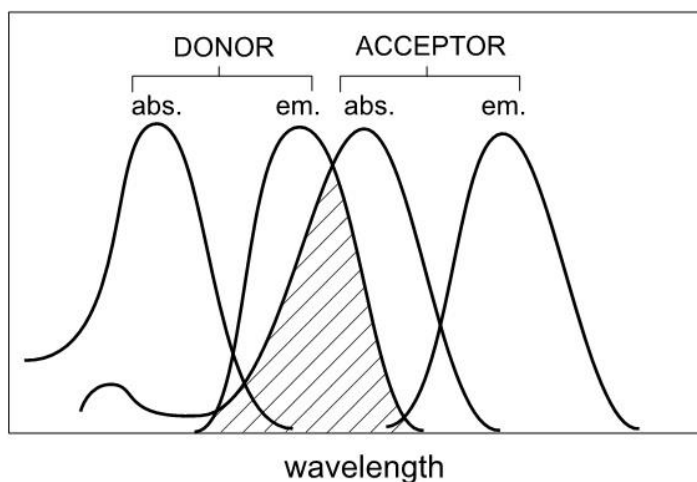


**Figure 8.** Spectral overlap for FRET.

### 1.3 Calixarene-based Fluorescent Chemosensors

Calixarenes have received much interest as basic molecular scaffolds for the construction of selective ionophores, many of which have been incorporated into fluorescent chemosensors.<sup>35</sup> Fluorophores such as anthracene, pyrene, dansyl, BODIPY, naphthalene, quinoline, rhodamine and fluorescein have been efficiently coupled to the upper and lower rims of calixarenes and showed good performance as fluorescent chemosensors.

#### 1.3.1 PET Chemosensors

Calixarene **1** (Figure 9) bearing four carbonyl groups, two of them being linked to pyrene and nitrobenzene at opposite sites on the lower rim, was prepared for Na<sup>+</sup> sensing.<sup>36</sup> As the free ligand, **1** shows fluorescence similar to that of **2**, but its intensity is 50 times weaker, suggesting that the fluorescence quenching in **1** is due to intramolecular PET between the nitrobenzyl acceptor and excited pyrene fluorophore, a conclusion supported by the fact that the fluorescence is not solvent sensitive. Binding of Na<sup>+</sup> to **1** in diethyl ether appears to cause a conformational change where the nitrobenzyl and pyrenyl substituents become more distant, leading to reduced PET seen as an enhancement in the fluorescence quantum yield from 0.0025 to 0.016.

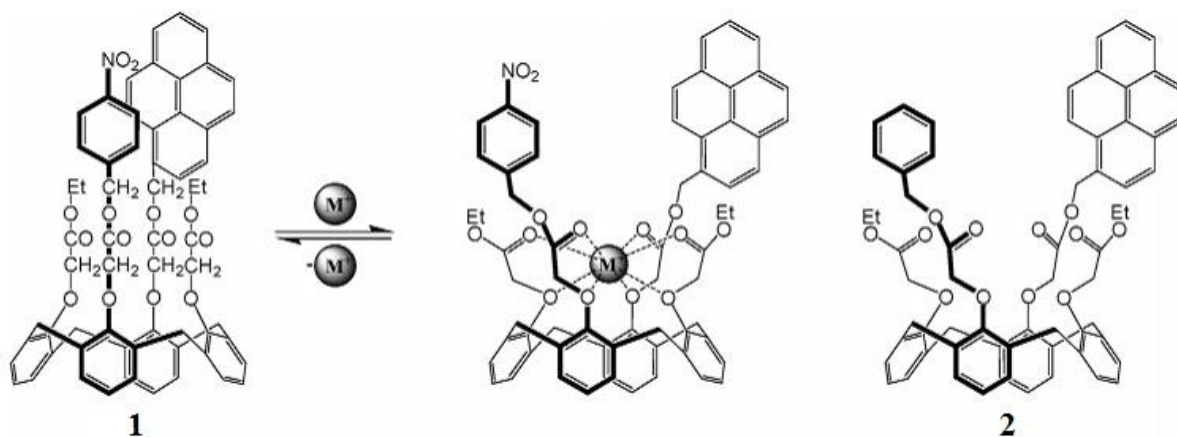


**Figure 9.** Structure of chemosensor **1** and **2**.

Dabestani and co-workers have reported Cs<sup>+</sup> PET sensors **3** and **4** (Figure 10) based on a calix[4]crown-6 ether in which a 9-cyanoanthracene fluorophore is linked to a phenyl ring

inserted into the crown.<sup>37</sup> In the absence of metal ion, their fluorescence is weak due to the PET from the oxygen atoms of the benzocrown to the excited singlet state of the cyanoanthracene fluorophore.  $\text{Cs}^+$  binding to the crown in  $\text{CH}_2\text{Cl}_2/\text{MeOH}$  (1:1 v/v) inhibits this PET effect, which induces an enhancement of the fluorescence emission. A 1:1 stoichiometry is found for compounds **3** and **4**, which leads to stability constants of  $4 \times 10^6$  and  $1.2 \times 10^7$ , respectively.

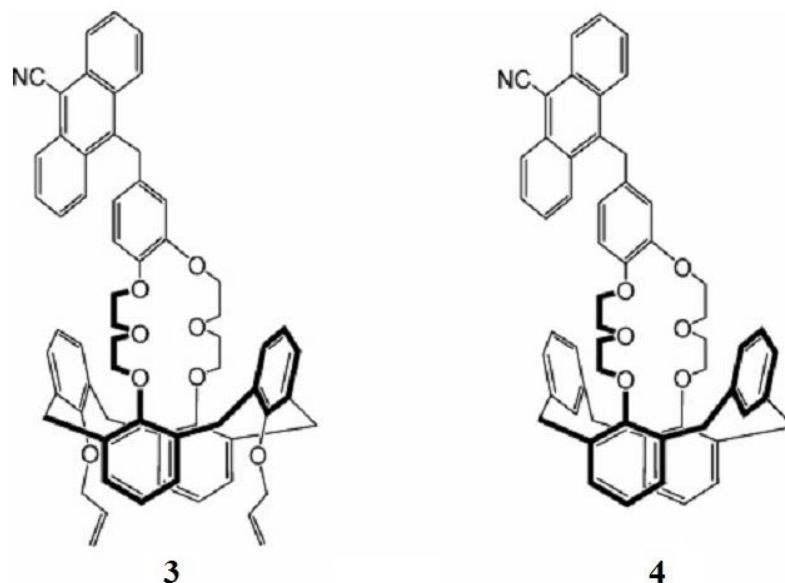


**Figure 10.** Structure of chemosensor **3** and **4**.

Fluorescence quenching commonly occurs by the PET mechanism described above in which the excited state acts as an oxidant, although the inverse phenomenon, termed reverse PET, is also sometimes observed. Chemosensor **5** (Figure 11) exhibited high selectivity towards  $\text{Fe}^{3+}$  ions by fluorescence quenching which was attributed to reverse photo-induced electron transfer (reverse PET) from pyrene units to the carbonyl oxygen atoms. Due to the  $\text{Fe}^{3+}$  played an important role in human body, and given that the better cell permeability and intracellular fluorescence imaging of sensor **5**, the author further attempted to apply sensor **5** to monitor  $\text{Fe}^{3+}$  in living cell.<sup>38</sup>

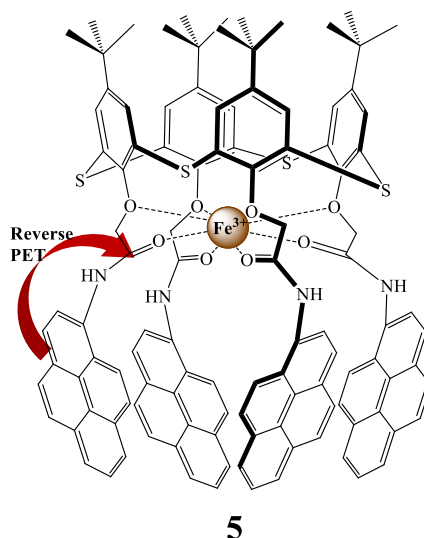


**Figure 11.** Structure of chemosensor **5**.

Apart from their application for metal ion sensing, calixarenes attached to a fluorophore can be used for pH sensing. The BODIPY-appended calixarene **6** (Figure 12) is such a sensor, acting through a PET mechanism. The emission intensity of **6** in  $\text{CH}_3\text{OH}/\text{H}_2\text{O}$  (1:1, v/v) is strongly and reversibly pH dependent. There are more than 10-fold changes in the emission intensity, maximizing in the pH range 5.6–8.2. PET in this system can be explained by electron transfer from the electron pair located on the phenolate to the BODIPY moiety.<sup>39</sup>

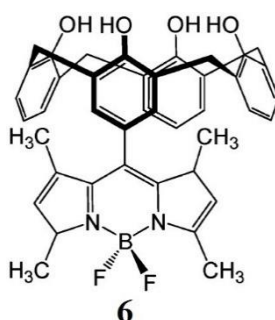


**Figure 12.** Structure of chemosensor **6**.

Chemosensor **7** exhibits a selective interaction with  $\text{CH}_3\text{COO}^-$  in  $\text{CH}_3\text{CN}$  (0.4%, v/v,  $\text{CHCl}_3$ ) over other anions tested (Figure 13). The addition of this anion to **7** leads to a quenching in fluorescence emission due to PET from nitrogen to the anthracene unit.  $^1\text{H}$  NMR spectra indicate that oxygen atoms of the anion interact with the anthracene 9H as well as the amide NH centers.<sup>40</sup>

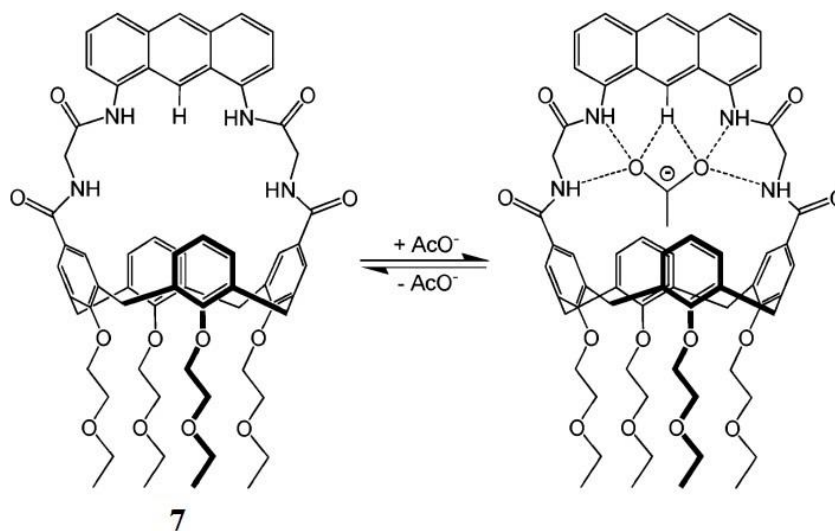


**Figure 13.** Proposed recognition mechanism of **7** towards  $\text{AcO}^-$ .

### 1.3.2 PCT Chemosensors

Chemosensor **8** and **9** containing one or four appended naphthalene fluorophores which contain the methoxy moiety as a donor unit and the carbonyl group as an acceptor in the PCT process (Figure 14).<sup>41</sup> They exhibit outstanding fluorescence enhancements upon cation binding and are very selective for  $\text{Na}^+$ . The complexation with metal ions induces a red shift of the UV-vis and fluorescence spectra associated with a major increase in fluorescence quantum yield due to the relative locations of the  $n\text{-}\pi^*$  and  $\pi\text{-}\pi^*$  levels depending on the charge density of the bound cation.

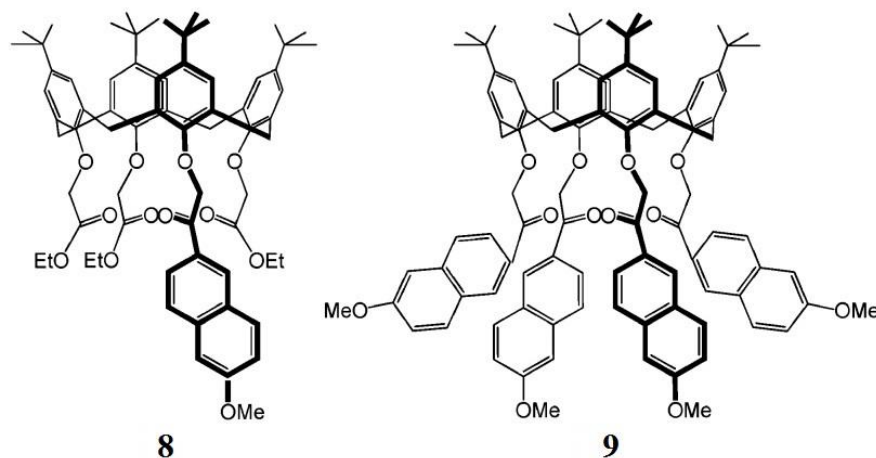


**Figure 14.** Structure of chemosensor **8** and **9**.

Kim *et al.* reported a calix[4]arene-based chemosensor **10** with two coumarin units attached via amido functions acting also as binding sites.<sup>42</sup> Complexation of  $F^-$  by sensor **10** resulted in red-shift of both UV-vis absorption and fluorescence emission, which was ascribed to the photo-induced charge transfer (PCT) mechanism induced by hydrogen bonding followed by deprotonation of NH-amide groups (Figure 15).

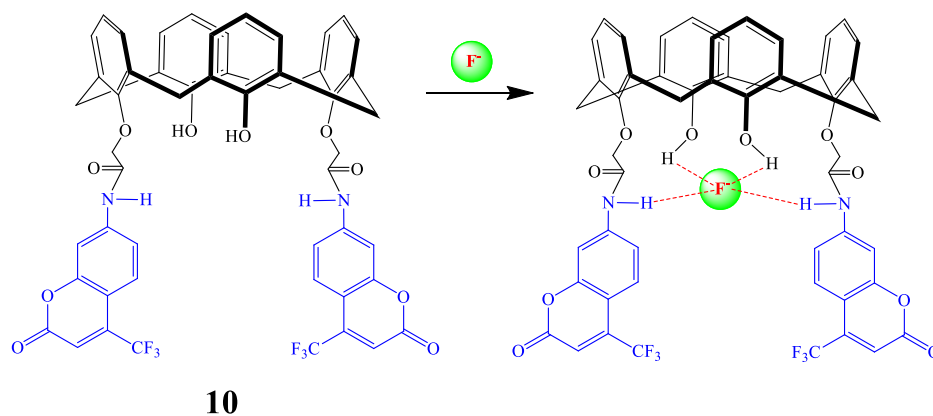


**Figure 15.** Proposed recognition mechanism of **10** towards  $F^-$ .

Similarly, Jain *et al.* reported a thiacalix[4]arene chemosensor **11** which employed quinoline as fluorophore. According to the UV-absorption and fluorescent emission spectra titration results, probe **11** exhibited highly selective recognize for  $F^-$  anion among other anions ( $Cl^-$ ,  $Br^-$ ,  $I^-$ ,  $OH^-$ ,  $CH_3COO^-$ ,  $H_2PO_4^-$  and  $PO_4^{3-}$ ). Quenching and red shift in emission spectra constituting the signature detection for fluoride. This may be attributed to the photo-induced charge transfer (PCT) mechanism which can be induced by deprotonation of acidic NH proton in the presence of fluoride ion (Figure 16).<sup>43</sup>

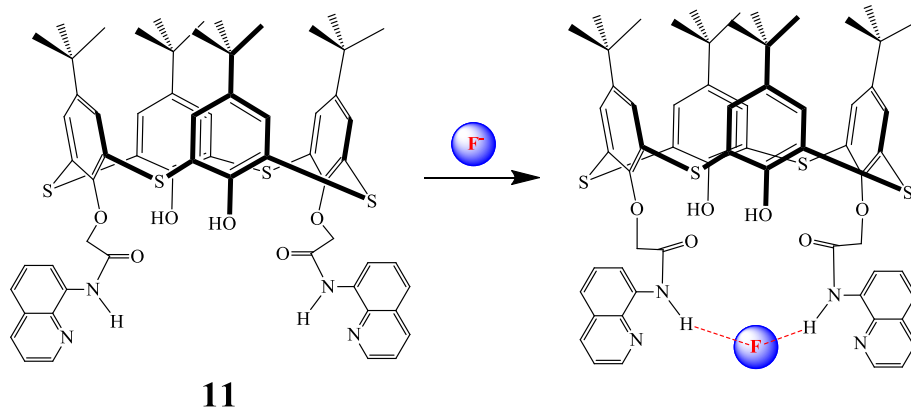


**Figure 16.** Proposed recognition mechanism of **11** towards  $F^-$ .

### 1.3.3 Excimer Chemosensors

As fluorogenic units, pyrene (Py) is regarded as one of the most useful sensing molecules because it may emit as a monomer near 370–380 nm or as an excimer near 480 nm. In molecules with two (or more) pyrenyl substituents, excimer formation can be efficient but is also sensitive to even subtle conformational changes such as may be induced by metal ion binding, so that the ratio (IE:IM) of excimer to monomer emission intensities can be an informative parameter in a variety of sensing systems. For this reason, pyrene is widely employed as signal unit for the design of fluorescent chemosensors.<sup>44</sup>

A ratiometric sensor **12** for  $\text{Cd}^{2+}$  and  $\text{Zn}^{2+}$  based on calix[4]arene bearing 1,2,3-triazole-linked pyrene units has been reported (Figure 17).<sup>45</sup> Sensor **12** showed strong excimer and weak monomer emissions, due to face-to-face  $\pi$ - $\pi$  interaction between the two pyrene moieties. Addition of  $\text{Cd}^{2+}$  or  $\text{Zn}^{2+}$  produced a ratiometric fluorescence change, with a decrease in excimer emission as well as an increase in monomer emission. This ratiometric behavior is due to the complexation of  $\text{Cd}^{2+}$  and  $\text{Zn}^{2+}$  by the triazole nitrogen atoms, which causes a change in the conformation of the pyrene arms. No other metal ions produced such ratiometric response, confirming the high selectivity of probe **12** for  $\text{Cd}^{2+}$  and  $\text{Zn}^{2+}$ .

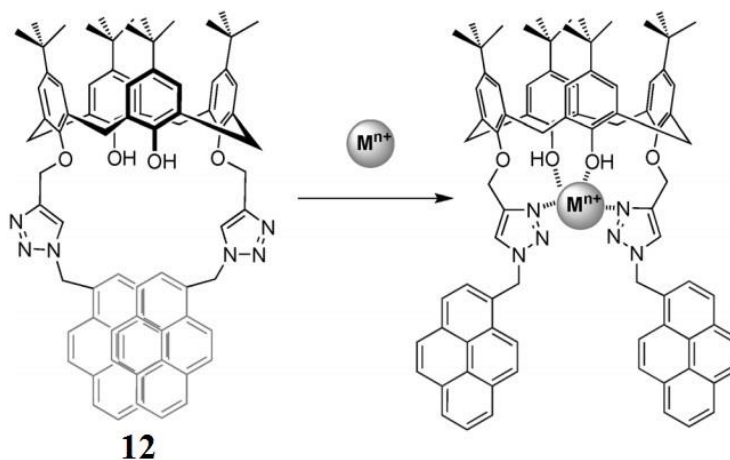


**Figure 17.** Fluorescent chemosensor **12** for sensing  $\text{Cd}^{2+}$  and  $\text{Zn}^{2+}$  ions.

Our group reported pyrene-linked triazole-modified homooxalix[3]arene **13** as a multi-functional fluorescent chemosensor for  $\text{Zn}^{2+}$  and  $\text{H}_2\text{PO}_4^-$  detection (Figure 18).<sup>46</sup> Chemosensor **13** showed ratiometric sensing of  $\text{Zn}^{2+}$  by enhancing the monomer emission



while weakening the excimer emission. Further studies revealed that the subsequent addition of  $\text{H}_2\text{PO}_4^-$  to the solution of  $\mathbf{13} \cdot \text{Zn}^{2+}$  complex resulted in a reversed ratiometric fluorescent change. This system exhibited a novel detection signal output for targeting cations and anions through switching of the excimer emission of pyrene from the “on-off” to the “off-on” type. In addition, an efficient logic circuit for a molecular traffic signal with the help of binary logic based on an INHIBIT and OR gate by using  $\text{Zn}^{2+}$  and  $\text{H}_2\text{PO}_4^-$  ions as different chemical inputs has been constructed and evaluated.

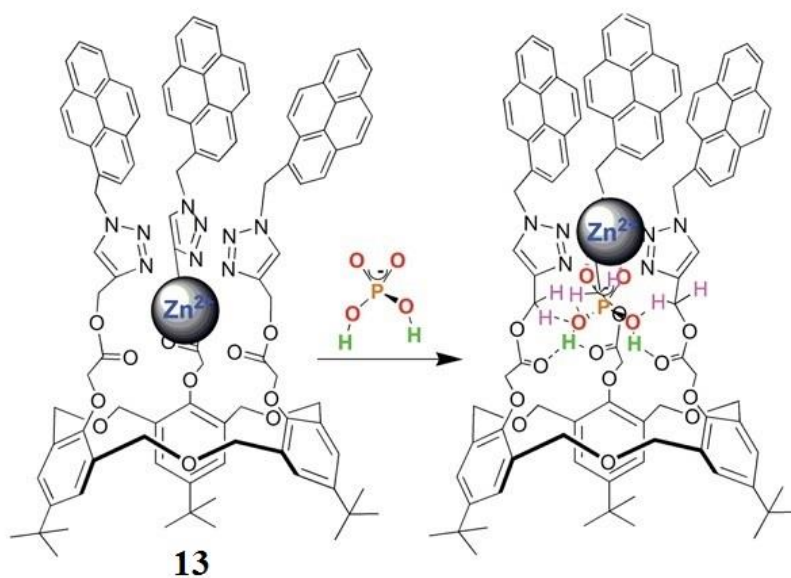


**Figure 18.** The proposed structure of  $\mathbf{13} \cdot \text{Zn}^{2+}$  for  $\text{H}_2\text{PO}_4^-$  anion.

On the basis of the above studies, our groups further designed and synthesized fluorescent chemosensors **14** and **15** based on thiocalix[4]arene with 1,3-alternate conformation (Figure 19).<sup>47</sup> The fluorescence spectra changes suggested that chemosensors **14** and **15** are highly selective for  $\text{Ag}^+$  over other metal ions by a ratiometric fluorescence response of pyrene. Furthermore, the competitive interaction of  $\text{Ag}^+$  ions in the presence of other cations was investigated, no significant interference in the detection of  $\text{Ag}^+$  ions was observed for sensor **14** and **15**. The  $^1\text{H}$  NMR titration analysis conformed that the  $\text{Ag}^+$  was selectively bound to the nitrogen atoms on the triazole rings.

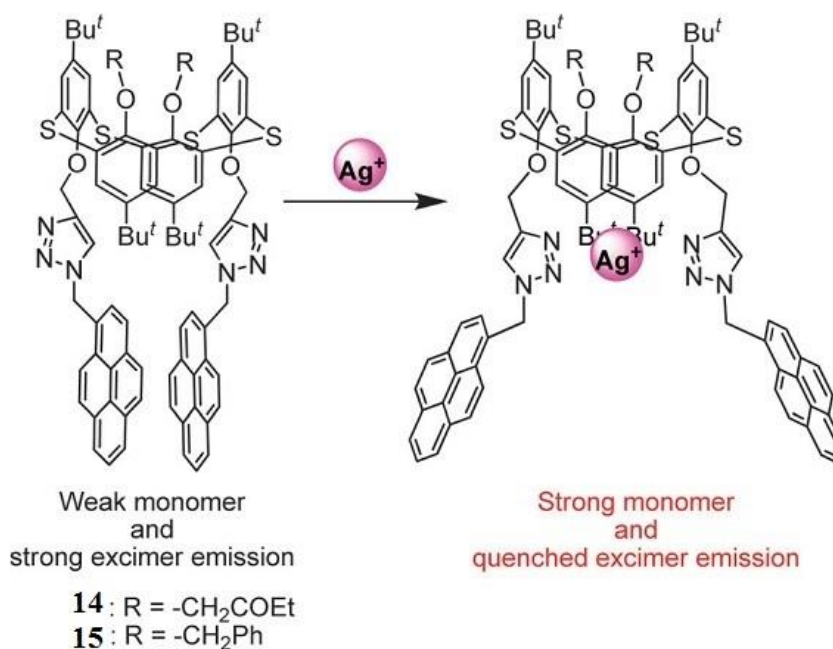


**Figure 19.** Fluorescent chemosensor **14** and **15** for sensing Ag<sup>+</sup>.

Kumar et al. reported fluorescent chemosensors **16** bearing thiourea moieties conjugated with naphthyl fluorophores.<sup>48</sup> Chemosensors **16** showed strong interactions with F<sup>-</sup> ions with an increase in excimer emission of the naphthyl groups. The binding of the NH protons of **16** with F<sup>-</sup> ions induced intermolecular binding which triggered intramolecular  $\pi$ - $\pi$  interactions between the two naphthyl groups and led to excimer formation (Figure 20).

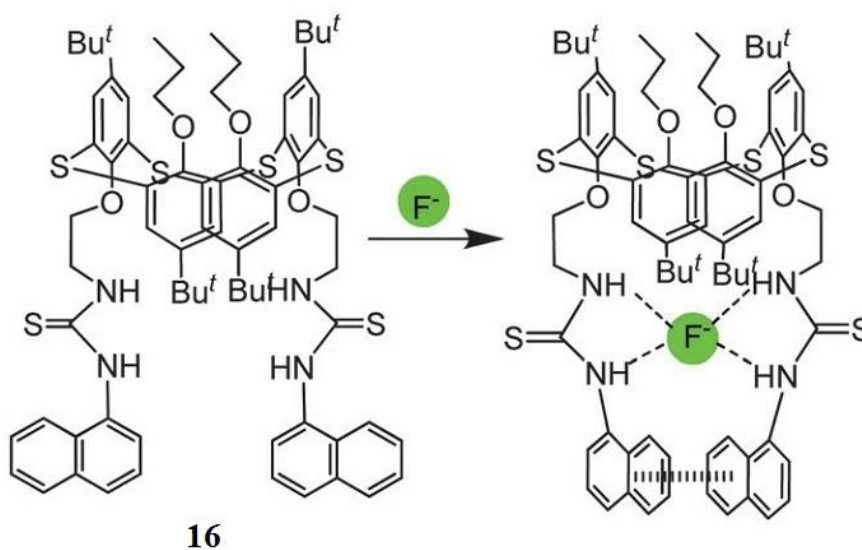


**Figure 20.** Fluproposed binding modes of **16** with F<sup>-</sup>.

### 1.3.4 FRET Chemosensors

Li *et al.* designed a fluorescent chemosensor **17**, bearing both BODIPY and rhodamine moieties for the detection of  $\text{Hg}^{2+}$  and  $\text{Ba}^{2+}$  (Figure 21).<sup>49</sup> In acetonitrile solution, probe **17** shows an absorption band centered at 499 nm, which is ascribed to absorbance of the BODIPY moiety. With excitation at 490 nm, the fluorescence intensity at 505 nm is very weak due to the efficient PET effect from the oxygen atoms in the oxa-crown-6 loop to the excited BODIPY fluorophore. The PET effect was canceled upon addition of 20 equiv. of  $\text{Ba}^{2+}$ , resulting in a 15-fold enhancement in fluorescence intensity at 505 nm. When  $\text{Hg}^{2+}$  was added to a solution containing **17**, the spirolactam form of rhodamine transferred to the ring-opened state, accompanied by an absorption band centered at 558 nm and a strong emission peak at 585 nm. This fluorescence enhancement at long wavelengths was attributed to the FRET effect from excited BODIPY to the ring-opening of the rhodamine moiety.

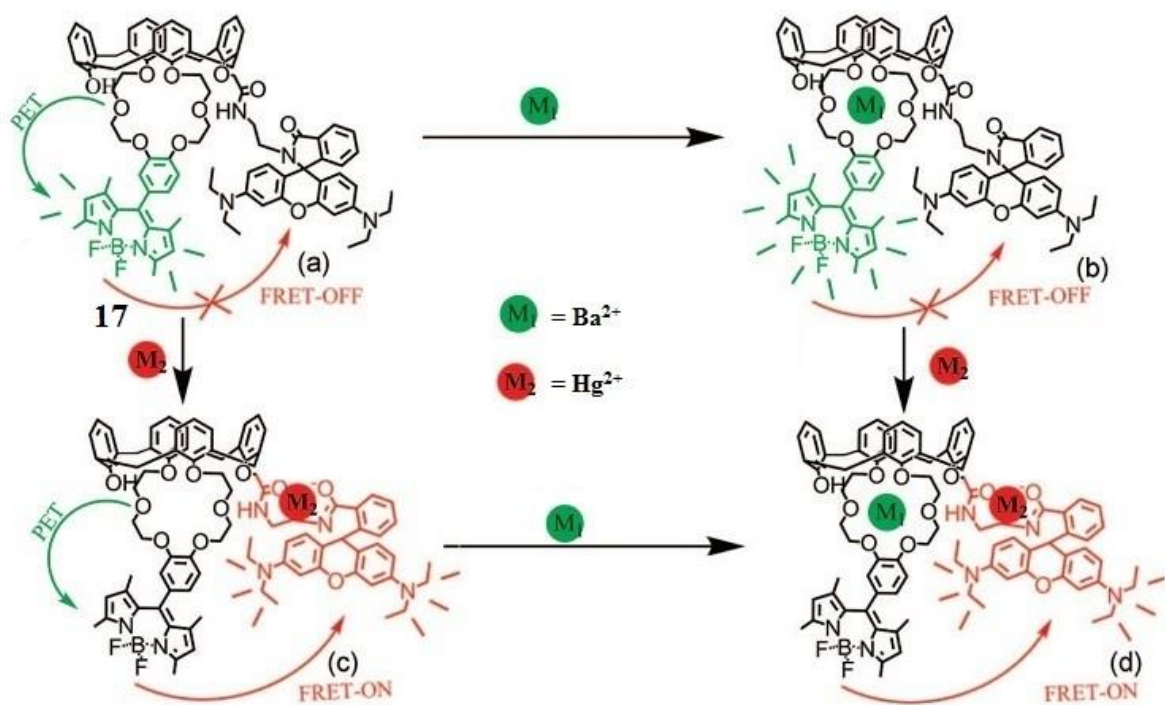


**Figure 21.** Proposed binding modes of **17** with  $\text{Hg}^{2+}$  and  $\text{Ba}^{2+}$ .

Vicens and Kim *et al.* reported a bis-calixarene **18** (Figure 22), combining two pyrenyl groups, which are potential energy donors, and a rhodamine group, which may act as an energy acceptor.<sup>50</sup> Fluorescence changes were observed in the case of complexation with

only the two different metal ions. Addition of  $\text{Hg}^{2+}$  to a  $\text{CH}_3\text{CN}$  solution of **18** resulted in significantly enhanced fluorescence at  $\sim 575$  nm via the FRET effect from the pyrenyl excimer to a ring-opened rhodamine moiety. In contrast, addition of  $\text{Al}^{3+}$  induced a distinct increase of pyrenyl excimer emission ( $\sim 475$  nm), while no obvious FRET-ON phenomenon was observed.

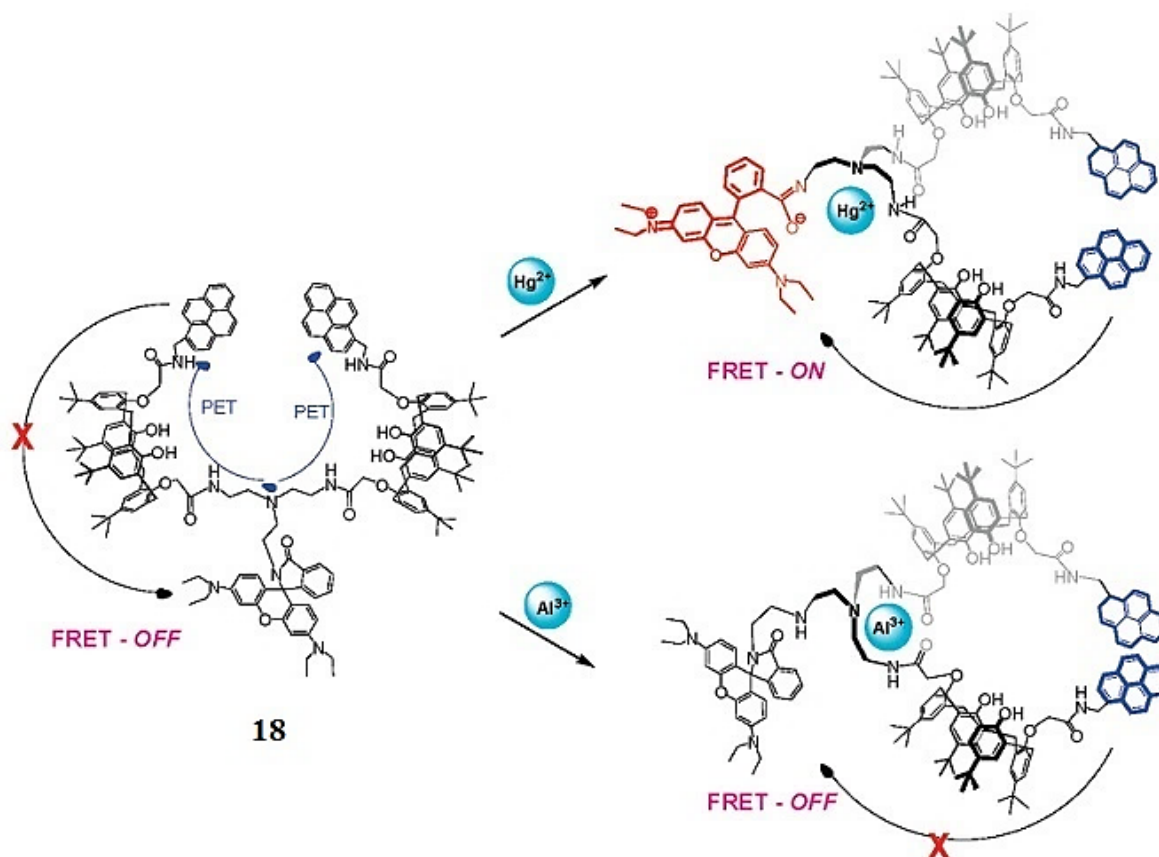


**Figure 22.** Proposed different complexation behaviors of **18** with  $\text{Hg}^{2+}$  and  $\text{Al}^{3+}$ .

Kim *et al.* designed a pyrene excimer-based calix[4]arene FRET chemosensor **19** (Figure 23), involving two pyrenyl and one rhodamine substituent, as a selective sensor for  $\text{Hg}^{2+}$ .<sup>51</sup> On the addition of 10 equiv. of  $\text{Hg}^{2+}$  to a solution of **19**, a new absorption band centered at 559 nm appears, with a color change from colorless to pink. In  $\text{CHCl}_3$ - $\text{CH}_3\text{CN}$  (50:50, v/v) solution, amide binding of  $\text{Hg}^{2+}$  promotes ring opening of rhodamine, resulting in FRET from the pyrene excimer to rhodamine. The intensity of the characteristic emission of the ring-opened rhodamine at 576 nm increases, with a concomitant decline in the pyrenyl

excimer emission intensity at 470 nm. The minimum detectable concentration of  $\text{Hg}^{2+}$  is about 5.0  $\mu\text{M}$ , based on linear variations in the fluorescence intensity.

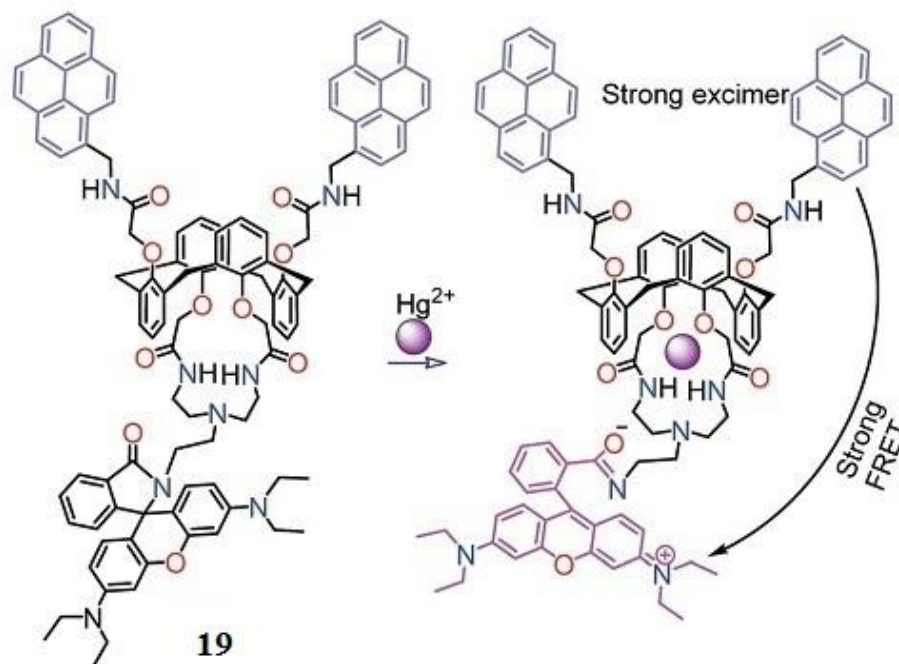


**Figure 23.** Schematic of  $\text{Hg}^{2+}$ -selective chemosensor **19** based on FRET.

### 1.3.5 Other Chemosensors

#### 1.3.5.1 Chemosensors Based on Spirolactam Ring-Opening

Spirocyclic derivatives of rhodamine and fluorescein dyes are useful sensing platforms because the ring-opening process leads to a turn-on fluorescence change. Since the first rhodamine-based fluorescent chemosensor for  $\text{Cu}(\text{II})$  was reported by Anthony W. Czarnik in 1997, a large number of papers involving fluorescent chemosensors based on spiroring-opening processes have been published.<sup>52</sup> They have also been employed as fluorophore to the design of fluorescent chemosensors based on the calixarene platforms.

Chemosensor **20** possessing rhodamine as a signaling unit exhibits a high binding affinity towards  $\text{Fe}^{3+}$  and  $\text{Cr}^{3+}$  in mixed aqueous solutions (Figure 24).<sup>53</sup> The addition of  $\text{Fe}^{3+}$  or  $\text{Cr}^{3+}$  to the solution of **20** induced ring-opening of the spirolactam resulting in a significant increase in the fluorescence emission (turn-on). Considerable color changes were also

observed with the addition of  $\text{Fe}^{3+}$  (from colorless to pink) and  $\text{Cr}^{3+}$  (from colorless to light purple) indicating that **20** could serve as a ‘‘naked-eye’’ chemosensor for  $\text{Fe}^{3+}$  or  $\text{Cr}^{3+}$  ions.

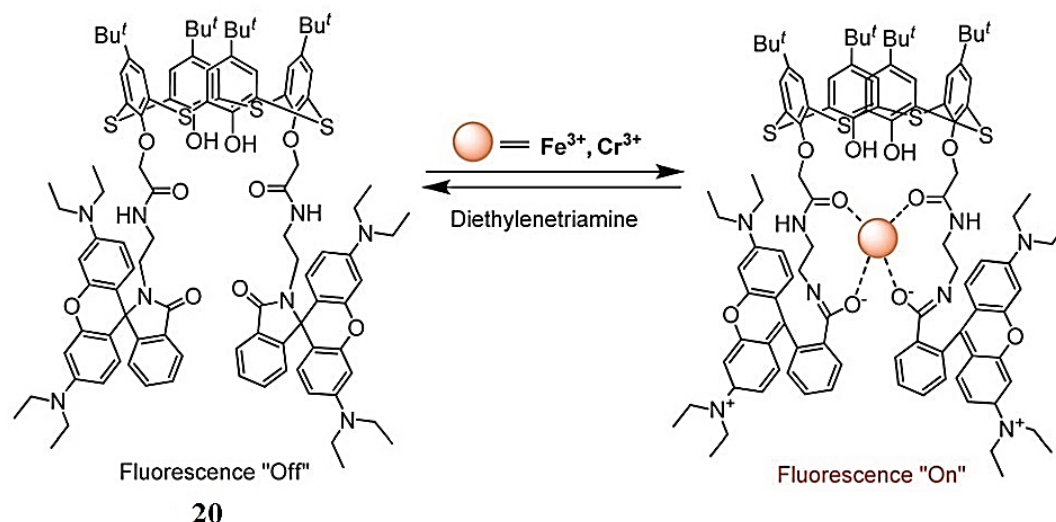


**Figure 24.** Proposed binding modes of **20** with  $\text{Fe}^{3+}$  or  $\text{Cr}^{3+}$ .

Kumar *et al.* synthesized a fluorescent probe **21** which shown a selective turn-on fluorescence response *via*  $\text{CN}^-$  ions induced spirolactone ring opening of fluorescein (Figure 25). Particularly, the resulting cyanide complex **21**· $\text{CN}^-$  can further selectively applied to detect copper ( $\text{Cu}^{2+}$ ) ions through fluorescence turn-off. Depending on the different chemical inputs ( $\text{CN}^-$  and  $\text{Cu}^{2+}$ ) and fluorescence signals as outputs (on and off), a sequential logic circuit was constructed.<sup>54</sup>

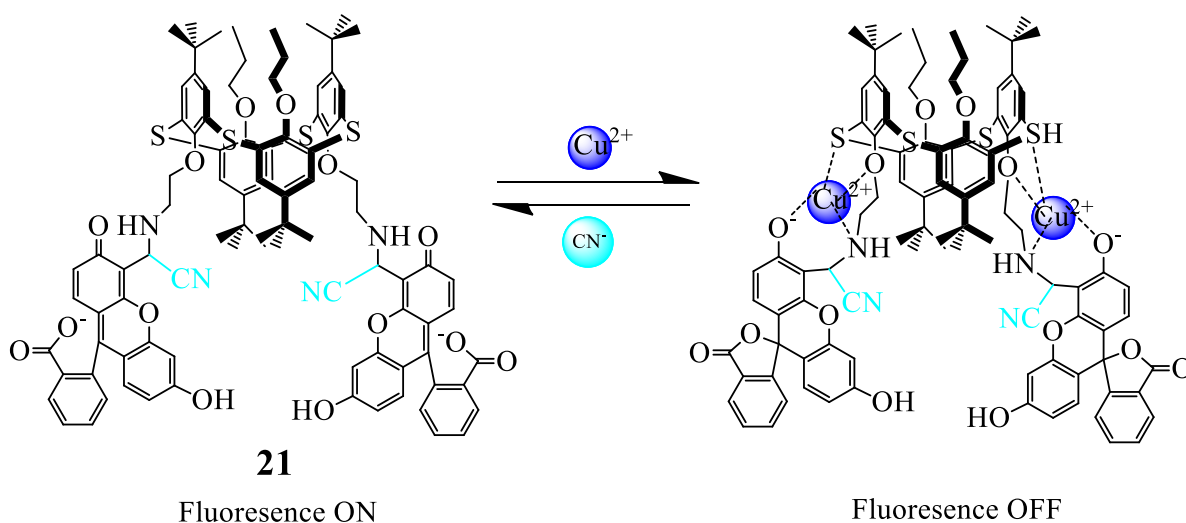


**Figure 25.** Proposed binding modes of **21** with  $\text{CN}^-$  and  $\text{Cu}^{2+}$  ions.



### 1.3.5.2 Chemosensors Based on ESIPT

Kim et al. reported a novel fluorescent chemosensor **22** with two amidoanthraquinone groups at the lower rim of *p*-*tert*-butylcalix[4]arene.<sup>55</sup> Significant changes of absorption and fluorescence bands showed that chemosensor **22** is selective toward fluoride ion ( $F^-$ ) over other anions such as  $Cl^-$ ,  $Br^-$ ,  $I^-$ ,  $CH_3COO^-$ , and  $OH^-$ . The ESIPT (excited-state intramolecular proton transfer) process of **22** is inhibited by the fluoride-induced H-bonding followed by deprotonation of NH groups in the amidoanthraquinone fragment (Figure 26), which strongly affected such properties of the compound as luminescence intensity, magnitude of Stokes shift, and photostability. The visible absorption and emission spectra in toluene, MeCN, and DMSO, as well as  $^1H$  NMR spectra in  $CDCl_3$  were studied. The emission spectra of **22** in toluene and acetonitrile contained bands corresponding to the ground (N,  $\lambda$  515 nm) and excited states (T,  $\lambda$  560 nm; Figure 26). The emission spectrum recorded in DMSO lacked ESIPT band due to facile formation of hydrogen bonds between the solvent and H-donors. Chemosensor **22** selectively recognizes  $F^-$  ion, presumably via intramolecular  $NH\cdots F^-$  hydrogen bonding (or deprotonation), which promotes  $\pi$ -electron delocalization through the amidoanthraquinone fragment and affects  $\pi$ - $\pi$  interaction. The originally colorless solution turns green. A small change of the band at  $\lambda$  560 nm (tautomeric emission) is accompanied by strong increase of the normal emission band at  $\lambda$  527 nm, indicating inhibition of ESIPT in the presence of  $F^-$  (Figure 27).

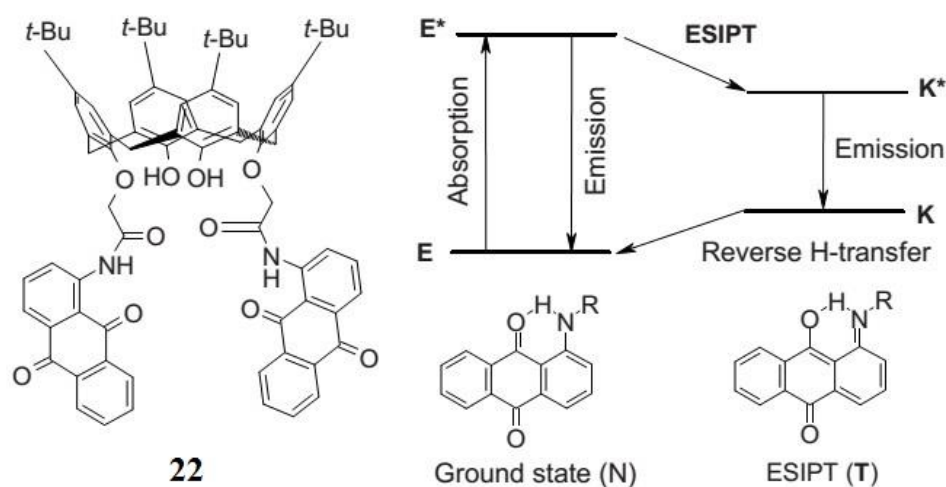


**Figure 26.** The structure of chemosensor **22** and the 1-Aminoanthraquinone groups in the ground (N) and excited (T) states.

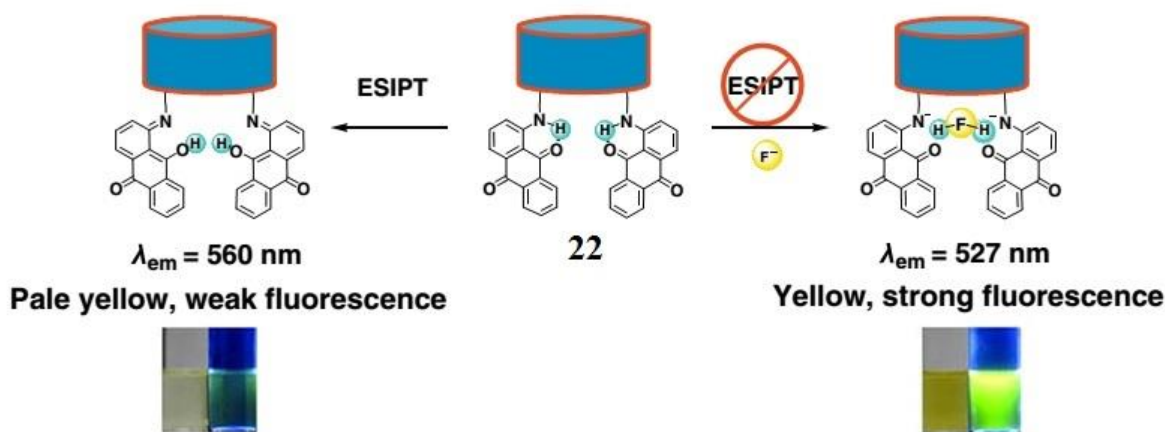


**Figure 27.** Proposed mechanism for the inhibition of ESIPT in **22** induced by  $F^-$  ion.

Chemosensor **23** based on a thiacalix[4]crown with a 1,3-alternate conformation has been synthesized.<sup>56</sup> The fluorescence of chemosensor **23** was quenched with addition of  $Fe^{3+}$  ions due to the inhibition of excited state intramolecular proton transfer (ESIPT, Figure 28). However, addition of  $Li^+$  ions and cysteine to the **23**· $Fe^{3+}$  complex generated *in situ* revealed that the emission occurred via two different mechanisms. The addition of  $Li^+$  ions triggered a negative allosteric behavior, and the addition of cysteine followed the displacement approach.

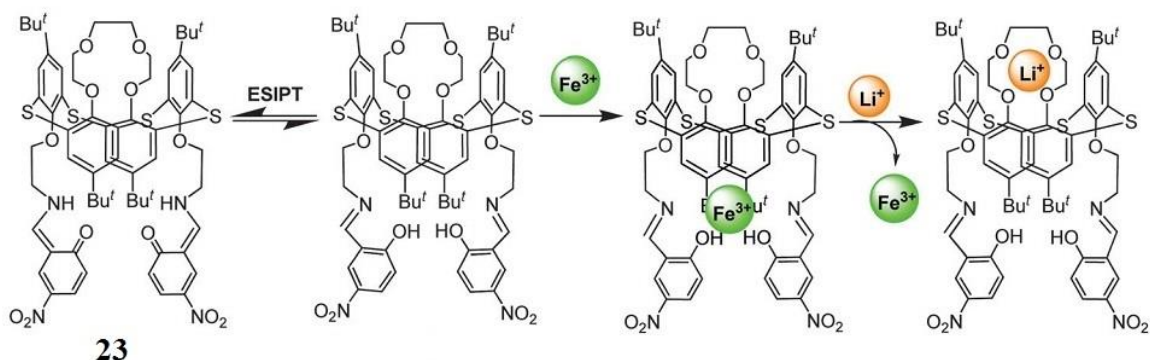


**Figure 28.** Structures of chemosensor **23** and proposed binding modes.

### 1.3.5.3 Chemosensors Based on Schiff-base

Schiff base calixarenes have been widely used as fluorescent chemosensors for various analytes. Zeng *et al.* designed a 1,3-alternate thiacalix[4]crown-shaped fluorescent chemosensor **24** which employed phenothiazine moieties as fluorophore (Figure 29). Chemosensor **24** exhibited strong fluorescence emission in THF-water due to multiple



noncovalent interactions within the molecule inhibit the intramolecular rotation. When  $\text{Fe}^{3+}$  or  $\text{Cr}^{3+}$  were gradually added to the solution of **24**, the fluorescence intensity of this solution was gradually decreased until completely quenched. However, there were no obviously change by the addition of any other tested metal ions. It suggested that chemosensor **24** was capable of selectively sensing  $\text{Fe}^{3+}$  and  $\text{Cr}^{3+}$  ions. Further study revealed the quenching mechanism was ascribed to the  $\text{Fe}^{3+}$  or  $\text{Cr}^{3+}$  ions catalyze the cleavage of the Schiff base group of **24**. In other word, chemosensor **24** was hydrolyzed in the presence of  $\text{Fe}^{3+}$  or  $\text{Cr}^{3+}$  ions *via* loss of the phenothiazine groups. This is the first case of fluorescence quenching is based on a hydrolysis mechanism.<sup>57</sup>

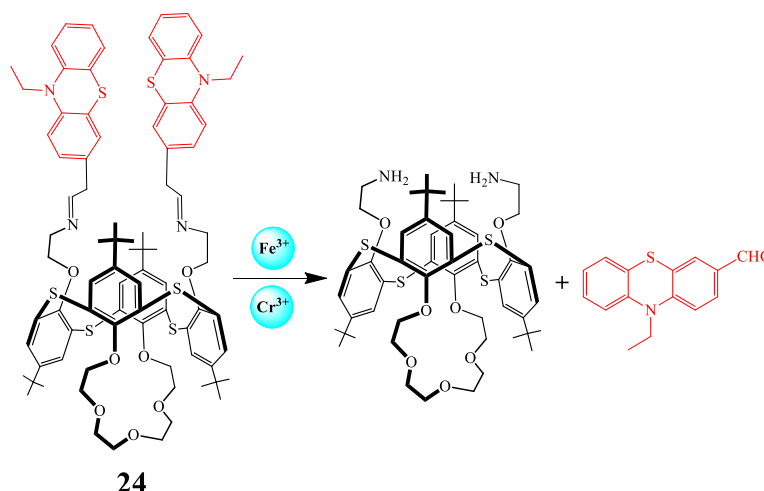


**Figure 29.** Proposed recognition mechanism of **24**.

Calixarene **25** exhibited a weak emission at 440 nm when excited at 320 or 390 nm. The addition of  $\text{Zn}^{2+}$  ions into the solution of **25** showed a progressive enhancement in the fluorescence intensity. The  $^1\text{H}$  NMR spectroscopic titration of **25** with  $\text{Zn}^{2+}$  ions exhibited that the intensity of the Schiff base OH and  $\text{CH}_2\text{OH}$  protons decreased, suggesting the binding of the  $\text{Zn}^{2+}$  ion inside the core of the Schiff base as shown in Figure 30. The triazole moieties are not involved in the coordination of the  $\text{Zn}^{2+}$  ion; however, it serves as a linker. Thus, a  $\text{Zn}^{2+}$ -selective chemosensor with a fluorescence off/on switch has been successfully synthesized.<sup>58</sup> On the basis of the above study, Rao and co-workers synthesized a series of salicylaldimine-appended triazole-linked calixarene derivatives **26–29** by using a click reaction and tested their selectivity for metal ions (Figure 31).<sup>59</sup>

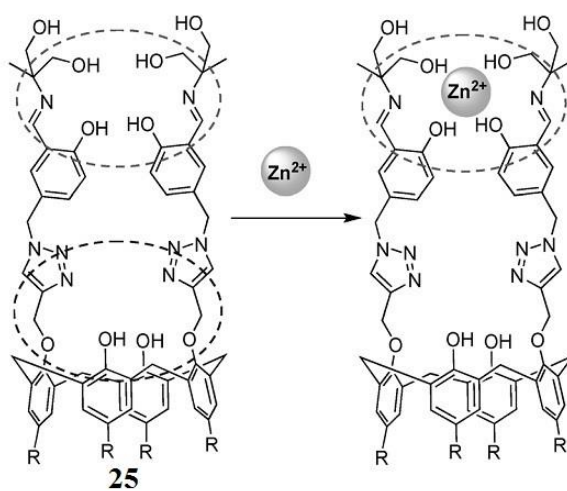


**Figure 30.** Proposed recognition mechanism of chemosensor **25**.

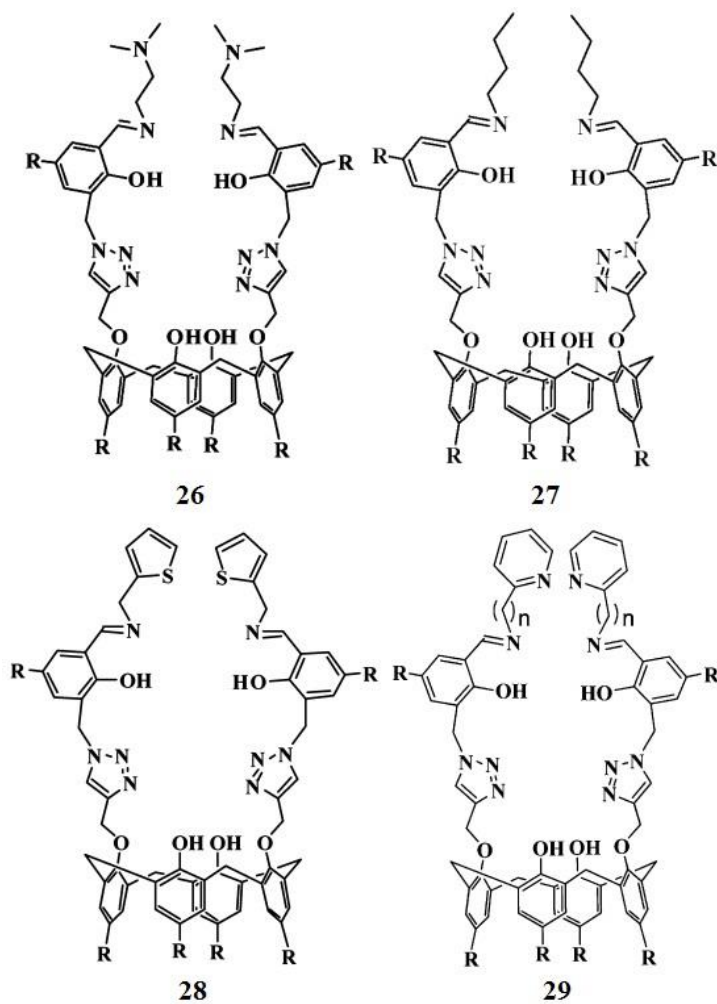


**Figure 31.** Structure of chemosensor **26**–**29**.

## 1.4 Conclusion

Calixarenes have attracted tremendous interest and have been extensively explored in various fields, including chemistry, biology, medicine, and environmental processes. Because of their inherent versatility and numerous possibilities of functionalization, calixarene derivatives have been widely used for the development of fluorescent chemosensors. The pre-organized core of calixarene is well-known for the complexation of ions and molecules of particular size and shape. The lower and upper rim modification of calixarene with various binding sites, such as N, O, S, and P, further tune and improve the binding efficiency and selectivity toward different guest molecules (hard or soft). These modifications make calixarene derivatives more flexible for efficient binding with guest species. Numerous calixarene derivatives exhibiting different binding properties have been developed for the sensitive and selective detection of anions, cations, and other biologically relevant analytes. Thus, the development of calixarene-based fluorescent chemosensors serves as a useful strategy for the determination of different analytes in environmental and biological systems.

## 1.5 References

1. (a) D. J. Cram, *Science*, 1988, **240**, 760–767; (b) J. M. Lehn, *Science*, 2002, **295**, 2400–2403; (c) J. W. Steed and J. L. Atwood, *Supramolecular Chemistry*, John Wiley & Sons, Ltd., West Sussex, 2nd edn, 2009; (d) H.-J. Schneider and A. Yatsimirsky, *Principles and Methods in Supramolecular Chemistry*, John Wiley & Sons, Ltd., West Sussex, 2000; (e) J. M. Lehn, *Supramolecular Chemistry: Concepts and Perspectives*, Wiley-VCH, New York, 1995.
2. (a) P. A. Gale, N. Busschaert, C. J. E. Haynes, L. E. Karagiannidis and I. L. Kirby, *Chem. Soc. Rev.*, 2014, **43**, 205–241; (b) M. Wenzel, J. R. Hiscock and P. A. Gale, *Chem. Soc. Rev.*, 2012, **41**, 480–520; (c) P. A. Gale, *Chem. Soc. Rev.*, 2010, **39**, 3746–3771; (d) E. Galbraith and T. D. James, *Chem. Soc. Rev.*, 2010, **39**, 3831–3842; (e) S. K. Kim and J. L. Sessler, *Chem. Soc. Rev.*, 2010, **39**, 3784–3809; (f) A. Zhang, J. L. Neumeyer and R. J. Baldessarini, *Chem. Rev.*, 2007, **107**, 274–302.
3. (a) Z. Liu, S. K. M. Nalluri and J. F. Stoddart, *Chem. Soc. Rev.*, 2017, **46**, 2459–2478; (b) L. F. Lindoy, K.-M. Park and S. S. Lee, *Chem. Soc. Rev.*, 2013, **42**, 1713–1727; (c) X. X.

- Zhang, J. S. Bradshaw and R. M. Izatt, *Chem. Rev.*, 1997, **97**, 3313–3362; (d) M. M. Conn and J. Rebek, Jr., *Chem. Rev.*, 1997, **97**, 1647–1668; (e) Y. Inoue and G. W. Gokel, *Cation Binding by Macrocycles*, Marcel Dekker, New York, 1990.
4. (a) J. Vicens and J. Harrowfield, *Calixarenes in the Nanoworld*, Springer, Dordrecht, The Netherlands, 2007; (b) C. D. Gutsche, *Acc. Chem. Res.*, 1983, **16**, 161–170.
  5. (a) G. W. Gokel, W. M. Leevy and M. E. Weber, *Chem. Rev.*, 2004, **104**, 2723–2750; (b) G. W. Gokel, *Crown Ethers and Cryptands*, The Royal Society of Chemistry, London, England, 1991.
  6. (a) G. Crini, *Chem. Rev.*, 2014, **114**, 10940–10975; (b) J. Szejtli, *Chem. Rev.*, 1998, **98**, 1743–1754; (c) J. Szejtli, *Cyclodextrins and their Inclusion Complexes*, Akademiai Kiado, Budapest, 1982.
  7. (a) C. D. Gutsche and M. Iqbal, *Org. Synth.*, 1990, **68**, 234; (b) C. D. Gutsche, B. Dhawan, M. Leonis and D. Stewart, *Org. Synth.*, 1990, **68**, 238; (c) J. H. Munch and C. D. Gutsche, *Org. Synth.*, 1990, **68**, 243; (d) C. D. Gutsche, M. Iqbal and D. Stewart, *J. Org. Chem.*, 1986, **51**, 742–745; (e) C. D. Gutsche, B. Dhawan, K. H. No and R. Muthukrishnan, *J. Am. Chem. Soc.*, 1981, **103**, 3782–3792; (f) C. D. Gutsche, M. Iqbal and D. Stewart, *J. Org. Chem.*, 1986, **51**, 742–745.
  8. D. R. Stewart and C. D. Gutsche, *J. Am. Chem. Soc.*, 1999, **121**, 4136–4146.
  9. (a) Z. Asfari, V. Böhmer, J. Harrowfield and J. Vicens, *Calixarenes 2001*, Kluwer Academic Publishers, Dordrecht, 2001; (b) W. Sliwa and M. Deska, *ARKIVOC*, 2011, 496–551.
  10. C. D. Gutsche and R. Muthukrishnan, *J. Org. Chem.*, 1978, **43**, 4905–4906.
  11. L. Baldini, F. Sansone, A. Casnati and R. Ungaro, Calixarenes in molecular recognition, in *Supramolecular Chemistry: from Molecules to Nanomaterials*, ed. J. W. Steed and P. A. Gale, John Wiley & sons, Chichester, 2012, vol. 3, pp 863–894.
  12. (a) C. D. Gutsche and L. J. Bauer, *J. Am. Chem. Soc.*, 1985, **107**, 6052–6059; (b) S. Shinkai, *Tetrahedron*, 1993, **49**, 8933–8968; (c) C. D. Gutsche and P. A. Reddy, *J. Org. Chem.*, 1991, **56**, 4783–4791; (d) A. Ikeda and S. Shinkai, *Chem. Rev.*, 1997, **97**, 1713–1734; (e) C. D. Gutsche, *Calixarenes: An Introduction*, Royal Society of Chemistry, Cambridge, 2nd edn, 2008.

13. (a) T. Sone, Y. Ohba, K. Moriya, H. Kumada and K. Ito, *Tetrahedron*, 1997, **53**, 10689–10698; (b) H. Kumagai, M. Hasegawa, S. Miyanari, Y. Sugawa, Y. Sato, T. Hori, S. Ueda, H. Kamiyama and S. Miyano, *Tetrahedron Lett.*, 1997, **38**, 3971–3972; (c) N. Iki, C. Kabuto, T. Fukushima, H. Kumagai, H. Takeya, S. Miyanari, T. Miyashi and S. Miyano, *Tetrahedron*, 2000, **56**, 1437–1443; (d) N. Morohashi, F. Narumi, N. Iki, T. Hattori and S. Miyano, *Chem. Rev.*, 2006, **106**, 5291–5316.
14. (a) B. Dhawan and C. D. Gutsche, *J. Org. Chem.*, 1983, **48**, 1536–1539; (b) P. Zerr, M. Mussrabi and J. Vicens, *Tetrahedron Lett.*, 1991, **32**, 1879–1880; (c) S. Kohmoto, Y. Someya, H. Masu, K. Yamaguchi and K. Kishikawa, *J. Org. Chem.*, 2006, **71**, 4509–4515; (d) W. Maes and W. Dehaen, *Chem. Soc. Rev.*, 2008, **37**, 2393–2402; (e) W. V. Rossom, K. Robeyns, M. Ovaere, L. V. Meervelt, W. Dehaen and W. Maes, *Org. Lett.*, 2011, **13**, 126–129; (f) J. Wm. Wackerly, M. Zhang, S. T. Nodder, S. M. Carlin and J. L. Katz, *Org. Lett.*, 2014, **16**, 2920–2922.
15. (a) I. U. Khan, H. Takemura, M. Suenaga, T. Shinmyozu and T. Inazu, *J. Org. Chem.*, 1993, **58**, 3158–3161; (b) K. Niikura and E. V. Anslyn, *J. Chem. Soc., Perkin Trans. 2*, 1999, 2769–2775; (c) H. Tsue, K. Ishibashi and R. Tamura, *Top. Heterocycl. Chem.*, 2008, **17**, 73–96; (d) K. V. Lawson, A. C. Barton and J. D. Spence, *Org. Lett.*, 2009, **11**, 895–898.
16. (a) M. Vysotsky, M. Saadioui and V. Böhmer, in *Calixarenes 2001*; Z. Asfari, V. Böhmer, J. Harrowfield and J. Vicens, Ed.; Kluwer Academic Publishers, Dordrecht, 2001, Chapter 13, pp 250–465; (b) M. H. Patela and P. S. Shrivastav, *Chem. Commun.*, 2009, 586–588; (c) Y.-X. Ma, Y. Han and C.-F. Chen, *J. Incl. Phenom. Macrocycl. Chem.*, 2014, **79**, 261–281.
17. (a) S. Ibach, V. Prautzsch, F. Vögtle, C. Chartroux and K. Gloe, *Acc. Chem. Res.*, 1999, **32**, 729–740; (b) J. Thomas, L. Dobrzańska, K. V. Hecke, M. P. Sonawane, K. Robeyns, L. V. Meervelt, K. Woźniak, M. Smet, W. Maes and W. Dehaen, *Org. Biomol. Chem.*, 2012, **10**, 6526–6536; (c) J. Thomas, W. Maes, K. Robeyns, M. Ovaere, L. V. Meervelt, M. Smet and W. Dehaen, *Org. Lett.*, 2009, **11**, 3040–3043; (d) J. Thomas, A. S. Gusak and W. Dehaen, In *Calixarenes and Beyond*; P. Neri, J. L. Sessler, M.-X. Wang, Ed.; Springer International Publishing: Switzerland, 2016, Chapter 16, pp 421–444.

18. (a) H. Stephan, T. Krüger-Rambusch, K. Gloe, W. Hasse, B. Ahlers, K. Cammann, K. Rissanen, G. Brodesser and F. Vögtle, *Chem. Eur. J.*, 1998, **4**, 434–440; (b) P. A. Gale, J. L. Sessler and V. Král, *Chem. Commun.*, 1998, 1–8; (c) V. Král, P. A. Gale, P. Anzenbacher Jr., K. Jursíková, V. Lynch, J. L. Sessler, V. Král and P. Anzenbacher Jr., *Chem. Commun.*, 1998, 9–10; (d) C. Kaewtong, S. Fuangswasdi, N. Muangsin, N. Chaichit, J. Vicens and B. Pulpoka, *Org. Lett.*, 2006, **8**, 1561–1564.
19. (a) K. Araki, N. Hashimoto, H. Otsuka and S. Shinkai, *J. Org. Chem.*, 1993, **58**, 5958–5963; (b) K. Araki, K. Inada, H. Otsuka and S. Shinkai, *Tetrahedron*, 1993, **49**, 9465–9478; (c) H. Matsumoto, S. Nishio, M. Takeshita and S. Shinkai, *Tetrahedron*, 1995, **51**, 4647–4654; (d) K. Tsubaki, T. Otsubo, T. Morimoto, H. Maruoka, M. Furukawa, Y. Momose, M. Shang and K. Fuji, *J. Org. Chem.*, 2002, **67**, 8151–8156; (e) X.-K. Jiang, Y. Ikejiri, X.-L. Ni, X. Zeng, C. Redshaw and T. Yamato, *J. Mol. Struct.*, 2016, **1120**, 274–280.
20. (a) D. T. McQuade, A. E. Pullen and T. M. Swager, *Chem. Rev.*, 2000, **100**, 2537–2574; (b) C. McDonagh, C. S. Burke and B. D. MacCraith, *Chem. Rev.*, 2008, **108**, 400–422; (c) S. Joo and R. B. Brown, *Chem. Rev.*, 2008, **108**, 638–651; (d) T.-H. Tran-Thi, R. Dagnelie, S. Crunaire and L. Nicole, *Chem. Soc. Rev.*, 2011, **40**, 621–639; (e) L. E. Kreno, K. Leong, O. K. Farha, M. Allendorf, R. P. V. Duyne and J. T. Hupp, *Chem. Rev.*, 2012, **112**, 1105–1125; (f) O. S. Wenger, *Chem. Rev.*, 2013, **113**, 3686–3733.
21. (a) G. H. Jeffery, J. Bassett, J. Mendham, R. C. Denny, *Vogel's Textbook of Quantitative Chemical Analysis*, 5th edn, Longman: Edinburgh Gate, England, 1996; (b) D. A. Skoog, F. J. Holler, and T. A. Nieman, *Principles of Instrumental Analysis*, 5th edn, Saunders College Publishing, New York, 1997; (c) B. K. Sharma, *Instrumental Methods of Chemical Analysis*, 23th edn, Goel Publishing House, Meerut, 2000.
22. (a) M. Vendrell, D. Zhai, J. C. Er and Y.-T. Chang, *Chem. Rev.*, 2012, **112**, 4391–4420; (b) S. K. Sahoo, D. Sharma, R. K. Bera, G. Crisponi and J. F. Callan, *Chem. Soc. Rev.*, 2012, **41**, 7195–7227; (c) K. P. Carter, A. M. Young and A. E. Palmer, *Chem. Rev.*, 2014, **114**, 4564–4601; (d) J. A. Cotruvo Jr., A. T. Aron, K. M. Ramos-Torres and C. J. Chang, *Chem. Soc. Rev.*, 2015, **44**, 4400–4414; (e) J. Yin, Y. Hu and J. Yoon, *Chem. Soc. Rev.*, 2015, **44**, 4619–4644; (f) X. Sun, Y. Wang and Y. Lei, *Chem. Soc. Rev.*, 2015, **44**, 8019–8061.

23. (a) A. P. de Silva, H. Q. N. Gunaratne, T. Gunnlaugsson, A. J. M. Huxley, C. P. McCoy, J. T. Rademacher and T. E. Rice, *Chem. Rev.*, 1997, **97**, 1515–1566; (b) B. Valeur and I. Leray, *Coord. Chem. Rev.*, 2000, **205**, 3–40; (c) B. Valeur, *Molecular Fluorescence: Principles and Applications*, Wiley-VCH Verlag GmbH: New York, 2001; (d) J. Wu, W. Liu, J. Ge, H. Zhang and P. Wang, *Chem. Soc. Rev.*, 2011, **40**, 3483–3495.
24. (a) R. A. Bissell, A. P. de Silva, H. Q. N. Gunaratne, P. L. M. Lynch, G. E. M. Maguire, C. P. McCoy and K. R. A. S. Sandanayake, *Top. Curr. Chem.*, 1993, **168**, 223–264; (b) A. P. de Silva, H. Q. N. Gunaratne, T. Gunnlaugsson, A. J. M. Huxley, C. P. McCoy, J. T. Rademacher and T. E. Rice, *Adv. Supramol. Chem.*, 1997, **4**, 1–53.
25. (a) B. Valeur, J. Bourson and J. Pouget, in *Fluorescent Chemosensors for Ion and Molecule Recognition*; A. W. Czarnik, Ed.; ACS Symposium Series 538, American Chemical Society, Washington, DC, 1993, Chapter 3, pp 25–44; (b) W. Rettig and R. Lapouyade, in *Topics in Fluorescence Spectroscopy: Volume 4: Probe Design and Chemical Sensing*, J. R. Lakowicz, Ed., Plenum, New York, 1994, pp 109–150.
26. H.-G. Löhr and F. Vögtle, *Acc. Chem. Res.*, 1985, **18**, 65–72.
27. E. U. Akkaya, M. E. Huston, A. W. Czarnik, *J. Am. Chem. Soc.*, 1990, **112**, 3590–3593.
28. (a) J. B. Birks, *Photophysics of Aromatic Molecules*, Wiley-Interscience, New York, 1970; (b) W. Klöpffer, In *Organic Molecular Photophysics*; J. B. Birks, Ed.; Wiley, New York, 1973, Chapter 7, pp 357–402.
29. J. B. Birks, M. D. Lumb and I. H. Munro, *Proc. R. Soc. London Series A*, 1964, **280**, 289–297.
30. (a) F. M. Winnik, *Chem. Rev.*, 1993, **93**, 587–614; (b) S. K. Kim, S. H. Lee, J. Y. Lee, J. Y. Lee, R. A. Bartsch and J. S. Kim, *J. Am. Chem. Soc.*, 2004, **126**, 16499–16506; (c) J. Y. Lee, S. K. Kim, J. H. Jung and J. S. Kim, *J. Org. Chem.*, 2005, **70**, 1463–1466; (d) S. H. Lee, S. H. Kim, S. K. Kim, J. H. Jung and J. S. Kim, *J. Org. Chem.*, 2005, **70**, 9288–9295.
31. (a) Y.-C. Wang and H. Morawetz, *J. Am. Chem. Soc.*, 1976, **98**, 3611–3615; (b) M. Goldenberg, J. Emert and H. Morawetz, *J. Am. Chem. Soc.*, 1978, **100**, 7171–7177; (c) M. A. Winnik, *Chem. Rev.*, 1981, **81**, 491–524.

32. (a) H. Nohta, H. Satozono, K. Koiso, H. Yoshida, J. Ishida and M. Yamaguchi, *Anal. Chem.*, 2000, **72**, 4199–4204; (b) A. Okamoto, T. Ichiba and I. Saito, *J. Am. Chem. Soc.*, 2004, **126**, 8364–8365.
33. (a) L. Stryer, *Ann. Rev. Biochem.*, 1978, **47**, 819–846; (b) B. W. Van Der Meer, G. Coker and S. Y. S Chen, *Resonance Energy Transfer: Theory and Data*, VCH, New York, 1994.
34. (a) J. R. Lakowicz, *Principles of Fluorescence Spectroscopy*, 3rd edn, Springer, New York, 2006; (b) M. Umadevi, S.R. Kavitha, P. Vanelle, T. Terme and O. Khoumeri, *J. Lumin.*, 2013, **142**, 1–7; (c) S.R. Kavitha, M. Umadevi, S.R. Janani, T. Balakrishnan and R. Ramanibai, *Spectrochim. Acta. Part A.*, 2014, **127**, 115–121.
35. (a) S. H. Kim, H. J. Kim, J. Yoon and J. S. Kim, in *Calixarenes in the Nanoworld*; J. Vicens and J. Harrowfield, Ed.; Springer, Dordrecht, The Netherlands, 2007, Chapter 15, pp 311–333; (b) J. S. Kim and D. T. Quang, *Chem. Rev.*, 2007, **107**, 3780–3799; (c) I. Leray and B. Valeur, *Eur. J. Inorg. Chem.*, 2009, 3525–3535; (d) R. Joseph and C. P. Rao, *Chem. Rev.*, 2011, **111**, 4658–4702; (e) Ü. Ocak, M. Ocak and R. A. Bartsch, *Inorg. Chim. Acta.*, 2012, **381**, 44–57; (f) M. Song, Z. Sun, C. Han, D. Tian, H. Li and J. S. Kim, *Chem. Asian J.*, 2014, **9**, 2344–2357.
36. I. Aoki, T. Sakaki and S. Shinkai, *J. Chem. Soc., Chem. Commun.*, 1992, 730–732.
37. H. F. Ji, R. Dabestani, G. M. Brown and R. A. Sachleben, *Chem. Commun.*, 2000, 833–834.
38. M. Kumar, R. Kumar, V. Bhalla, P. R. Sharma, T. Kaur and Y. Qurishi, *Dalton Trans.*, 2012, **41**, 408–412.
39. C. N. Baki and E. U. Akkaya, *J. Org. Chem.*, 2001, **66**, 1512–1513.
40. R. Miao, Q.-Y. Zheng, C.-F. Chen and Z.-T. Huang, *Tetrahedron Lett.*, 2005, **46**, 2155–2158.
41. I. Leray, J.-P. Lefevre, J.-F. Delouis, J. Delaire and B. Valeur, *Chem. Eur. J.*, 2001, **7**, 4590–4598.
42. S. H. Lee, H. J. Kim, Y. O. Lee, J. Vicens and J. S. Kim, *Tetrahedron Lett.*, 2006, **47**, 4373–4376.
43. S. M. Darjee, D. R. Mishra, K. D. Bhatt, D. J. Vyas, K. M. Modi and V. K. Jain, *Tetrahedron Lett.*, 2014, **55**, 7094–7098.



44. (a) B. Schazmann, N. Alhashimy and D. Diamond, *J. Am. Chem. Soc.*, 2006, **128**, 8607–8614; (b) Z. Xu, N. J. Singh, J. Lim, J. Pan, H. N. Kim, S. Park, K. S. Kim and J. Yoon, *J. Am. Chem. Soc.*, 2009, **131**, 15528–15533; (c) Y. Zhou, C.-Y. Zhu, X.-S. Gao, X.-Y. You and C. Yao, *Org. Lett.*, 2010, **12**, 2566–2569; (d) Y. Zhou, J. Y. Jung, H. R. Jeon, Y. Kim, S.-J. Kim and J. Yoon, *Org. Lett.*, 2011, **13**, 2742–2745; (e) E. Manandhar, J. H. Broome, J. Myrick, W. Lagrone, P. J. Cragg and K. J. Wallace, *Chem. Commun.*, 2011, **47**, 8796–8798; (f) S. A. Ingale and F. Seela, *J. Org. Chem.*, 2012, **77**, 9352–9356; (g) E. Manandhar and K. J. Wallace, *Inorg. Chim. Acta.*, 2012, **381**, 15–43.
45. S. Y. Park, J. H. Yoon, C. S. Hong, R. Souane, J. S. Kim, S. E. Matthews and J. Vicens, *J. Org. Chem.*, 2008, **73**, 8212–8218.
46. X. L. Ni, X. Zeng, C. Redshaw and T. Yamato, *J. Org. Chem.*, 2011, **76**, 5696–5702.
47. X. L. Ni, X. Zeng, C. Redshaw and T. Yamato, *Tetrahedron*, 2011, **67**, 3248–3253.
48. M. Kumar, R. Kumar and V. Bhalla, *Tetrahedron*, 2009, **65**, 4340–4344.
49. M. Yuan, W. Zhou, X. Liu, M. Zhu, J. Li, X. Yin, H. Zheng, Z. Zuo, C. Ouyang, H. Liu, Y. Li and D. Zhu, *J. Org. Chem.*, 2008, **73**, 5008–5014.
50. A. B. Othman, J. W. Lee, J.-S. Wu, J. S. Kim, R. Abidi, P. Thuéry, J.-M. Strub, A. Van Dorsselaer and J. Vicens, *J. Org. Chem.*, 2007, **72**, 7634–7640.
51. Y. H. Lee, M. H. Lee, J. F. Zhang and J. S. Kim, *J. Org. Chem.*, 2010, **75**, 7159–7165.
52. (a) Y. Yang, C.-Y. Gao, J. Liu and D. Dong, *Anal. Methods*, 2016, **8**, 2863–2871; (b) H. N. Kim, M. H. Lee, H. J. Kim, J. S. Kim and J. Yoon, *Chem. Soc. Rev.*, 2008, **37**, 1465–1472; (c) M. Beija, C. A. M. Afonso and J. M. G. Martinho, *Chem. Soc. Rev.*, 2009, **38**, 2410–2433; (d) X. Chen, T. Pradhan, F. Wang, J. S. Kim and J. Yoon, *Chem. Rev.*, 2012, **112**, 1910–1956.
53. X. Y. Zheng, W. J. Zhang, L. Mu, X. Zeng, S. F. Xue, Z. Tao and T. Yamato, *J. Inclusion Phenom. Macrocyclic Chem.*, 2010, **68**, 139–146.
54. N. Sharma, S. I. Reja, V. Bhalla and M. Kumar, *Dalton Trans.*, 2014, **43**, 15929–15936.
55. H. S. Jung, H. J. Kim, J. Vicens and J. S. Kim, *Tetrahedron Lett.*, 2009, **50**, 983–987.
56. M. Kumar, N. Kumar and V. Bhalla, *Dalton Trans.*, 2013, **42**, 981–986.
57. Q. Sun, L. Mu, X. Zeng, J. Zhao, T. Yamato and J. Zhang, *Sci. China Chem.*, 2015, **58**, 539–544.
58. R. K. Pathak, S. M. Ibrahim and C. P. Rao, *Tetrahedron Lett.*, 2009, **50**, 2730–2734.

59. (a) R. K. Pathak, V. K. Hinge, K. Mahesh, A. Rai, D. Panda and C. P. Rao, *Anal. Chem.*, 2012, **84**, 6907–6913; (b) R. K. Pathak, A. G. Dikundwar, T. N. G. Row, C. P. Rao, *Chem. Commun.*, 2010, **46**, 4345–4347; (c) R. K. Pathak, V. K. Hinge, M. Mondal and C. P. Rao, *J. Org. Chem.*, 2011, **76**, 10039–10049; (d) R. K. Pathak, K. Tabbasum, A. Rai, D. Panda and C. P. Rao, *Anal. Chem.*, 2012, **84**, 5117–5123; (e) R. K. Pathak, K. Tabbasum, V. K. Hinge and C. P. Rao, *Chem. Eur. J.*, 2011, **17**, 13999–14003; (f) R. K. Pathak, V. K. Hinge, A. Rai, D. Panda and C. P. Rao, *Inorg. Chem.*, 2012, **51**, 4994–5005.

## **Chapter 2**

# **Click Synthesis of Quinoline-functionalized Homooxacalix[3]arene as Turn-on Fluorescence Chemosensor for Fe<sup>3+</sup>**

*This chapter described a novel quinoline-functionalized homooxacalix[3]arene L was synthesized via Click chemistry and its chemosensing properties with various metal ions were investigated. The designed chemosensor L exhibited a high selectivity and antidisturbance for Fe<sup>3+</sup> among environmentally and biologically relevant metal ions, leading to a prominent off-on-type fluorescent signaling behavior. Further study demonstrates the detection limit on fluorescence response of the sensor to Fe<sup>3+</sup> is down to 10<sup>-7</sup> M range.*

## 2.1 Introduction

The development of chemosensors capable of recognizing and sensing metal ions have attracted considerable attention because of their fundamental role in biological, environmental, and chemical processes.<sup>1</sup> As one of the most essential trace elements in life system, ferric ion ( $\text{Fe}^{3+}$ ) plays important roles in oxygen metabolism, enzyme catalysis, and DNA synthesis.<sup>2</sup> Deficiency or overloading of iron result in various pathological disorders, such as anemia, liver and kidney damages, diabetes, and heart diseases.<sup>3</sup> Therefore, development of simple and sensitive chemosensors for detection of  $\text{Fe}^{3+}$  is of great importance in environmental and life science.

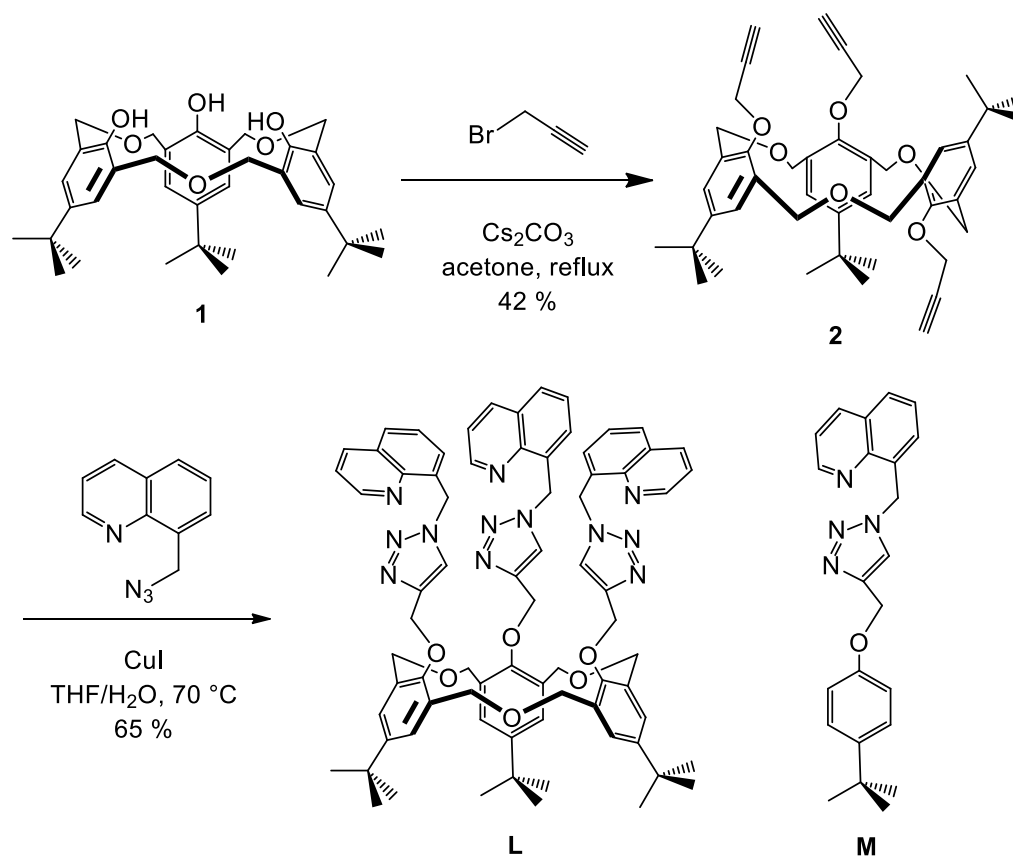
Fluorescent chemosensor strategy has proven to be a convenient and efficient approach for metal ions detection due to its superiority over other methods, which characterized high sensitivity and selectivity, easiness of manipulating, non-destructive analysis, and rapid response.<sup>4</sup> Because of the paramagnetic nature of  $\text{Fe}^{3+}$ , most reported  $\text{Fe}^{3+}$  fluorescent chemosensors are based on a fluorescence quenching mechanism.<sup>5</sup> However, fluorescence quenching is not only a disadvantage for high signal output upon recognition but also hampers temporal separation of spectrally similar complexes with time-resolved fluorometry.<sup>6</sup> Thus, the development of chemosensors that exhibit fluorescence enhancement upon binding with  $\text{Fe}^{3+}$  would be more attractive.

Homooxacalix[3]arenes including three ethereal linkages are relatively flexible and thus can provide a suitable binding environment for species that require trigonal-planar, tetrahedral, or octahedral coordination.<sup>7</sup> Based on this excellent structure characteristic, homooxacalix[3]arenes have been used as ideal molecular platforms for the development of chemosensors in the molecular recognition of chemical and biological targets.<sup>8</sup> On the other hand, we noted that quinoline derivatives possess desirable photo-physical properties, they usually used as fluorophore to construct fluorescence chemosensors for heavy and transition metal ions. In particular, the nitrogen atom in heterocyclic quinoline can act as a chelating site towards metal ions.<sup>9</sup> Taking advantage of the easily-synthesized triazole binding site, it prompted us to synthesize the quinoline-functionalized homooxacalix[3]arene by Click chemistry. In the present manuscript, we

reported a quinoline-functionalized triazole linked homooxacalix[3]arene **L** as a fluorescence turn on chemosensor for  $\text{Fe}^{3+}$  among the different metal ions studied. The role of the calixarene platform has been addressed by making a noncalixarene-based analogue of this. Furthermore, the binding mechanism was confirmed by  $^1\text{H}$  NMR titration analysis.

## 2.2 Results and Discussion

### 2.2.1 Synthesis and Characterization of Chemosensor **L**



**Scheme 1.** The synthetic route of chemosensor **L**.

The synthetic route for the current sensor is depicted in Scheme 1. The  $\text{Cu}^{\text{I}}$ -catalyzed 1,3-dipolar cycloaddition reaction of compound **2** with 8-azidomethyl quinoline under Click conditions afforded the chemosensor **L** in 65% yield. All compounds synthesized in this work were fully characterized by spectroscopic data including  $^1\text{H}$ ,  $^{13}\text{C}$  NMR spectroscopy and HRMS.  $^1\text{H}$  NMR spectra (Figure 1) of **L** revealed the disappearance of the three

terminal alkyne protons, whereas the new singlet appearing around  $\delta = 7.84$  ppm was attributed to the protons of the newly formed H<sub>d</sub> on the triazole groups. Furthermore, the other peaks were observed as three singlets assignable to the protons H<sub>a</sub>, H<sub>c</sub> and H<sub>e</sub>, and an AB quartet for the H<sub>b</sub> protons. These findings supported the conclusion that the homooxacalix[3]arene skeleton was immobilized in the *cone* conformation and possesses a C<sub>3</sub> symmetry. Furthermore, in order to demonstrate the role of calixarene platform clearly, compound **M** was synthesized as a reference.

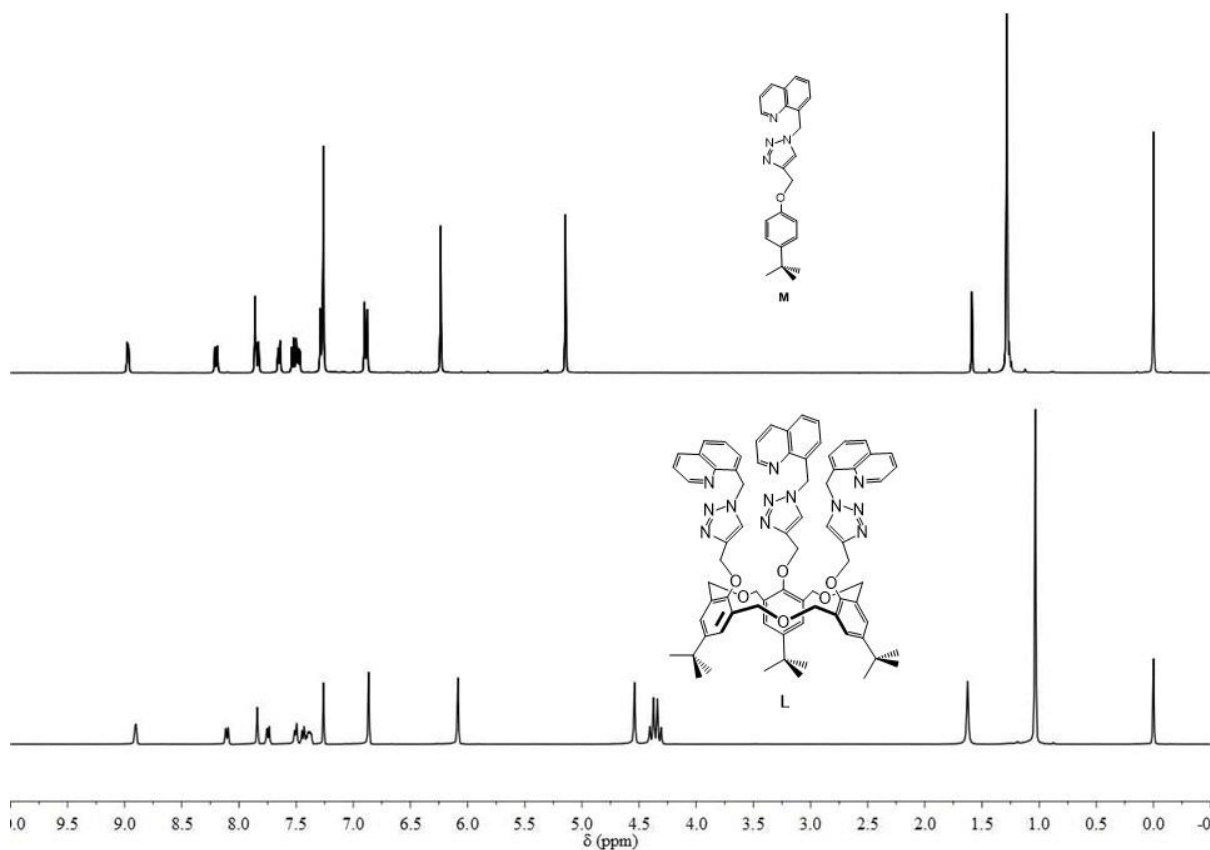


**Figure 1.** The <sup>1</sup>H NMR spectra of compounds **L** and **M**.

### 2.2.2 Chemosensing Properties of **L** for Fe<sup>3+</sup>

The recognition behavior of chemosensor **L** toward various metal cations was investigated by fluorescence measurement. The fluorescence spectrum of **L** exhibited weak fluorescence emission when excited at 314 nm in CH<sub>3</sub>CN solution (Figure 2). Upon addition of Fe<sup>3+</sup> ions to the solution of **L**, remarkable enhancement of emission intensity was observed

at 414 nm. Under the same conditions as used for  $\text{Fe}^{3+}$ , no significant change of the fluorescence spectrum was observed in the presence of other metal cations, indicating a  $\text{Fe}^{3+}$ -selective off-on fluorescent signaling behavior. The possible mechanism for the observed fluorescence enhancement may be explained as follows. Before coordinated with  $\text{Fe}^{3+}$ , free **L** showed the weak fluorescence because of the lone electron pairs of the nitrogen atom in the triazole moieties being located adjacent to the quinoline fluorophores, which resulted in an intramolecular photo-induced electron transfer (PET). The deexcitation of the tautomer occurred mainly via a nonradiative pathway. When **L** was coordinated with  $\text{Fe}^{3+}$ , the nonradiative channel was inhibited simultaneously, and thus the **L**- $\text{Fe}^{3+}$  system exhibited the enhanced fluorescence.<sup>10</sup>

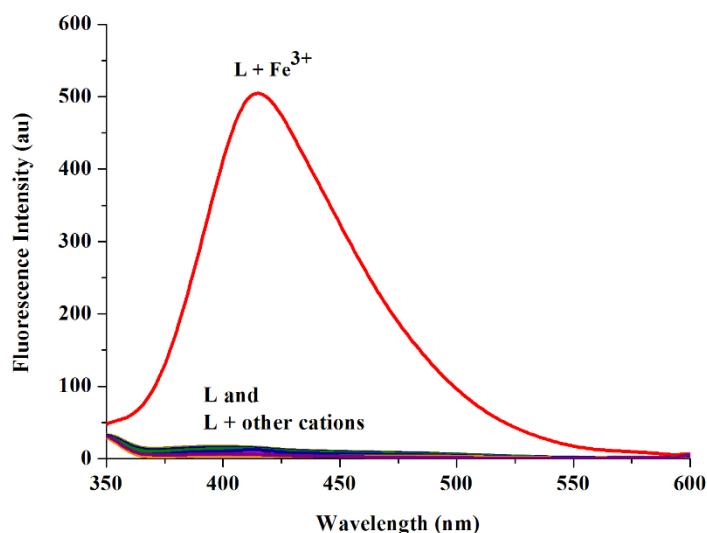


**Figure 2.** Fluorescence emission spectra of **L** (1.0  $\mu\text{M}$ ) in the presence of various metal ions ( $\text{Li}^+$ ,  $\text{Na}^+$ ,  $\text{K}^+$ ,  $\text{Cs}^+$ ,  $\text{Ag}^+$ ,  $\text{Cu}^{2+}$ ,  $\text{Pb}^{2+}$ ,  $\text{Zn}^{2+}$ ,  $\text{Co}^{2+}$ ,  $\text{Ni}^{2+}$ ,  $\text{Cr}^{3+}$ ,  $\text{Fe}^{3+}$ ,  $\text{Al}^{3+}$ ,  $\text{Cd}^{2+}$ ,  $\text{Hg}^{2+}$  and  $\text{Fe}^{2+}$ , 20.0  $\mu\text{M}$ ) in  $\text{CH}_3\text{CN}$ .

To further investigate the chemosensing properties of **L** for  $\text{Fe}^{3+}$ , UV-vis and fluorescence titration experiments were performed on 5.0  $\mu\text{M}$  and 1.0  $\mu\text{M}$  solutions of **L** in  $\text{CH}_3\text{CN}$  respectively. The UV-vis spectrum of compound **L** exhibits absorption bands at 255, 261, 280 and 314 nm. Upon the addition of  $\text{Fe}^{3+}$ , the absorption bands at 255, 261 and 280 nm gradually decreased, while the absorption intensity at 314 nm increased (Figure 3). The isosbestic point observed at 293 nm indicates a transition between the unbound and the

complexed species. The stoichiometry of the complex formed between **L** and  $\text{Fe}^{3+}$  has been derived to be 1:1 based on Job's plot (Figure 4).

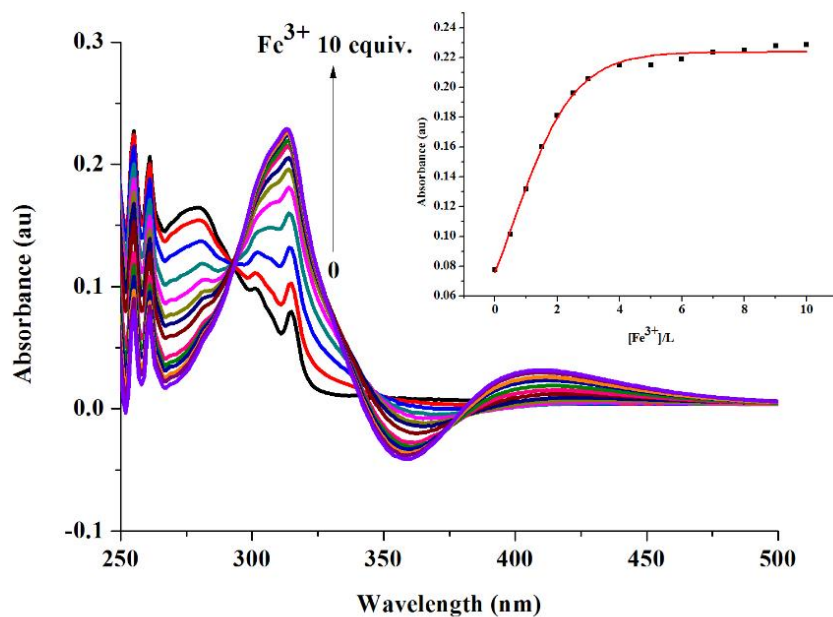


**Figure 3.** Absorption spectra obtained during the titration of **L** (5.0  $\mu\text{M}$ ) with  $\text{Fe}^{3+}$  in  $\text{CH}_3\text{CN}$ . The inset shows the plot of absorbance at 314 nm vs  $[\text{Fe}^{3+}]/[\text{L}]$  mole ratio.

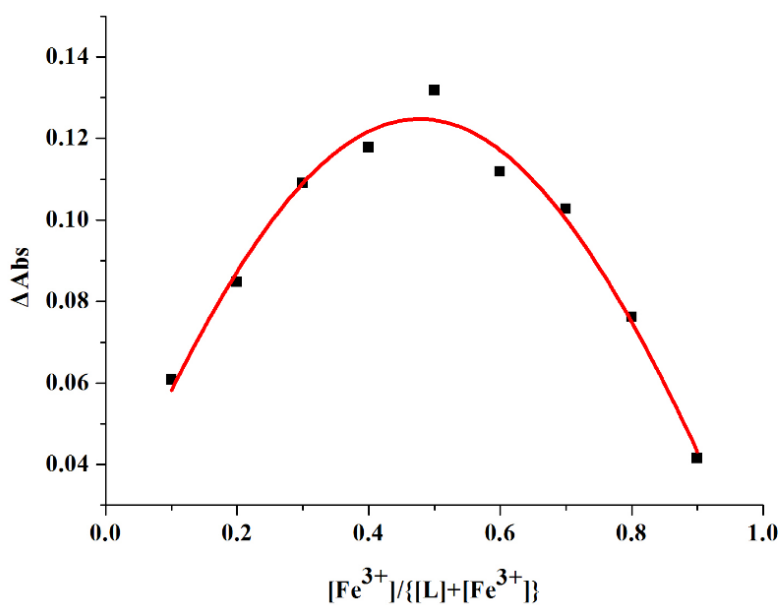


**Figure 4.** Job's plot obtained from the absorption titration of **L** with  $\text{Fe}^{3+}$  at 314 nm, indicating a 1:1 binding stoichiometry.



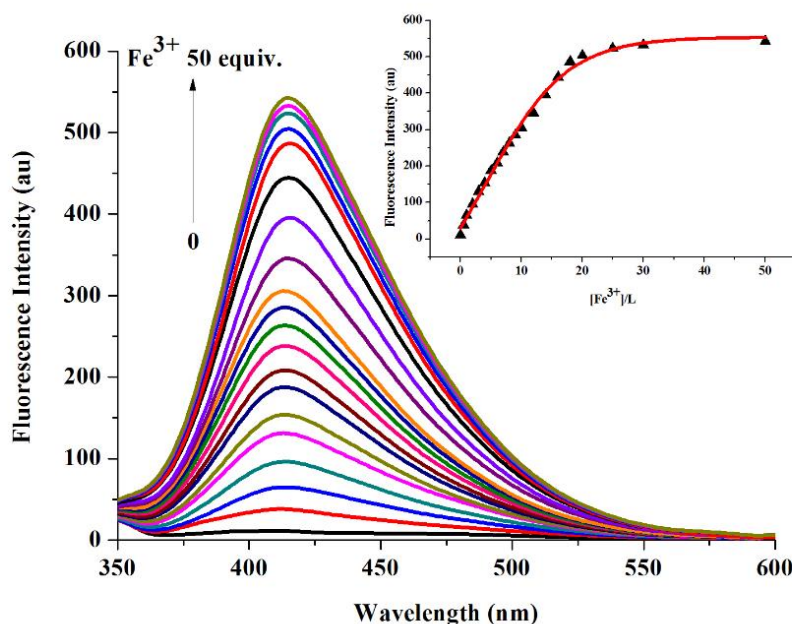


**Figure 5.** Fluorescence spectra obtained during the titration of **L** (1.0 μM) with Fe<sup>3+</sup> in CH<sub>3</sub>CN. The inset shows the relative fluorescence intensity as a function of the [Fe<sup>3+</sup>]/[**L**] mole ratio.

As seen in Figure 5, with the stepwise addition of Fe<sup>3+</sup> to a solution of **L**, the fluorescence emission intensity of **L** at 414 nm was gradually increased. When the concentration of Fe<sup>3+</sup> ran up to about 20.0 equiv, the fluorescence intensity of **L** reached a plateau and almost contained a constant. From the fluorescence titration profiles, the association constant between **L** and Fe<sup>3+</sup> was calculated to be  $1.18 \times 10^5 \text{ M}^{-1}$  according to the Benesi–Hildebrand method by plotting  $1/(I-I_0)$  against  $1/[M]$  (Figure 6).<sup>11</sup> Moreover, the corresponding detection limit for Fe<sup>3+</sup> was estimated to be  $2.25 \times 10^{-7} \text{ M}$  on the basis of reported methods (Figure 7),<sup>12</sup> which is much lower than the maximum level ( $0.3 \text{ mg L}^{-1}$ , equivalent to  $5.4 \text{ μM}$ ) of Fe<sup>3+</sup> permitted in drinking water by the U.S. Environmental Protection Agency.<sup>13</sup>

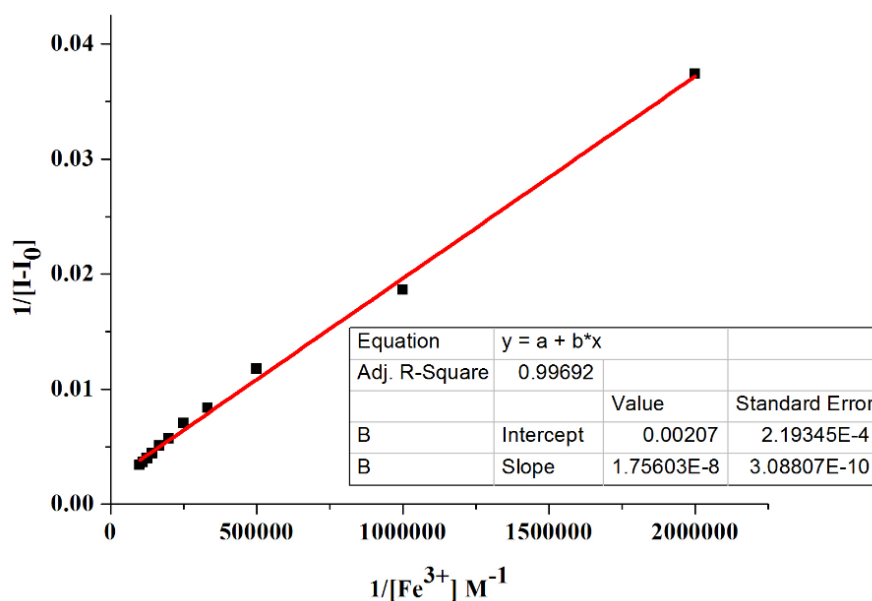


**Figure 6.** Association constant ( $K_a$ ) determined with fluorescence data using Benesi-Hildebrand equation.

Association constant  $K_a = 0.00207/(1.756E-8) = 1.18 \times 10^5 \text{ M}^{-1}$ .

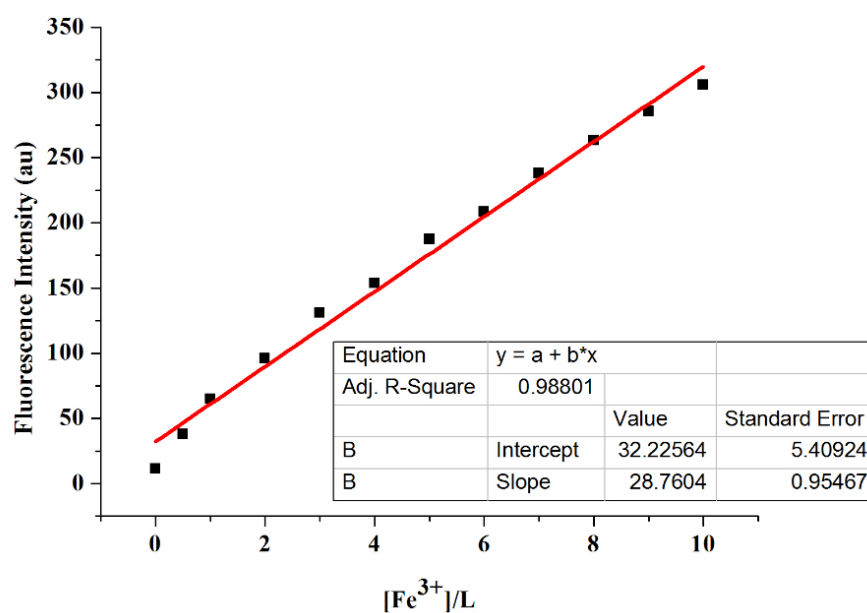


**Figure 7.** The linear dynamic fluorescence response for the titration of **L** with  $\text{Fe}^{3+}$  to determine the detection limit (LOD). The calculation method for LOD is based on the standard deviation of the response ( $\sigma$ ) and the slope of the calibration curve ( $K$ ) according to the formula:  $\text{LOD} = 3\sigma/K = 2.25 \times 10^{-7} \text{ M}$ .

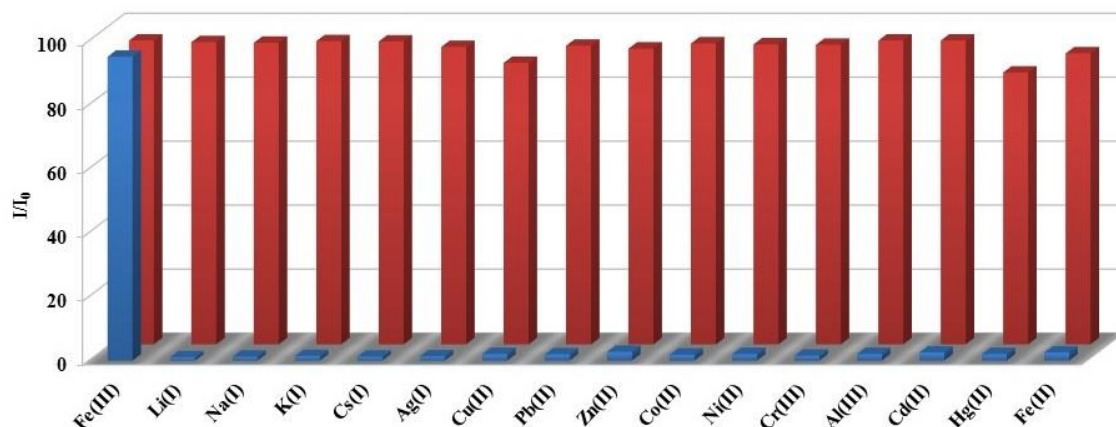


**Figure 8.** Fluorescence response of **L** (1.0  $\mu$ M) to 20 equiv. of metal cations (the blue bar) and to the mixture of 20 equiv. of other metal ions with  $\text{Fe}^{3+}$  (the red bar).  $I_0$  is fluorescent emission intensity at 414 nm of free **L**, and  $I$  is the fluorescent intensity after adding metal cations.

In order to explore the practical utility of **L** to detect  $\text{Fe}^{3+}$  selectively even in the presence of other metal ions, competition experiments were carried out (Figure 8). No significant variation was observed in the presence of other competitive metal ions in comparison to the solution containing only  $\text{Fe}^{3+}$ . Thus it may be concluded that **L** could be used as a potential  $\text{Fe}^{3+}$ -selective fluorescent chemosensor. The potency of the synthesized chemosensor **L** for the detection of  $\text{Fe}^{3+}$  was evaluated and compared with that of already described sensors in the literatures.

### 2.2.3 Sensing Mechanism of **L** for $\text{Fe}^{3+}$

In order to get insight into the sensing mechanism of sensor **L** for  $\text{Fe}^{3+}$ , the interaction of sensor **L** with  $\text{Fe}^{3+}$  was further investigated by  $^1\text{H}$  NMR titration experiments. As shown in Figure 9, the  $^1\text{H}$  NMR signals for the protons of both quinoline and triazole moieties of **L** showed the downfield shifts in the presence of  $\text{Fe}^{3+}$ , the detail chemical shifts were summarized in Table 1. This phenomenon may be attributed to the electron shielding effect of  $\text{Fe}^{3+}$  on protons in its proximity. Furthermore, the AB quartet of the methylene bridge protons  $\text{H}_b$  was split as a pair of doublet, which indicated that there must be a conformational change of sensor **L** for the binding with

$\text{Fe}^{3+}$  ions. As a matter of fact, it is believed that the conformation of homooxacalix[3]arene can be pre-organized for the binding of metal cations in solution in a manner that is similar to the examples described by previous reports.<sup>14</sup>

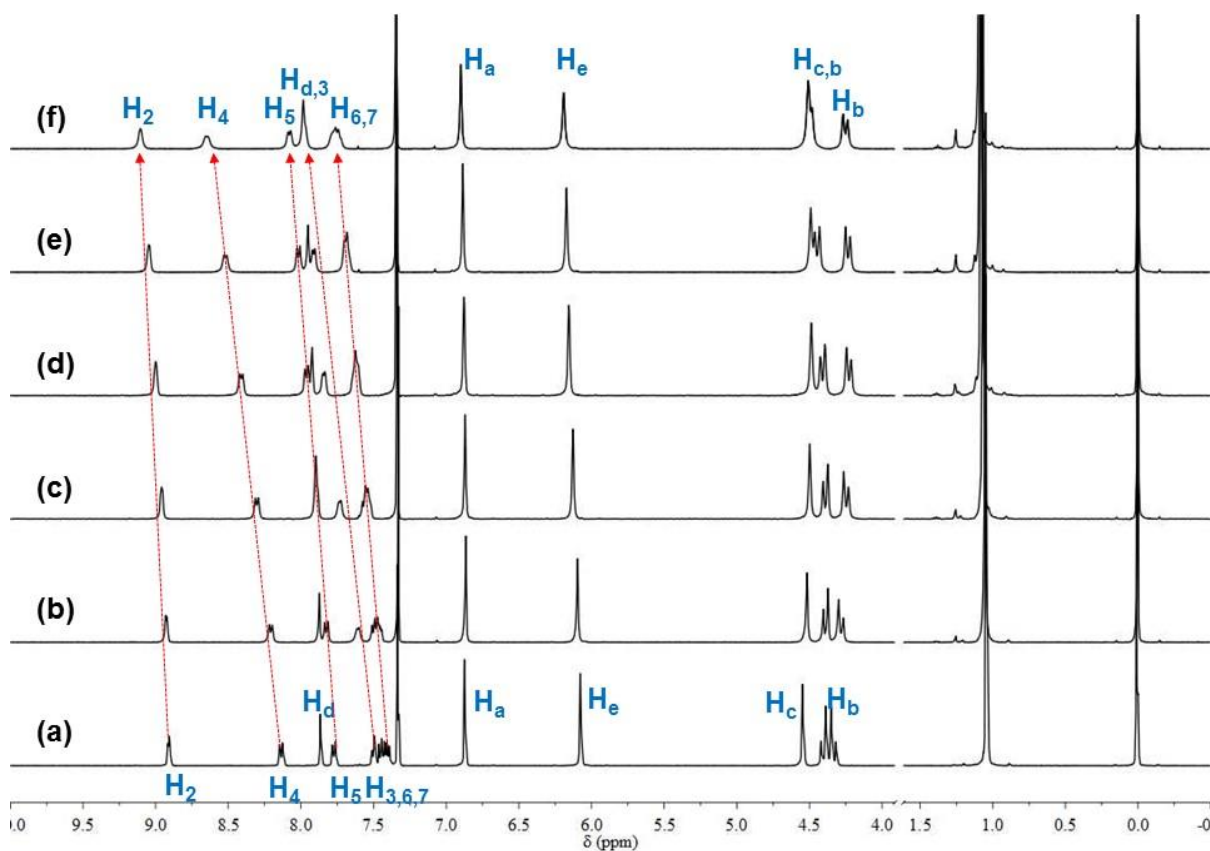


**Figure 9.**  $^1\text{H}$  NMR titration spectra of **L** (5.0 mM) in the presence of increasing amounts of  $\text{Fe}^{3+}$  in  $\text{CDCl}_3/\text{CD}_3\text{CN}$  (10:1, v/v). (a) **L** only, (b c d e and f) in the presence of 0.2, 0.4, 0.6, 0.8 and 1.0 equiv. of  $\text{Fe}^{3+}$ , respectively.

**Table 1** Selected proton chemical shifts ( $\delta$ , ppm) of **L** and **L-Fe<sup>3+</sup>** complex.<sup>a</sup>

Compound	$\text{H}_2$	$\text{H}_3$	$\text{H}_4$	$\text{H}_5$	$\text{H}_6$	$\text{H}_7$	$\text{H}_d$
<b>L</b>	8.90	7.43	8.10	7.74	7.43	7.50	7.84
<b>L-Fe<sup>3+</sup></b>	9.10	7.98	8.64	8.07	7.76	7.76	7.98
$\Delta\delta^{\text{b,c}}$	+0.20	+0.55	+0.54	+0.33	+0.33	+0.26	+0.14

<sup>a</sup> The midpoint values of multiplet are indicated.

<sup>b</sup>  $\Delta\delta$  value is the difference of the chemical shift between **L** and **L-Fe<sup>3+</sup>** complex.

<sup>c</sup> A plus sign (+) denotes a shift to lower magnetic field.

Lacking the calixarene platform, the reference compound **M** showed no appreciable fluorescence changes to  $\text{Fe}^{3+}$ . This phenomenon suggested that the three triazole ligands and three quinoline moieties exhibited a synergistic action to bind  $\text{Fe}^{3+}$ , and hence supports the necessity of calixarene platform for selective recognition of  $\text{Fe}^{3+}$ . Based on the above results, we deduced that the triazole and quinoline moieties of **L** jointly coordinated with  $\text{Fe}^{3+}$  to form the **L**- $\text{Fe}^{3+}$  complex as illustrated in Figure 10, which inhibited the intramolecular photoinduced electron transfer (PET) from electron-donating group triazole to electron-receptor quinoline group and thus led to the enhanced fluorescence of **L**- $\text{Fe}^{3+}$  system.

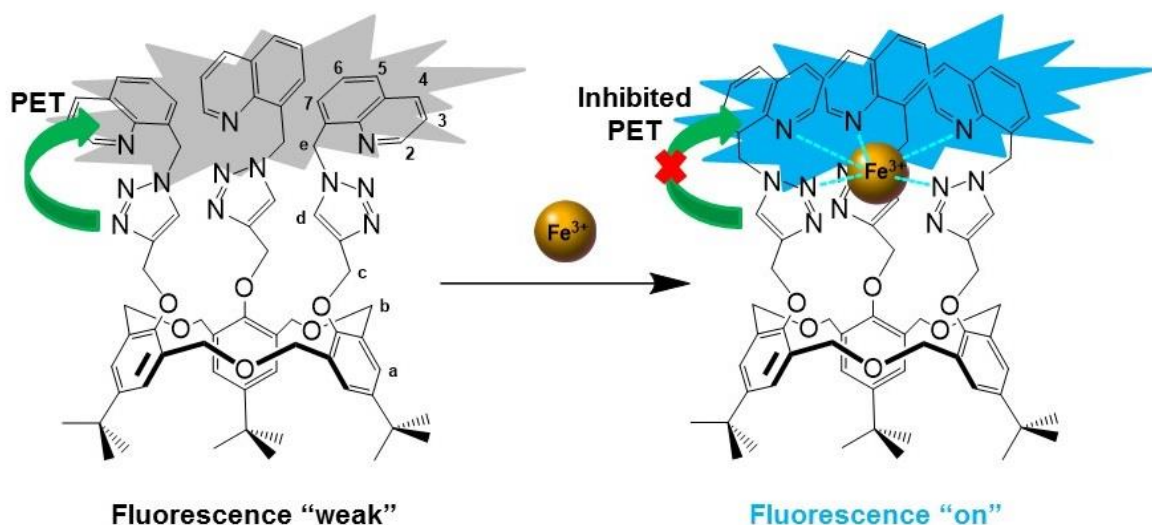


**Figure 10.** Proposed sensing mechanism of **L** for  $\text{Fe}^{3+}$ .

## 2.3 Conclusions

In summary, we have successfully developed a quinoline-functionalized homooxacalix[3]arene **L** as fluorescence chemosensor for highly sensitive and specific detection of  $\text{Fe}^{3+}$ . This non-fluorescent chemosensor **L** exhibited a dramatic fluorescence turn-on response for  $\text{Fe}^{3+}$ , among the sixteen different metal ions studied. Chemosensor **L** formed a 1:1 complex with  $\text{Fe}^{3+}$ , and the  $\text{Fe}^{3+}$  binding behavior has been confirmed by  $^1\text{H}$  NMR titration analysis. Comparison with a noncalixarene analogue **M**, indicating the

necessity of the homooxacalix[3]arene platform in sensing. The sensing mechanism may be ascribed to the inhibited PET process from the coordination of  $\text{Fe}^{3+}$  and **L**.

## 2.4 Experimental Section

### 2.4.1 General

Unless otherwise stated, all reagents were purchased from commercial sources and used without further purification. All solvents were dried and distilled by the usual procedures before use. Melting points were determined using a Yanagimoto MP-S1.  $^1\text{H}$  NMR and  $^{13}\text{C}$  NMR spectra were recorded on a Nippon Denshi JEOL FT-300 NMR spectrometer and a Varian-400MRvnmrs400 with  $\text{SiMe}_4$  as an internal reference: *J*-values are given in Hz. UV spectra were measured by a Shimadzu UV-3150UV-vis-NIR spectrophotometer. Fluorescence spectroscopic studies of compounds in solution were performed in a semi-micro fluorescence cell (Hellma®, 104F-QS,  $10 \times 4$  mm, 1400  $\mu\text{L}$ ) with a Varian Cary Eclipse spectrophotometer. Mass spectra were obtained on a Nippon Denshi JMS-01SG-2 mass spectrometer at an ionization energy of 70 eV using a direct inlet system through GLC.

### 2.4.2 General Procedure for Synthesis of Sensor **L**

Compounds **2**<sup>15</sup> and 8-azidomethyl quinoline<sup>16</sup> were prepared following the reported procedures. Copper iodide (10 mg) was added to compound **2** (200 mg, 0.29 mmol) and 8-azidomethyl quinoline (177 mg, 0.96 mmol) in a 30 mL mixture of THF/ $\text{H}_2\text{O}$  (5:1, v/v) and the mixture was heated at 70 °C for 24 h. The resulting solution was cooled and extracted twice with  $\text{CH}_2\text{Cl}_2$ . The organic layers were combined, dried over  $\text{MgSO}_4$  and the solvent was removed under reduced pressure. The residue obtained was purified using a silica gel column eluting with 1:1 hexane/ethyl acetate to give desired compound **L** as white solid in 65 % yield. m.p. 146–147 °C.  $^1\text{H}$  NMR (400 MHz,  $\text{CDCl}_3$ ):  $\delta$  = 1.03 (s, 27H, *t*Bu), 4.31–4.41 (ABq, 12H, ether bridge, *J* = 13.2 Hz), 4.54 (s, 6H, ArO– $\text{CH}_2$ –triazole), 6.08 (s, 6H, triazole– $\text{CH}_2$ –quinoline), 6.87 (s, 6H, Ar*H*), 7.39–7.45 (m, 6H, Quin–*H*), 7.50 (d, 3H, Quin–*H*, *J* = 6.8 Hz), 7.74 (d, 3H, Quin–*H*, *J* = 8.0 Hz), 7.84 (s, 3H, triazole–*H*), 8.10 (d, 3H,

Quin-*H*,  $J = 8.4$  Hz), 8.90 (d, 3H, Quin-*H*,  $J = 2.4$  Hz).  $^{13}\text{C}$  NMR (100 MHz,  $\text{CDCl}_3$ )  $\delta =$  31.42, 34.16, 49.65, 67.36, 69.30, 121.50, 124.42, 125.86, 126.36, 128.20, 128.59, 129.59, 130.98, 133.51, 136.14, 143.96, 145.72, 146.21, 150.11, 152.00. HRMS  $m/z$  Calcd for  $\text{C}_{75}\text{H}_{79}\text{N}_{12}\text{O}_6$   $[\text{M}+\text{H}]^+$ : 1243.6246 Found: 1243.6246  $[\text{M}+\text{H}]^+$ .

The monomeric compound **M** was also synthesized in 68 % yield as a reference compound by following a similar protocol.  $^1\text{H}$  NMR (400 MHz,  $\text{CDCl}_3$ ):  $\delta =$  1.28 (s, 9H, *t*Bu), 5.14 (s, 2H, ArO- $\text{CH}_2$ -triazole), 6.24 (s, 2H, triazole- $\text{CH}_2$ -quinoline), 6.88 (d, 2H, Ar*H*,  $J = 8.8$  Hz), 7.26 (d, 2H, Ar*H*,  $J = 10.0$  Hz), 7.48-7.54 (m, 2H, Quin-*H*), 7.64 (d, 1H, Quin-*H*,  $J = 6.8$  Hz), 7.83 (d, 1H, Quin-*H*,  $J = 8.4$  Hz), 7.86 (s, 1H, triazole-*H*), 8.19 (d, 1H, Quin-*H*,  $J = 8.4$  Hz), 8.97 (d, 1H, Quin-*H*,  $J = 4.0$  Hz).  $^{13}\text{C}$  NMR (100 MHz,  $\text{CDCl}_3$ )  $\delta =$  31.48, 34.05, 49.86, 62.14, 114.17, 121.62, 123.75, 126.21, 126.43, 128.36, 128.91, 129.91, 133.20, 136.39, 143.76, 144.18, 145.82, 150.17, 155.99. HRMS  $m/z$  Calcd for  $\text{C}_{73}\text{H}_{24}\text{N}_4\text{O}$   $[\text{M}]^+$ : 372.1950 Found: 372.1950  $[\text{M}]^+$ .

### 2.4.3 General Procedure for the UV-vis and Fluorescence Titrations

For absorption or fluorescence measurements, compounds were dissolved in acetonitrile to obtain stock solutions (1 mM). The stock solutions were diluted with acetonitrile to the desired concentration. Stock solutions ( $10^{-3}$  M) of perchlorate salts ( $\text{Li}^+$ ,  $\text{Na}^+$ ,  $\text{K}^+$ ,  $\text{Cs}^+$ ,  $\text{Ag}^+$ ,  $\text{Cu}^{2+}$ ,  $\text{Pb}^{2+}$ ,  $\text{Zn}^{2+}$ ,  $\text{Co}^{2+}$ ,  $\text{Ni}^{2+}$ ,  $\text{Cr}^{3+}$ ,  $\text{Al}^{3+}$ ,  $\text{Cd}^{2+}$ ,  $\text{Hg}^{2+}$ ,  $\text{Fe}^{2+}$  and  $\text{Fe}^{3+}$ ) were prepared with water. In titration experiments, typically, aliquots of freshly prepared standard solutions ( $10^{-3}$  M to  $10^{-6}$  M) of various analytes in water were added to record the UV-vis and fluorescence spectra. The fluorescence spectra were performed with the excitation wavelength 314 nm.

### 2.5 References

1. (a) J. Yin, Y. Hu and J. Yoon, *Chem. Soc. Rev.*, 2015, **44**, 4619–4644; (b) K. P. Carter, A. M. Young and A. E. Palmer, *Chem. Rev.*, 2014, **114**, 4564–4601; (c) H. N. Kim, W. X. Ren, J. S. Kim and J. Yoon, *Chem. Soc. Rev.*, 2012, **41**, 3210–3244; (d) J. F. Zhang, Y. Zhou, J. Yoon and J. S. Kim, *Chem. Soc. Rev.*, 2011, **40**, 3416–3429; (e) D. T. Quang and J. S. Kim, *Chem. Rev.*, 2010, **110**, 6280–6301.

2. (a) L. He, C. Liu and J. H. Xin, *Sens. Actuators B*, 2015, **213**, 181–187; (b) A. Kamal, S. Kumar, V. Kumar and R. K. Mahajan, *Sens. Actuators B*, 2015, **221**, 370–378; (c) C. D. Kaplan and J. Kaplan, *Chem. Rev.*, 2009, **109**, 4536–4552; (d) P. Aisen, M. Wessling-Resnick and E. A. Leibold, *Curr. Opin. Chem. Biol.*, 1999, **3**, 200–206; (e) R. Meneghini, *Free Radical Biol. Med.*, 1997, **23**, 783–792; (f) R. S. Eisenstein, *Annu. Rev. Nutr.*, 2000, **20**, 627–662.
3. (a) C. Brugnara, *Clin. Chem.*, 2003, **49**, 1573–1578; (b) E. Beutler, V. Felitti, T. Gelbart and N. Ho, *Drug. Metab. Dispos.*, 2001, **29**, 495–499; (c) F. O. Omara and B. R. Blakley, *J. Nutr.*, 1993, **123**, 1649–1655
4. (a) Y. Li, K. Li and J. He, *Talanta*, 2016, **153**, 381–385; (b) J.-L. Tang, C.-Y. Li, Y.-F. Li, X. Lu and H.-R. Qi, *Anal. Chim. Acta*, 2015, **888**, 155–161; (c) A. Wang, Y. Yang, F. Yu, L. Xue, B. Hu, W. Fan and Y. Dong, *Talanta*, 2015, **132**, 864–870.
5. (a) L. Zhao, X. Xin, P. Ding, A. Song, Z. Xie, J. Shen and G. Xu, *Anal. Chim. Acta*, 2016, **926**, 99–106; (b) P. Li, M. Zhang, X. Sun, S. Guan, G. Zhang, M. Baumgarten and K. Müllen, *Biosens. Bioelectron.*, 2016, **85**, 785–791; (c) X. Yang, X. Chen, X. Lu, C. Yan, Y. Xu, X. Hang, J. Qu and R. Liu, *J. Mater. Chem. C*, 2016, **4**, 383–390; (d) Y.-H. He, J.-P. Lai, H. Sun, Z.-M. Chen and S. Lan, *Sens. Actuators B*, 2016, **225**, 405–412; (e) K. Kaur, S. Chaudhary, S. Singh and S. K. Mehta, *Sens. Actuators B*, 2016, **232**, 396–401; (f) S. Joshi, S. Kumari, R. Bhattacharjee, A. Sarmah, R. Sakhuja and D. D. Pant, *Sens. Actuators B*, 2015, **220**, 1266–1278.
6. (a) C. Wu, J.-L. Zhao, X.-K. Jiang, C.-Z. Wang, X.-L. Ni, X. Zeng, C. Redshaw and T. Yamato, *Dalton Trans.*, 2016, **45**, 14948–14953; (b) R. Martínez, F. Zapata, A. Caballero, A. Espinosa, A. Tárraga and P. Molina, *Org. Lett.*, 2006, **8**, 3235–3238; (c) K. Rurack, U. Resch-Genger and W. Rettig, *J. Photochem. Photobiol. A*, 1998, **118**, 143–149.
7. (a) C. Wu, Y. Ikejiri, X. Zeng, M. R. J. Elsegood, C. Redshaw and T. Yamato, *Org. Lett.*, 2017, **19**, 66–69; (b) K. Griffiths, K. Sharma, P. M. Marcos, J. R. Ascenso, J. Nind, K. Cottet and P. J. Cragg, *Supramol. Chem.*, 2015, **27**, 167–173; (c) K. Cottet, P. M. Marcos and P. J. Cragg, *Beilstein J. Org. Chem.*, 2012, **8**, 201–226.
8. (a) X.-K. Jiang, Y. Ikejiri, C.-C. Jin, C. Wu, J.-L. Zhao, X.-L. Ni, X. Zeng, C. Redshaw and T. Yamato, *Tetrahedron*, 2016, **72**, 4854–4858; (b) C. Wu, Y. Ikejiri, J.-L. Zhao, X.-K. Jiang, X.-L. Ni, X. Zeng, C. Redshaw and T. Yamato, *Sens. Actuators B*, 2016, **228**,



- 480–485; (c) C. Wu, J.-L. Zhao, X.-K. Jiang, X.-L. Ni, X. Zeng, C. Redshaw and T. Yamato, *Anal. Chim. Acta*, 2016, **936**, 216–221.
9. (a) H. Liu, Y. Dong, B. Zhang, F. Liu, C. Tan, Y. Tan and Y. Jiang, *Sens. Actuators B*, 2016, **234**, 616–624; (b) M.-H. Kao, T.-Y. Chen, Y.-R. Cai, C.-H. Hu, Y.-W. Liu, Y. Jhong and A.-T. Wu, *J. Lumin.*, 2016, **169**, 156–160; (c) D. Sarkar, A. Pramanik, S. Jana, P. Karmakar and T. K. Mondal, *Sens. Actuators B*, 2015, **209**, 138–146; (d) E. J. Song, G. J. Park, J. J. Lee, S. Lee, I. Noh, Y. Kim, S.-J. Kim, C. Kim and R. G. Harrison, *Sens. Actuators B*, 2015, **213**, 268–275; (e) H. Kim, G. R. You, G. J. Park, J. Y. Choi, I. Noh, Y. Kim, S.-J. Kim, C. Kim and R. G. Harrison, *Dyes Pigm.*, 2015, **113**, 723–729.
10. (a) B. Valeur, *Molecular fluorescence: principles and applications*, Wiley-VCH, Weinheim, 2002; (b) B. Valeur and I. Leray, *Coord. Chem. Rev.*, 2000, **205**, 3–40; (c) A. P. de Silva, H. Q. N. Gunaratne, T. Gunnlaugsson, A. J. M. Huxley, C. P. McCoy, J. T. Rademacher and T. E. Rice, *Adv. Supramol. Chem.*, 1997, **4**, 1–53; (d) R. A. Bissell, A. P. de Silva, H. Q. N. Gunaratne, P. L. M. Lynch, G. E. M. Maguire, C. P. McCoy and K. R. A. S. Sandanayake, *Top. Curr. Chem.*, 1993, **168**, 223–264.
11. (a) S. Elçin, H. Deligöz, A. A. Bhatti, M. Oguz, S. Karakurt and M. Yilmaz, *Sens. Actuators B*, 2016, **234**, 345–352; (b) S.-L. Kao and S.-P. Wu, *Sens. Actuators B*, 2015, **212**, 382–388; (c) S.-Q. Jiang, Z.-Y. Zhou, S.-P. Zhuo, G.-G. Shan, L.-B. Xing, H.-N. Wang and Z.-M. Su, *Dalton Trans.*, 2015, **44**, 20830–20833; (d) V. V. S. Mummidivarapu, A. Nehra, V. K. Hinge and C. P. Rao, *Org. Lett.*, 2012, **14**, 2968–2971; (e) L.-Y. You, S.-G. Chen, X. Zhao, Y. Liu, W.-X. Lan, Y. Zhang, H.-J. Lu, C.-Y. Cao and Z.-T. Li, *Angew. Chem.*, 2012, **124**, 1689–1693.
12. (a) Y.-C. Liao, P. Venkatesan, L.-F. Wei and S.-P. Wu, *Sens. Actuators B*, 2016, **232**, 732–737; (b) K. Boonkitpatarakul, J. Wang, N. Niamnont, B. Liu, L. McDonald, Y. Pang and M. Sukwattanasinitt, *ACS Sens.*, 2016, **1**, 144–150; (c) J.-R. Lin, C.-J. Chu, P. Venkatesan and S.-P. Wu, *Sens. Actuators B*, 2015, **207**, 563–570; (d) Z. Liu, W. He, M. Pei and G. Zhang, *Chem. Commun.*, 2015, **51**, 14227–14230.
13. J. A. Ho, H.-C. Chang and W.-T. Su, *Anal. Chem.*, 2012, **84**, 3246–3253.
14. (a) A. Ikeda, H. Udzu, Z. Zhong, S. Shinkai, S. Sakamoto and K. Yamaguchi, *J. Am. Chem. Soc.*, 2001, **123**, 3872–3877; (b) M. Takeshita, F. Inokuchi and S. Shinkai, *Tetrahedron Lett.*, 1995, **36**, 3341–3344.

15. X.-L. Ni, S. Wang, X. Zeng, Z. Tao and T. Yamato, *Org. Lett.*, 2011, **13**, 552–555.
16. R. K. Pathak, J. Dessingou, V. K. Hinge, A. G. Thawari, S. K. Basu and C. P. Rao, *Anal. Chem.*, 2013, **85**, 3707–3714.

## Chapter 3

### A Novel Fluorescence “On–Off–On” Chemosensor for $\text{Hg}^{2+}$ via a Water-assistant Blocking Heavy Atom Effect

*This chapter described a upper rim pyrene-functionalized hexahomotrioxacalix[3]arene L, which can be utilized as a highly selective and sensitive fluorescent chemosensor to  $\text{Hg}^{2+}$  with a detection limit in nM level. Interestingly, the quenched fluorescence emission can be successfully revived upon the addition of water. In this process, the heavy atom effect and blocking thereof were demonstrated within the same system by the use of a  $C_3$ -symmetric homooxacalix[3]arene scaffold.*

### 3.1 Introduction

Heavy and transition metal (HTM) ions play an important role in living systems and can have an extremely toxic impact on the environment.<sup>1</sup> Fluorescent chemosensors are powerful tools for the monitoring *in vitro* and/or *in vivo* of HTM ions because of the simplicity and high sensitivity of fluorescence.<sup>2</sup> However, fluorescence quenching is usually observed when HTM ions are bound to sensors due to the heavy atom enhanced intersystem crossing (e.g.  $\text{Hg}^{2+}$ )<sup>3</sup> or energy/electron transfer (e.g. paramagnetic  $\text{Cu}^{2+}$ ).<sup>4</sup> Fluorescence quenching is not only a disadvantage for high signal output upon recognition but also hampers temporal separation of spectrally similar complexes with time-resolved fluorometry.<sup>5</sup> Thus, fluorescence enhancement induced by complexation with HTM ions is highly desirable in the field of fluorescent chemosensor research.

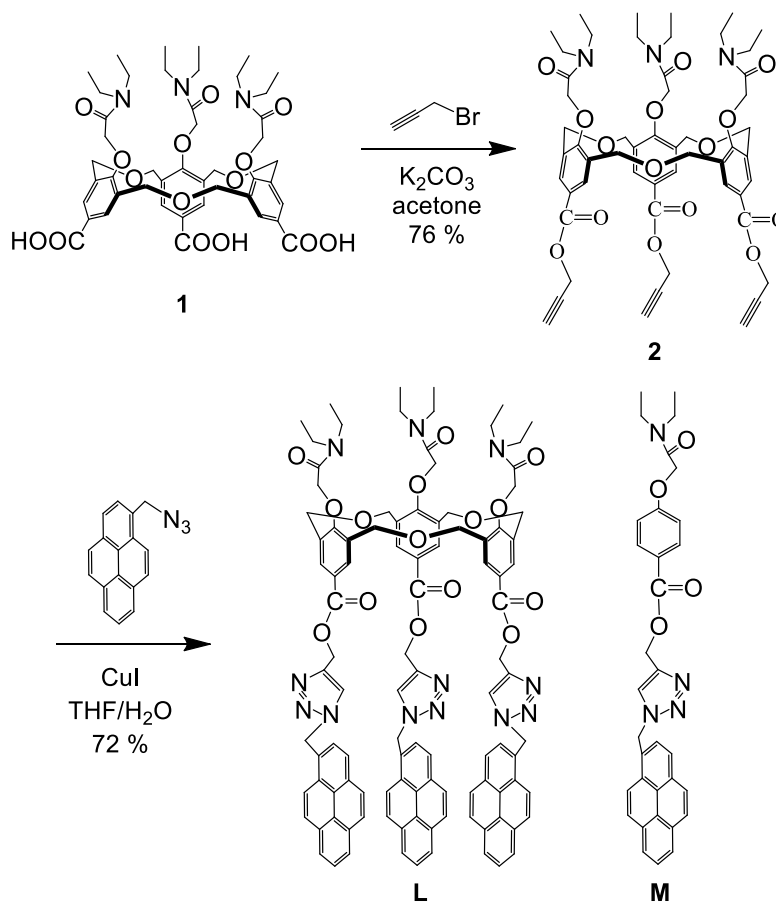
Since McClure (1952)<sup>3</sup> and Wehry (1972)<sup>4</sup> demonstrated the principle of heavy atom effect quenching on fluorescence emission, there have been many literature reports focusing on the “Why” of the intrinsic quenching behaviour of HTM ions,<sup>6</sup> but not providing the “How” to block the quenching effect. Therefore, one might consider whether the heavy atom effect caused by HTM ions can be blocked or indeed avoided? Undoubtedly, if so, it may open up a new strategy to develop new fluorescence turn on sensors for HTM ions.

In 2010, Xu *et al.* presented three general strategies to prevent fluorescence quenching and preserve the ability for fluorescence enhancement to take place upon binding of the HTM ions: (i) preventing the close proximity of the HTM ions to the fluorophore; (ii) increasing the oxidation potential of the fluorophore; (iii) introducing sacrificial donors that participate in single electron transfer with the HTM ions instead of the fluorophore.<sup>7</sup> Recently, we reported the first evidence of the blocking of the heavy atom effect via the water-assisted and time-dependent fluorescence enhancement detection of  $\text{Hg}^{2+}$  by utilizing the unique fluorescence ratiometric signal of the excimer/monomer emission (IE/IM) of the pyrene moiety appended to a  $C_3$ -symmetric homooxacalix[3]arene scaffold.<sup>8</sup> In connection with our continuing interest in the development of chemosensors for HTM ions, we herein report the synthesis and sensing properties of a new pyrene-functionalized hexahomotrioxacalix[3]arene chemosensor L, which exhibited an “on–off–on” fluorescence

response toward  $\text{Hg}^{2+}$  via the water-assistant blocking heavy atom effect. The present studies provided further evidence for the blocking heavy atom effect.

## 3.2 Results and Discussion

### 3.2.1 Synthesis and Characterization



**Scheme 1.** The synthesis route of chemosensor **L**.

The synthetic route for the current sensor is depicted in Scheme 1. Compound **2** was synthesized by the reaction of hexahomotrioxacalix[3]arene (**1**)<sup>9</sup> with propargyl bromide in acetone in the presence of  $\text{K}_2\text{CO}_3$ . The  $\text{Cu}^{\text{I}}$ -catalyzed 1,3-dipolar cycloaddition reaction of compound **2** with 1-azidomethylpyrene under Click conditions afforded the chemosensor **L** in 72 % yield. Reference compound **M** was synthesized in 78 % yield by using a method similar to that used in the preparation of **L**. All compounds synthesized in this work were fully characterized by spectroscopic data including  $^1\text{H}$ ,  $^{13}\text{C}$  NMR spectroscopy and HRMS.

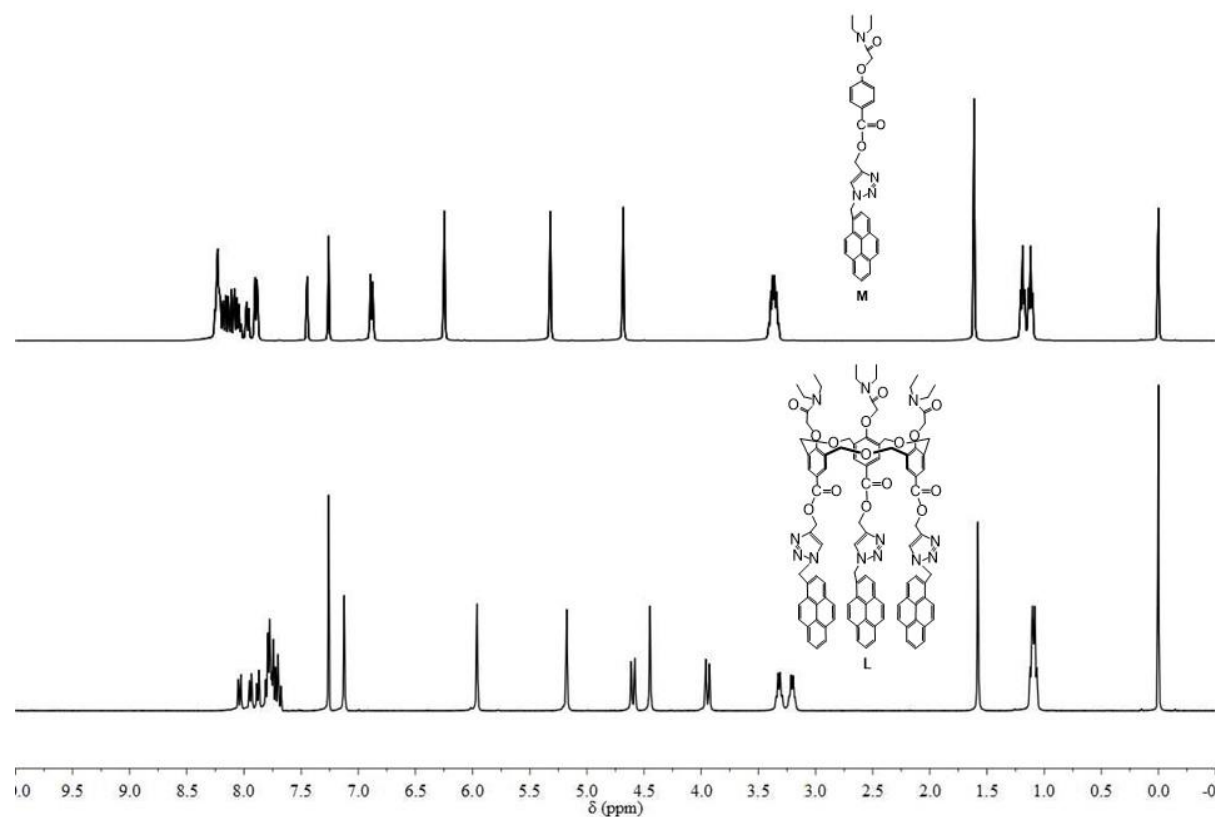


**Figure 1.** The  $^1\text{H}$  NMR spectra of compounds **L** and **M**.

### 3.2.2 Chemosensing properties of **L**

The spectroscopic properties of **L** and **M** were then studied via UV-vis and fluorescence spectroscopies. The UV-vis absorption spectra of compound **L** exhibit typical pyrene absorption bands in the region 320 – 360 nm. Interaction of **L** with 10 equiv. of various metal cations did not result in any significant changes in the absorption spectrum (Figure 2). On the other hand, the fluorescence properties of **L** and **M** were investigated in  $\text{CH}_3\text{CN}$ . On excitation at 343 nm, the maximum absorption wavelength of pyrene, **L** displays very weak monomer emission (379 nm and 398 nm) but strong excimer emission (around 484 nm), whereas reference compound **M** exhibited only the monomer band at 379 nm and 398 nm. The excimer emission band was attributed to the interaction of the neighbouring pyrene units engaging in intramolecular  $\pi$ - $\pi$  stacking, which was fixed by the oxacalix[3]arene scaffold.

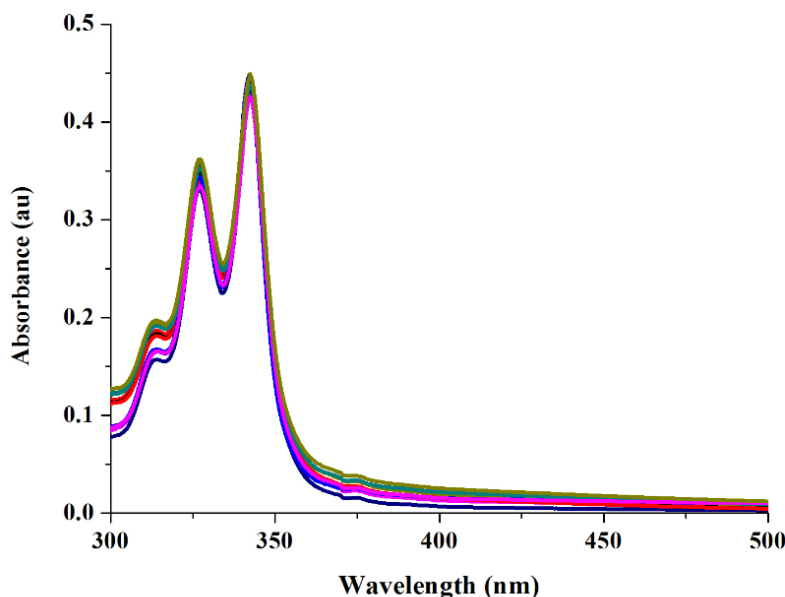


**Figure 2.** The UV-vis spectra of **L** (5.0  $\mu\text{M}$ ), in the presence of 10 equiv. of various metal cations (including  $\text{Li}^+$ ,  $\text{Na}^+$ ,  $\text{K}^+$ ,  $\text{Cs}^+$ ,  $\text{Ag}^+$ ,  $\text{Cu}^{2+}$ ,  $\text{Pb}^{2+}$ ,  $\text{Zn}^{2+}$ ,  $\text{Co}^{2+}$ ,  $\text{Ni}^{2+}$ ,  $\text{Cr}^{3+}$ ,  $\text{Al}^{3+}$ ,  $\text{Fe}^{3+}$ ,  $\text{Cd}^{2+}$  and  $\text{Hg}^{2+}$ ) in  $\text{CH}_3\text{CN}$  solutions. The molar absorption coefficient values were calculated by the Beer-Lambert Law ( $A = \epsilon bc$ ): 327 nm ( $\epsilon = 6.7 \times 10^4 \text{ M}^{-1} \cdot \text{cm}^{-1}$ ), 343 nm ( $\epsilon = 8.5 \times 10^4 \text{ M}^{-1} \cdot \text{cm}^{-1}$ ).

To explore the potential application of **L** as a fluorescent chemosensor for the detection of HTM ions, the fluorescence response of **L** in  $\text{CH}_3\text{CN}$  toward several common metal cations, including  $\text{Li}^+$ ,  $\text{Na}^+$ ,  $\text{K}^+$ ,  $\text{Cs}^+$ ,  $\text{Ag}^+$ ,  $\text{Cu}^{2+}$ ,  $\text{Pb}^{2+}$ ,  $\text{Zn}^{2+}$ ,  $\text{Co}^{2+}$ ,  $\text{Ni}^{2+}$ ,  $\text{Cr}^{3+}$ ,  $\text{Al}^{3+}$ ,  $\text{Fe}^{3+}$ ,  $\text{Cd}^{2+}$  and  $\text{Hg}^{2+}$  by using their perchlorate salts (10 equiv.) was investigated. The fluorescence changes are depicted in Figure 3, where addition of  $\text{Hg}^{2+}$  led to significant fluorescence quenching of up to 96 %.  $\text{Cu}^{2+}$  ions also resulted in quenching (32 %) but on a much smaller scale than observed for  $\text{Hg}^{2+}$ . Moreover, upon interaction with other metal cations, a much weaker response is observed when compared to  $\text{Hg}^{2+}$ . To evaluate the specific fluorescence response toward  $\text{Hg}^{2+}$ , a group of metal cations and an ion mixture were chosen as the interferential ions to perform the fluorescence tests (Figure 4). Except for  $\text{Cu}^{2+}$ , it was found that the rest of the metal cations exerted a negligible or very small influence on the fluorescence spectra of **L**. Thus, **L** can be used as a  $\text{Hg}^{2+}$  selective fluorescent chemosensor in the presence of most competitive metal cations.

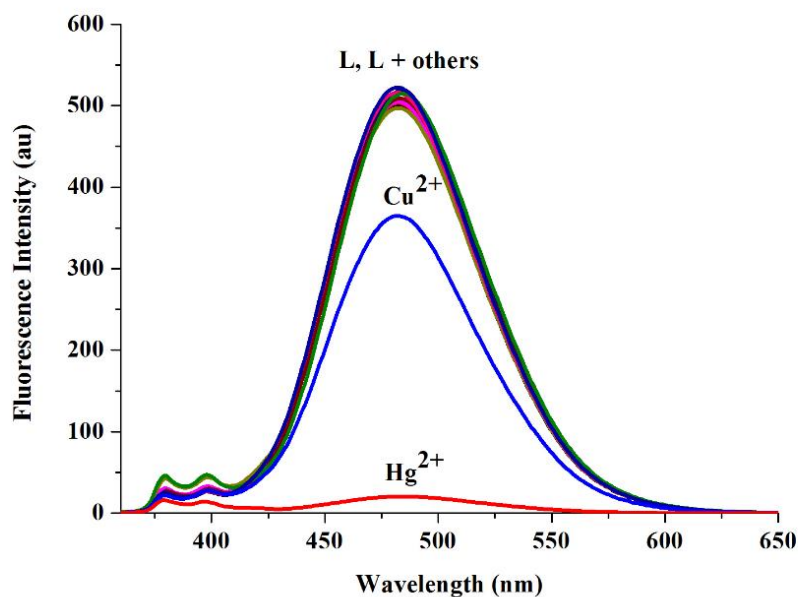


**Figure 3.** Fluorescence spectra of **L** (1.0  $\mu\text{M}$ ) on addition of various metal cations in  $\text{CH}_3\text{CN}$ ,  $\lambda_{\text{ex}} = 343$  nm.

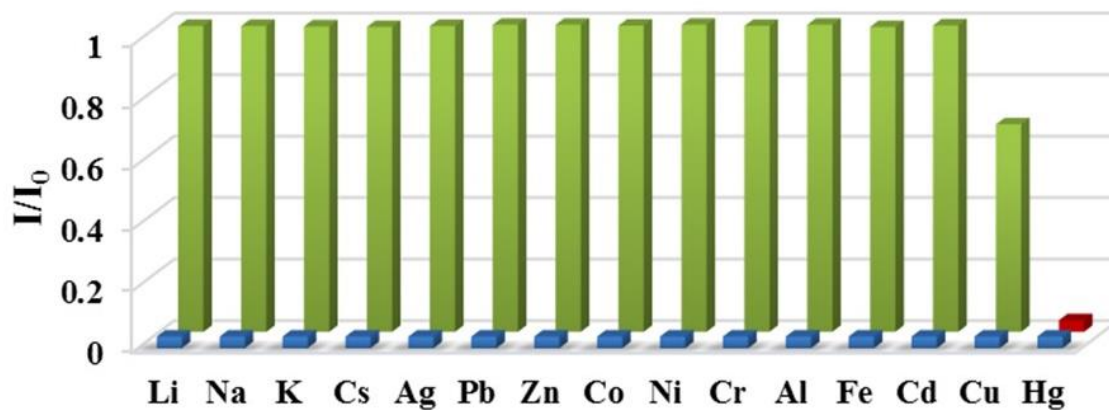


**Figure 4.** Fluorescence response of **L** (1.0  $\mu\text{M}$ ) to 10 equiv. of metal cations (the green bar) and to the mixture of 10 equiv. of other metal ions with  $\text{Hg}^{2+}$  (the blue bar) and the fluorescence response of **L** toward  $\text{Hg}^{2+}$  + all metal ions (the red bar).  $I_0$  is fluorescent emission intensity at 484 nm of free **L**, and  $I$  is the fluorescent intensity after adding metal cations.



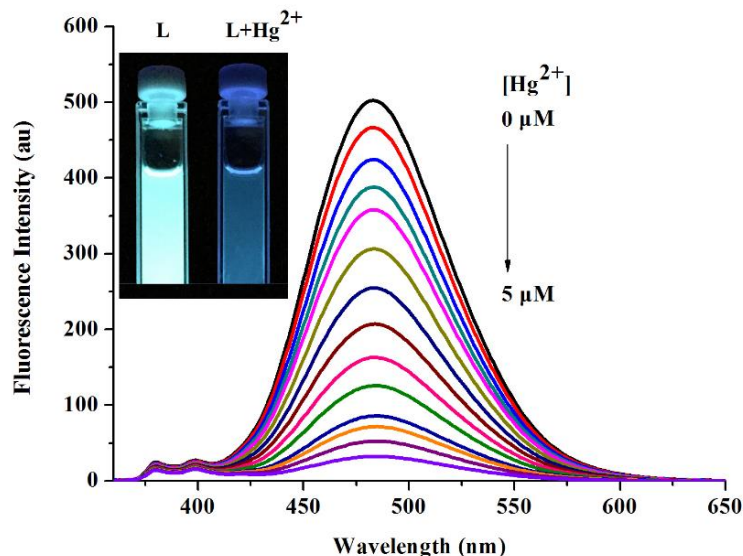


**Figure 5.** Fluorescence spectra of **L** (1.0  $\mu\text{M}$ ) upon the addition of increasing amount of  $\text{Hg}^{2+}$  in  $\text{CH}_3\text{CN}$ .  $\lambda_{\text{ex}} = 343 \text{ nm}$ . The inset shows the fluorescence colour of **L** before and after the addition of  $\text{Hg}^{2+}$ .

To demonstrate the ability of **L** as fluorescent sensor for  $\text{Hg}^{2+}$ , we performed the fluorescence quenching titration with  $\text{Hg}^{2+}$  in  $\text{CH}_3\text{CN}$  (Figure 5). The titration profiles revealed that the initial emission intensity of **L** was gradually quenched upon the addition of increasing amounts of  $\text{Hg}^{2+}$ . The addition of 5 equiv. of  $\text{Hg}^{2+}$  to the solution of **L** resulted in both the monomer and excimer emission becoming quenched due to the heavy atom effect imparted by  $\text{Hg}^{2+}$ , which increases the probability for intersystem crossing to the triplet state because of large spin-orbit coupling contribution.<sup>6a,10</sup> A good linear relationship was observed between the emission intensities and concentration of  $\text{Hg}^{2+}$ , and the limit of detection (LOD) was found to be  $3.48 \times 10^{-8} \text{ M}$  based on the formula  $\text{LOD} = 3\sigma/K$  (Figure 6).<sup>11</sup> The detection limits were sufficiently low to allow for the detection the sub-millimolar concentrations of  $\text{Hg}^{2+}$  ion found in many chemical and biological systems. The Job's method monitored by fluorescence intensities was applied to examine the stoichiometry of the **L**/ $\text{Hg}^{2+}$  complex, which indicated a 1:1 stoichiometry of **L** to  $\text{Hg}^{2+}$  in the complex (Figure 7). The association constant ( $K_a$ ) was calculated to be  $3.3 \times 10^5 \text{ M}^{-1}$  according to the spectral titration data using the Benesi–Hildebrand equation (Figure 8).<sup>12</sup> These results indicated that **L** has an excellent sensitivity toward  $\text{Hg}^{2+}$  with a detection limit in the nM level, and can even be applied to the quantitative detection of  $\text{Hg}^{2+}$ .

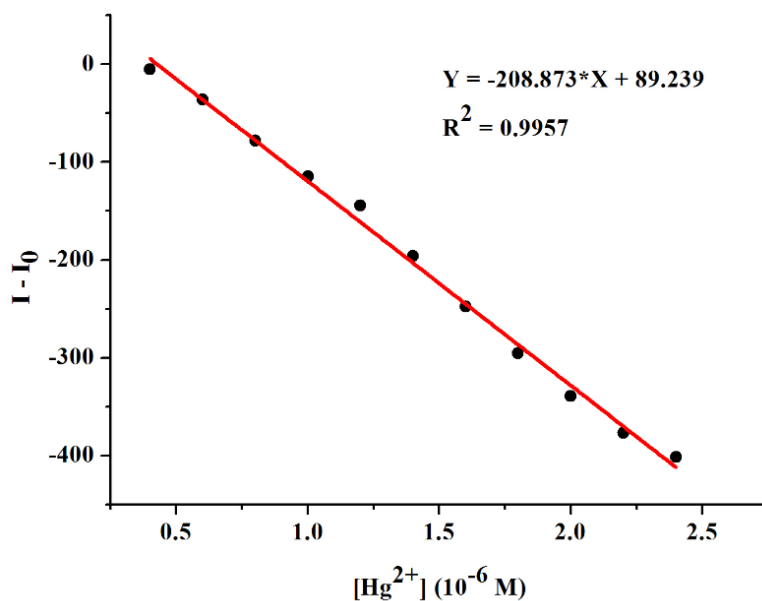


**Figure 6.** Linear concentration range of  $\text{Hg}^{2+}$  ( $\text{L}$ :  $1.0 \mu\text{M}$ ) in  $\text{CH}_3\text{CN}$ .  $I_0$  is fluorescence emission intensity at 484 nm for free  $\text{L}$ , and  $I$  is the fluorescent intensity after adding  $\text{Hg}^{2+}$  ions. The calculation method for LOD is based on the standard deviation of the response ( $\sigma$ ) and the slope of the calibration curve ( $K$ ) according to the formula:  $\text{LOD} = 3\sigma/K = 3.48 \times 10^{-8} \text{ M}$ .

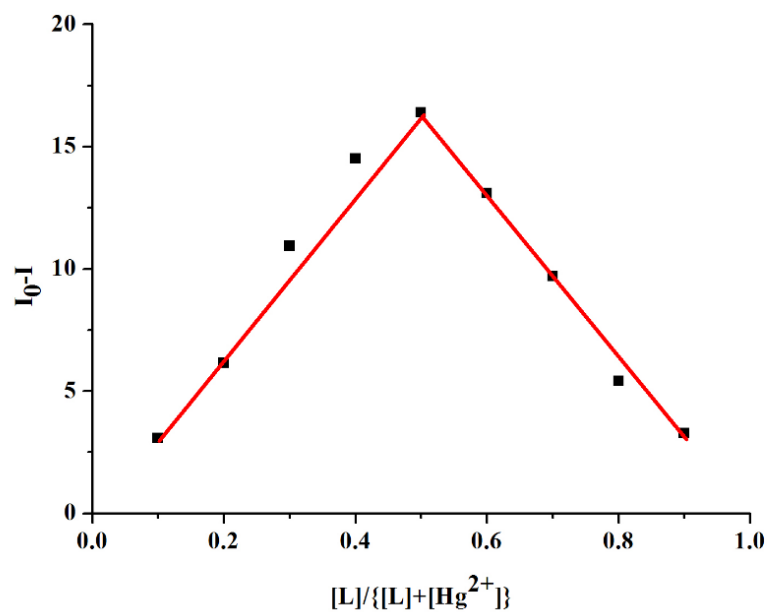


**Figure 7.** Job's plot for complexation of  $\text{L}$  with  $\text{Hg}^{2+}$  ion, indicating a 1:1 binding stoichiometry.

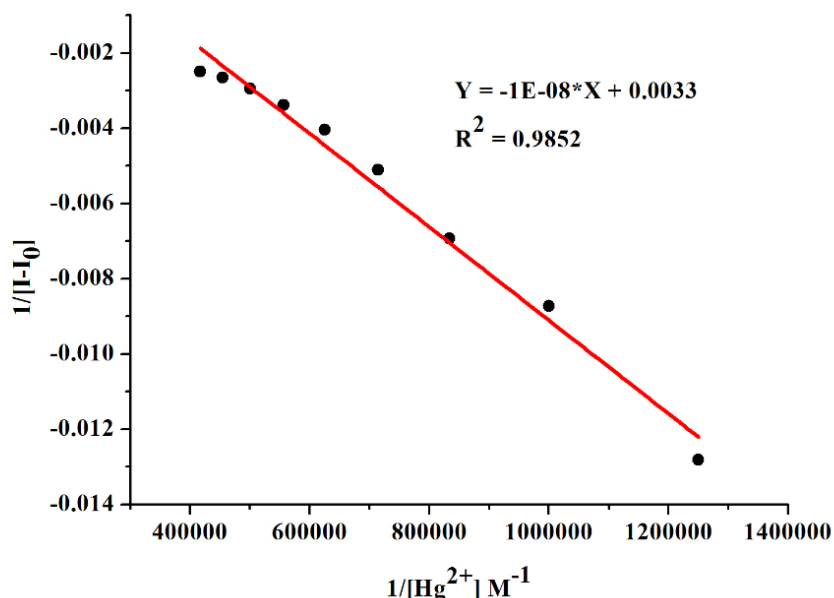


**Figure 8.** Benesi-Hildebrand plot of **L** in  $CH_3CN$ . The association constant was determined using a reported procedure for a 1:1 binding mode. Association constant  $K_a = 0.0033/(1E-08) = 3.3 \times 10^5 M^{-1}$ .

For practical applications, the effect of water as a solvent on the detection of  $Hg^{2+}$  was also monitored. To study the selective detection of  $Hg^{2+}$  from aqueous samples, the fluorescence response of **L** (in  $CH_3CN$ ) upon addition of water was initially monitored. The addition of water showed a negligible effect on the fluorescence intensity and the spectrum remained unaffected even after 1 h (Figure 9). Consequently, we further checked the selectivity of **L** for  $Hg^{2+}$  in a  $H_2O-CH_3CN$  (v/v, 1:10) mixed solvent system. Unexpectedly, upon the addition of  $Hg^{2+}$  to the mixed solvent system, the fluorescence spectrum does not show any significant change. Motivated by these results, we expanded this study in order to systematically investigate the role of the water molecules in the **L**/ $Hg^{2+}$  complex. In a specially designed experiment, 5 equiv. of  $Hg^{2+}$  was added to quench the fluorescence emission of **L** in  $CH_3CN$ , and then different volumes of distilled water were added to the original  $CH_3CN$  solution of the **L**/ $Hg^{2+}$  complex and the corresponding emissions were monitored.

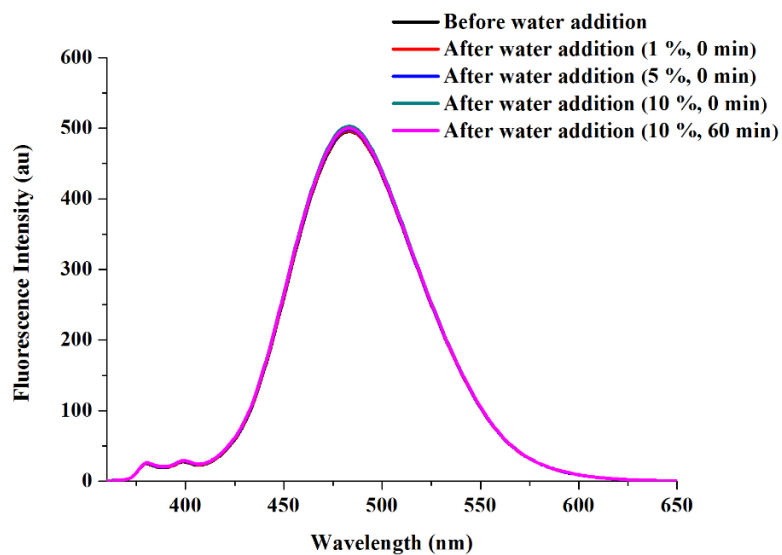


**Figure 9.** Effect of water on fluorescence spectrum of **L** dispersed in  $\text{CH}_3\text{CN}$ .

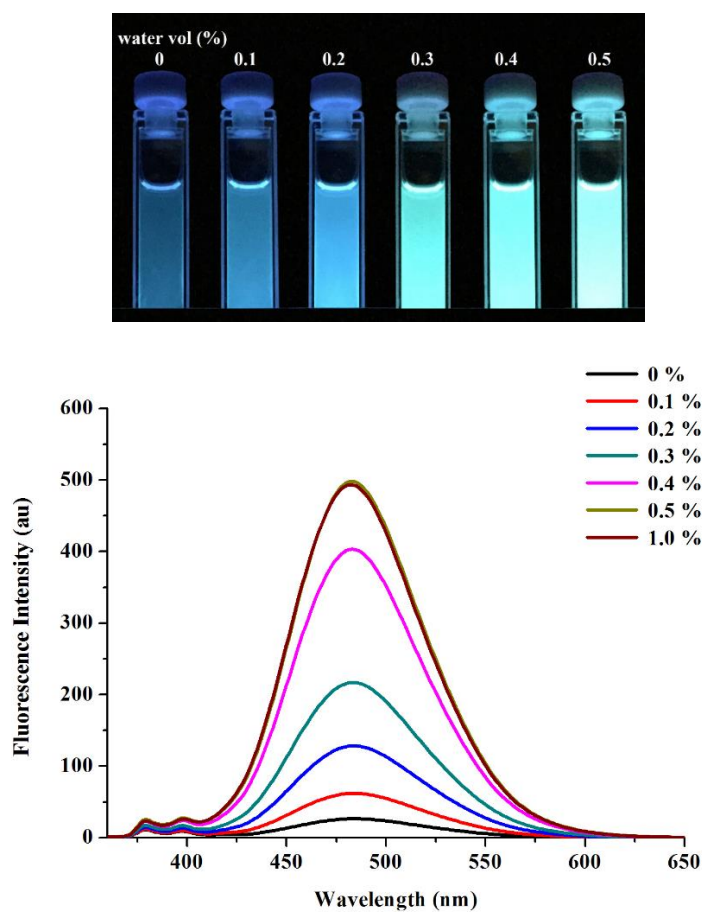


**Figure 10.** Fluorescence emission spectra for the  $\text{L}/\text{Hg}^{2+}$  complex in  $\text{CH}_3\text{CN}$  with the incremental addition of water and the digital photos of  $\text{L}/\text{Hg}^{2+}$  complex in  $\text{H}_2\text{O}-\text{CH}_3\text{CN}$  mixtures under irradiation at 365 nm.

Figure 10 illustrates the fluorescence spectral changes of the  $\text{L}/\text{Hg}^{2+}$  complex in  $\text{CH}_3\text{CN}$  upon addition of water. Interestingly, the incremental addition of water to the solution of  $\text{L}/\text{Hg}^{2+}$  complex resulted in a rapid enhancement of the excimer emission. This process is saturated when about 0.5 % content of water added, with the fluorescence intensity almost revived to that of the original chemosensor **L**. The revival of fluorescence emission is clearly observed under illumination at 365 nm. Additionally, in order to determine the impact of time on this process, an estimation of the time-dependent fluorescence spectral changes of  $\text{L}/\text{Hg}^{2+}$  complex was carried out. As shown in Figure 11, the fluorescence emission was enhanced immediately after adding water, and the fluorescence intensity could remain stable over a long period. Following this observation, we found that other polar solvents such as  $\text{CH}_3\text{OH}$  and  $\text{CH}_3\text{CH}_2\text{OH}$  also have the ability to revive the fluorescence emission of the  $\text{L}/\text{Hg}^{2+}$  complex (Figure 12 and 13), but on a much smaller scale than observed for  $\text{H}_2\text{O}$ . Thus, there must be a strong interaction between the water molecules and the  $\text{L}/\text{Hg}^{2+}$  complex, which leads to the revival of the fluorescence intensity.

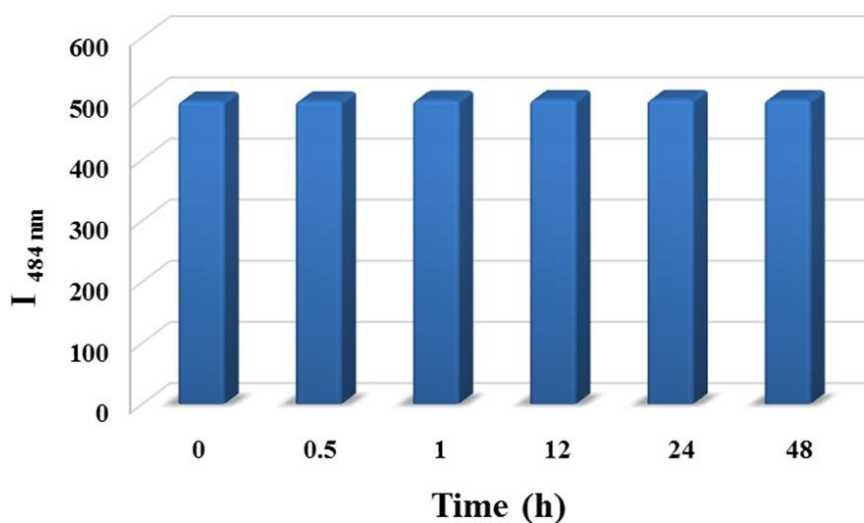


**Figure 11.** Time-dependent fluorescent intensity changes at 484 nm of  $\text{L}/\text{Hg}^{2+}$  complex in  $\text{H}_2\text{O}/\text{CH}_3\text{CN}$  (v/v, 1:200).

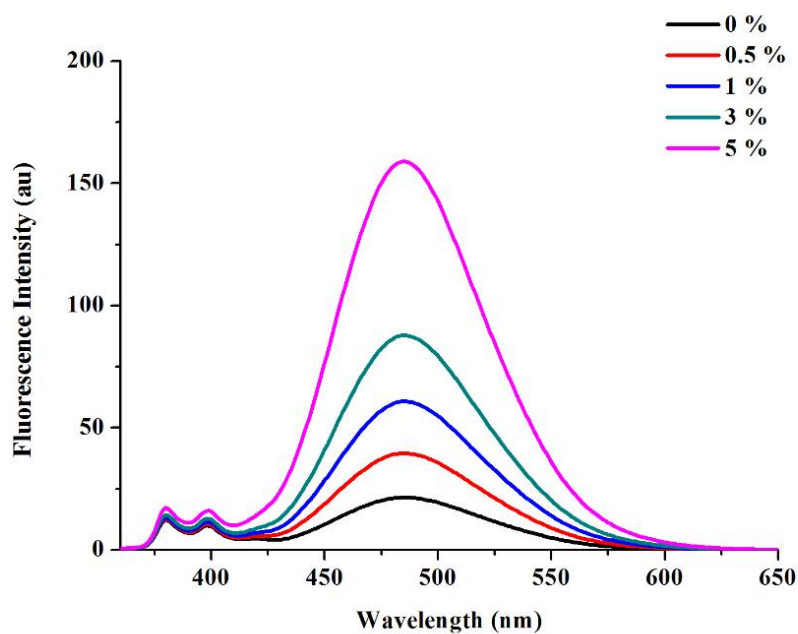


**Figure 12.** Fluorescence emission spectra for the L/Hg<sup>2+</sup> complex in CH<sub>3</sub>CN with the incremental addition of CH<sub>3</sub>OH.

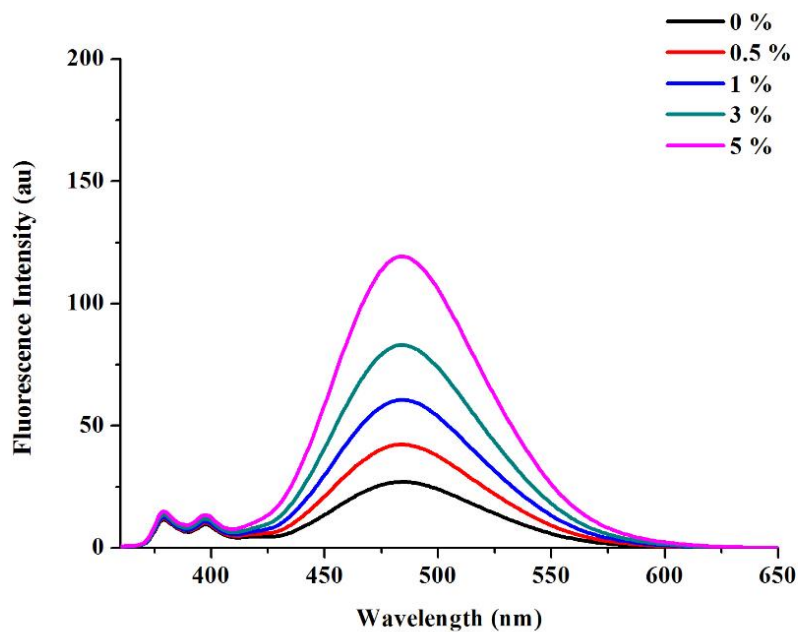


**Figure 13.** Fluorescence emission spectra for the L/Hg<sup>2+</sup> complex in CH<sub>3</sub>CN with the incremental addition of CH<sub>3</sub>CH<sub>2</sub>OH.

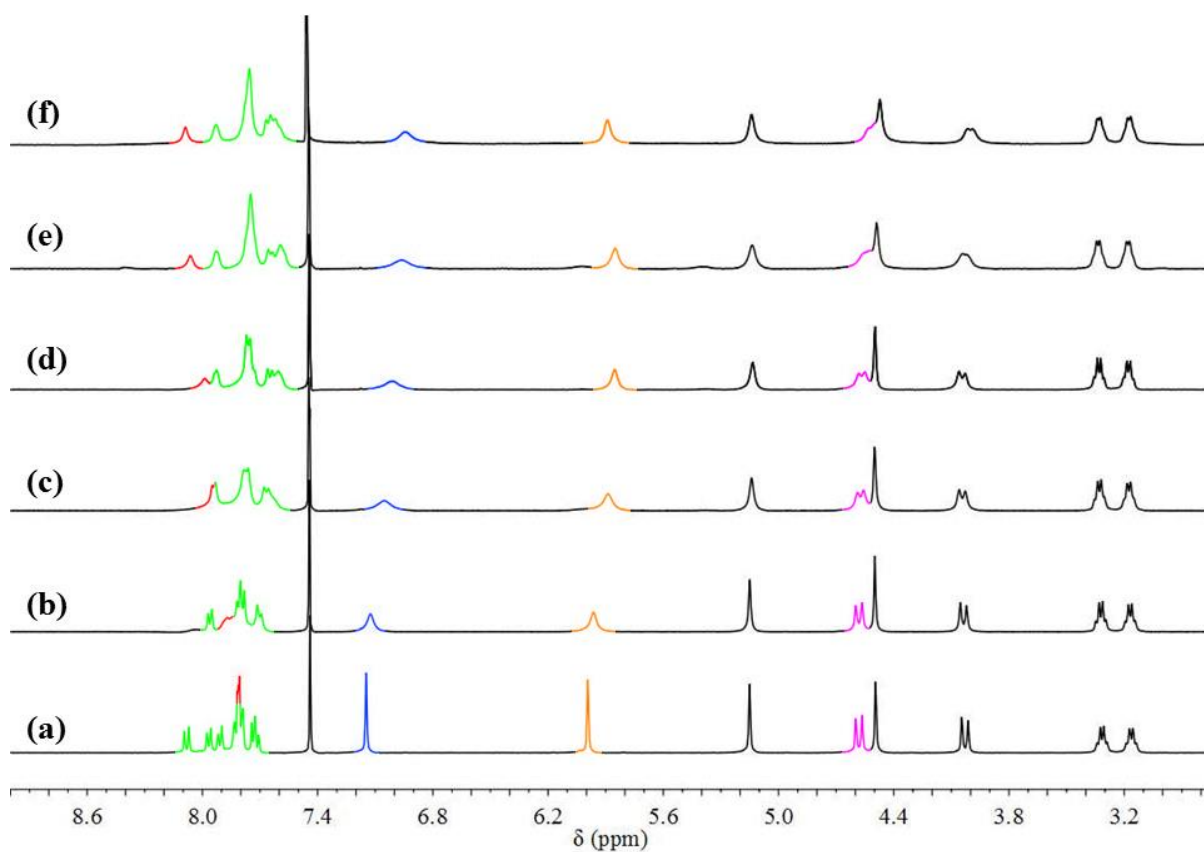


**Figure 14.** Partial  $^1\text{H}$  NMR spectra of **L** (5.0 mM) in  $\text{CDCl}_3/\text{CD}_3\text{CN}$  (v/v, 2:1): (a) **L** only; (b, c, d and e) in the presence of 0.3, 0.5, 0.8 and 1.0 equiv. of  $\text{Hg}^{2+}$ , respectively; (f) **L**/ $\text{Hg}^{2+}$  complex in the presence 10  $\mu\text{L}$   $\text{D}_2\text{O}$ .

For an in-depth understanding of the complexation properties of **L** with  $\text{Hg}^{2+}$  ions in the presence of water molecules,  $^1\text{H}$  NMR titration experiments were performed in  $\text{CDCl}_3/\text{CD}_3\text{CN}$  (v/v, 2:1) co-solvent. The spectral differences are depicted in Figure 14. Some significant spectral changes are observed in the  $^1\text{H}$  NMR spectra on addition of  $\text{Hg}^{2+}$ . For example, upon interaction with  $\text{Hg}^{2+}$ , the proton on the triazole rings undergoes a down-field shift by  $\Delta\delta$  0.26 ppm to 8.07 (red colour), whereas the triazole- $\text{CH}_2$ -pyrene linker proton is shifted from 5.99 to 5.87 ppm (brown colour). These chemical shift changes reflect the involvement of the triazole rings in the metal ion binding.<sup>13</sup> Furthermore, the chemical shifts of the aromatic (blue colour) and  $\text{ArCH}_2(\text{ax})\text{O}$  bridge methylene (pink colour) protons also experienced an up-field shift, which can be attributed to the conformational change of oxacalix[3]arene scaffold upon

complexation with the  $\text{Hg}^{2+}$ . As a matter of fact, it is believed that the conformation of the hexahomotrioxacalix[3]arene can be pre-organized for the binding of  $\text{Hg}^{2+}$  ion in solution in a manner that is similar to the examples described by Shinkai and coworkers.<sup>14</sup> Importantly, it should be noted that the proton signals of pyrene (green colour) obviously shifted up-field as the concentration of  $\text{Hg}^{2+}$  increased. It suggests that the pyrene moieties still maintain the  $\pi$ - $\pi$  stacking and exhibit the excimer emission. This is different from our recent reports in which the pyrene protons experienced a down-field shift, behaving as separate pyrene moieties with an enhancement of the monomer emission.<sup>8,15</sup>

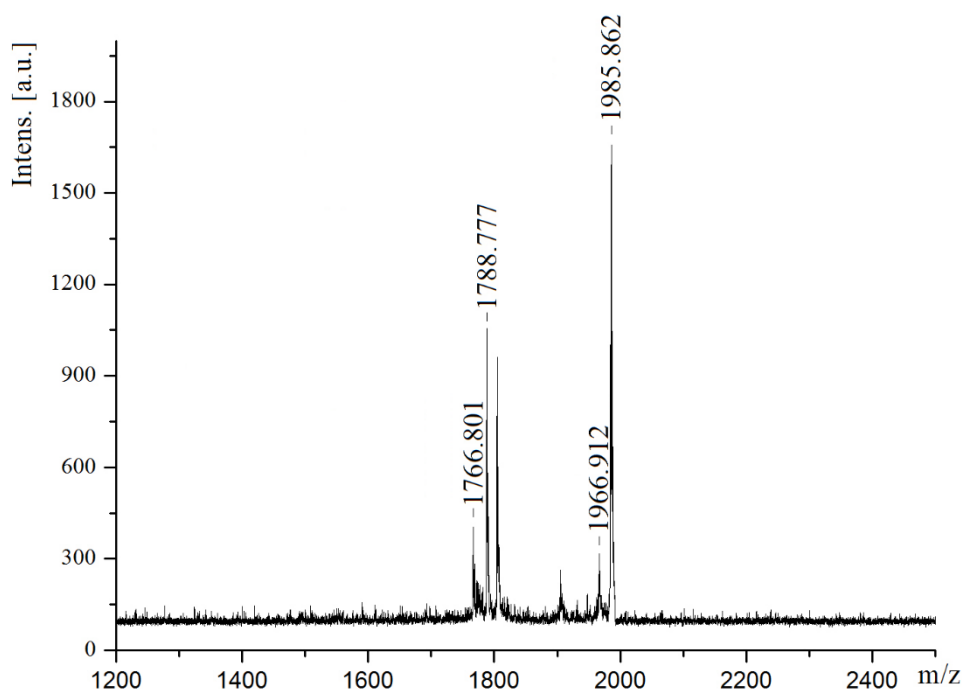


**Figure 15.** MALDI-TOF-MS spectrum of  $\text{L-Hg}^{2+}$ ,  $[\text{L} + \text{Hg}^{2+} + \text{H}_2\text{O} + \text{H}]^+$ ,  $m/z$  1985.862.

On further addition of 10  $\mu\text{L}$   $\text{D}_2\text{O}$  into the solution of  $\text{L/Hg}^{2+}$  complex, no significant chemical shift changes of the protons on the  $\text{L/Hg}^{2+}$  complex were observed (Fig. 5f). This result suggested that the enhancement of the excimer emission of pyrene in the present system should be ascribed to the additional coordination of a water molecule to the  $\text{Hg}^{2+}$  ion rather than the dissociation of the  $\text{L/Hg}^{2+}$  complex and the release of free **L**. Moreover, mass spectrometry (MALDI-TOF) was also used to investigate the complexation. When the  $\text{Hg}^{2+}$



ion was added to a  $\text{CH}_3\text{CN}$  solution of **L** in the presence of 1 % water, a new peak appeared at  $m/z$  1985.862, corresponding to  $[\text{L} + \text{Hg}^{2+} + \text{H}_2\text{O} + \text{H}]^+$ , which revealed the water molecule involvement of  $\text{Hg}^{2+}/\text{L}$  complexation (Figure 15). Thus we presumed that binding of a water molecule to the  $\text{Hg}^{2+}$  center of the  $\text{L}/\text{Hg}^{2+}$  complex causes a redistribution in the energy levels of the  $\text{L}/\text{Hg}^{2+}$  complex,<sup>16</sup> or alternatively a water molecule may act as a donor ligand and reduces the electron withdrawing ability of the positive center of the  $\text{Hg}^{2+}$  ion *versus* the pyrene fluorophore.<sup>6c,17</sup> Both cases thus result in the enhancement of the fluorescence emission of pyrene in the  $\text{L}/\text{Hg}^{2+}$  complex.

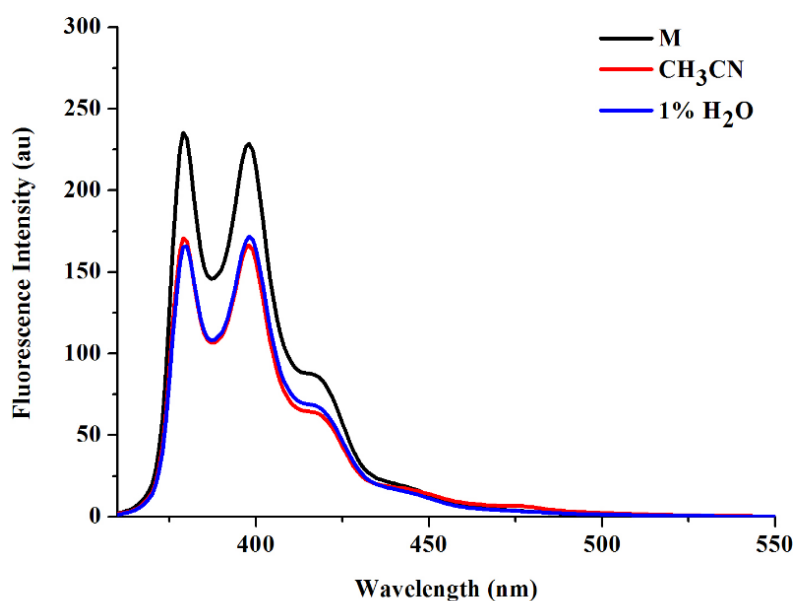


**Figure 16.** Fluorescence spectral changes of **M** (1.0  $\mu\text{M}$ ) upon sequential addition of 50 equiv. of  $\text{Hg}^{2+}$  and water in  $\text{CH}_3\text{CN}$ .  $\lambda_{\text{ex}} = 343$  nm.

Additionally, a monomeric analogue **M** was also synthesized as a reference compound and the fluorescence properties were evaluated under the same analytical conditions as used for **L**. It was found that the monomer emission of **M** was also quenched by the addition of 50 equiv. of  $\text{Hg}^{2+}$ , but the emission intensity cannot be retrieved in the presence of water (Figure 16). These results suggested that the three triazole ligands of the  $C_3$ -symmetric homooxacalix[3]arene scaffold play an important role in the complexation between the water molecule and  $\text{L}/\text{Hg}^{2+}$  complex.

On the basis of the fluorescence and NMR spectral evidence as well as our previous results, a plausible coordination-assisted fluorescence enhancement detection of  $\text{Hg}^{2+}$  is therefore depicted in Figure 17. A usual tetrahedral  $\text{Hg}^{2+}$ -ligand coordination structure may involve an intramolecular assembly process,<sup>18</sup> and the heavy atom effect of  $\text{Hg}^{2+}$  can be blocked by the complexation of the water molecule. Thus, the fluorescence emission of pyrene in the  $\text{L}/\text{Hg}^{2+}$  complex can be successfully revived.

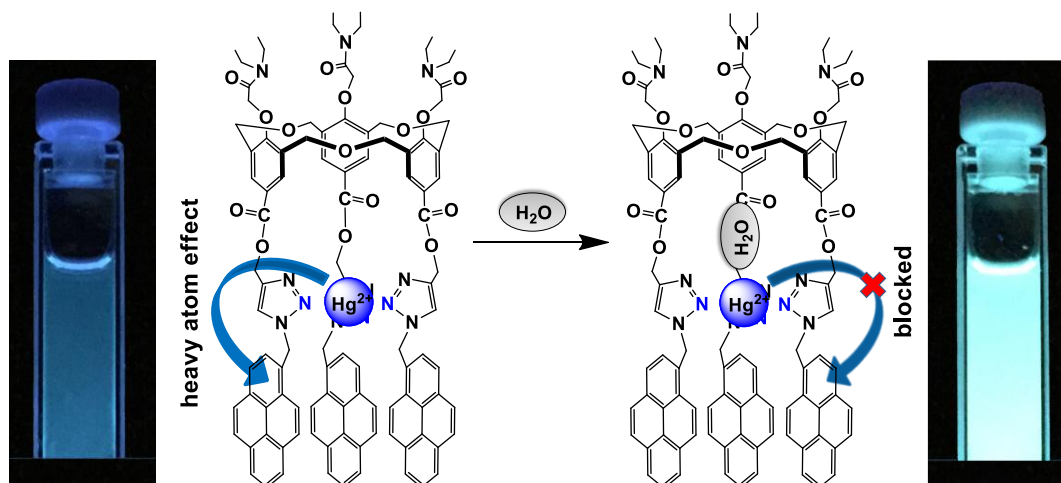


**Figure 17.** A plausible mechanism for the heavy atom effect blocked by water in the  $\text{L}/\text{Hg}^{2+}$  complex.

### 3.3 Conclusions

In conclusion, we have developed a novel fluorescence “on–off–on” chemosensor for  $\text{Hg}^{2+}$  via a water-assisted blocking heavy atom effect. Most importantly, the heavy atom effect and blocking thereof were demonstrated within the same system by the use of a  $C_3$ -symmetric homooxacalix[3]arene scaffold. The information obtained in this work can be considered an interesting contribution to the understanding of the blocking heavy atom effect and could be particularly useful in the design of new fluorescence enhancement chemosensors for HTM ions.

### 3.4 Experimental Section

### 3.4.1 General

Unless otherwise stated, all reagents used were purchased from commercial sources and used without further purification. All solvents used were dried and distilled by the usual procedures before use. All melting points were determined using a Yanagimoto MP-S1.  $^1\text{H}$  NMR and  $^{13}\text{C}$  NMR spectra were recorded on a Nippon Denshi JEOL FT-300 NMR spectrometer and a Varian-400MRvnmrs400 with  $\text{SiMe}_4$  as an internal reference:  $J$ -values are given in Hz. IR spectra were measured as KBr pellets or as liquid films on NaCl plates in a Nippon Denshi JIR-AQ2OM spectrophotometer. UV spectra were measured by a Shimadzu UV-3150UV-vis-NIR spectrophotometer. Fluorescence spectroscopic studies of compounds in solution were performed in a semi-micro fluorescence cell (Hellma®, 104F-QS,  $10 \times 4$  mm, 1400  $\mu\text{L}$ ) with a Varian Cary Eclipse spectrophotometer. Mass spectra were obtained on a Nippon Denshi JMS-01SG-2 mass spectrometer at an ionization energy of 70 eV using a direct inlet system through GLC.

### 3.4.2 Materials

Compounds **1**<sup>9</sup> and 1-azidomethylpyrene<sup>19</sup> were prepared following the reported procedures.

#### 3.4.2.1 Synthesis of compound **2**

A solution of compound **1** (300 mg, 0.34 mmol), propargyl bromide (134 mg, 1.12 mmol) in acetone (50 mL) and  $\text{K}_2\text{CO}_3$  (470 mg, 3.4 mmol) were heated at reflux for 24 h. The solvent was evaporated and the residue partitioned between 10% HCl and  $\text{CH}_2\text{Cl}_2$ . The organic layer was separated and dried ( $\text{MgSO}_4$ ) and the solvents were evaporated. The residue was purified by column chromatography on silica gel with chloroform as eluent to yield the desired compound **2** (224 mg, 76 %). M.p. 131–132°C.  $^1\text{H}$  NMR (400 MHz,  $\text{CDCl}_3$ ):  $\delta$  = 1.12–1.21 (dt, 18H,  $\text{NCH}_2\text{CH}_3$ ), 2.51 (s, 3H,  $-\text{C}\equiv\text{CH}$ ), 3.28–3.41 (dq, 12H,  $\text{NCH}_2\text{CH}_3$ ), 4.49–4.52 (d, 6H,  $\text{ArCH}_2(\text{eq})\text{O}$ ,  $J$  = 13.2 Hz), 4.66 (s, 6H,  $\text{ArO}-\text{CH}_2$ ), 4.86 (s, 6H,  $\text{C}=\text{O}-\text{OCH}_2$ ), 4.87–4.91 (d, 6H,  $\text{ArCH}_2(\text{ax})\text{O}$ ,  $J$  = 13.2 Hz), 7.58 (s, 6H,  $\text{ArH}$ ).  $^{13}\text{C}$  NMR

(100 MHz, CDCl<sub>3</sub>)  $\delta$  = 12.98, 14.32, 40.11, 41.06, 52.19, 68.93, 72.26, 74.72, 78.13, 125.08, 131.86, 132.03, 159.90, 164.72, 166.84. HRMS  $m/z$  Calcd for C<sub>54</sub>H<sub>64</sub>N<sub>3</sub>O<sub>15</sub> [M+H]<sup>+</sup>: 994.4337 Found: 994.4335 [M+H]<sup>+</sup>.

### 3.4.2.2 Synthesis of compound **L**

Copper iodide (10 mg) was added to compound **2** (200 mg, 0.20 mmol) and 1-azidomethylpyrene (170 mg, 0.66 mmol) in a 30 mL mixture of THF/H<sub>2</sub>O (5:1, v/v) and the mixture was heated at 70 °C for 24 h. The resulting solution was cooled and extracted twice with CH<sub>2</sub>Cl<sub>2</sub>. The organic layer was dried over MgSO<sub>4</sub> and the solvent was removed under reduced pressure. The residue obtained was purified over a silica gel column eluting with ethyl acetate to afford the desired material **L** (242 mg, 72 %) as a white solid. M.p. 184–185 °C. <sup>1</sup>H NMR (400 MHz, CDCl<sub>3</sub>):  $\delta$  = 1.06–1.12 (q, 18H, NCH<sub>2</sub>CH<sub>3</sub>), 3.18–3.34 (dq, 12H, NCH<sub>2</sub>CH<sub>3</sub>), 3.93–3.96 (d, 6H, ArCH<sub>2</sub>(eq)O,  $J$  = 12.8 Hz), 4.45 (s, 6H, ArO–CH<sub>2</sub>), 4.58–4.61 (d, 6H, ArCH<sub>2</sub>(ax)O,  $J$  = 12.8 Hz), 5.18 (s, 6H, C=O–OCH<sub>2</sub>), 5.96 (s, 6H, triazole–CH<sub>2</sub>–pyrene), 7.12 (s, 6H, ArH), 7.68–7.81 (m, 21H, pyrene–H (18H) and triazole–H (3H); overlapped), 7.87–7.89 (d, 3H, pyrene–H,  $J$  = 8.0 Hz), 7.93–7.95 (d, 3H, pyrene–H,  $J$  = 8.0 Hz), 8.03–8.05 (d, 3H, pyrene–H,  $J$  = 8.0 Hz). <sup>13</sup>C NMR (100 MHz, CDCl<sub>3</sub>)  $\delta$  = 12.91, 14.21, 39.96, 40.89, 51.94, 57.97, 68.68, 71.96, 121.76, 123.99, 124.36, 124.48, 124.61, 124.71, 125.32, 125.42, 125.88, 126.79, 126.85, 127.40, 127.75, 128.51, 130.13, 130.72, 131.57, 131.70, 131.77, 143.54, 159.96, 165.21, 166.81. HRMS  $m/z$  Calcd for C<sub>105</sub>H<sub>97</sub>N<sub>12</sub>O<sub>15</sub> [M+H]<sup>+</sup>: 1766.7230 Found: 1766.7228 [M+H]<sup>+</sup>.

The monomeric compound **M** was also synthesized in 78 % yield as a reference compound by following a similar protocol. M.p. 66–67 °C. <sup>1</sup>H NMR (400 MHz, CDCl<sub>3</sub>):  $\delta$  = 1.10–1.21 (dt, 6H, NCH<sub>2</sub>CH<sub>3</sub>), 3.32–3.41 (m, 4H, NCH<sub>2</sub>CH<sub>3</sub>), 4.68 (s, 2H, ArO–CH<sub>2</sub>), 5.32 (s, 2H, C=O–OCH<sub>2</sub>), 6.25 (s, 2H, triazole–CH<sub>2</sub>–pyrene), 6.87–6.89 (d, 2H, ArH,  $J$  = 8.0 Hz), 7.45 (s, 1H, triazole–H), 7.88–7.90 (d, 2H, ArH,  $J$  = 8.0 Hz), 7.96–7.98 (d, 1H, pyrene–H,  $J$  = 8.0 Hz), 8.04–8.25 (m, 8H, pyrene–H). <sup>13</sup>C NMR (100 MHz, CDCl<sub>3</sub>)  $\delta$  = 12.74, 14.26, 40.34, 41.48, 52.38, 57.77, 67.18, 114.21, 121.82, 122.80, 123.69, 124.38, 124.89, 124.98, 125.76, 125.86, 126.31, 126.56, 127.14, 127.60, 128.23, 128.99, 129.20, 130.48, 131.08, 131.73, 132.08, 143.35, 161.90, 165.81, 166.16. HRMS  $m/z$  Calcd for C<sub>33</sub>H<sub>31</sub>N<sub>4</sub>O<sub>4</sub> [M+H]<sup>+</sup>: 547.2345 Found: 547.2344 [M+H]<sup>+</sup>.

### 3.4.3 General Procedure for the UV-vis and Fluorescence Titrations

For absorption or fluorescence measurements, compounds were dissolved in acetonitrile to obtain stock solutions (1 mM). The stock solutions were diluted with acetonitrile to the desired concentration. Stock solutions ( $10^{-3}$  M) of perchlorate salts ( $\text{Li}^+$ ,  $\text{Na}^+$ ,  $\text{K}^+$ ,  $\text{Cs}^+$ ,  $\text{Ag}^+$ ,  $\text{Cu}^{2+}$ ,  $\text{Pb}^{2+}$ ,  $\text{Zn}^{2+}$ ,  $\text{Co}^{2+}$ ,  $\text{Ni}^{2+}$ ,  $\text{Cr}^{3+}$ ,  $\text{Al}^{3+}$ ,  $\text{Cd}^{2+}$ ,  $\text{Hg}^{2+}$ ,  $\text{Fe}^{2+}$  and  $\text{Fe}^{3+}$ ) were prepared with water. In titration experiments, typically, aliquots of freshly prepared standard solutions ( $10^{-3}$  M to  $10^{-6}$  M) of various analytes in water were added to record the UV-vis and fluorescence spectra. The fluorescence spectra were performed with the excitation wavelength 343 nm.

### 3.5 References

1. (a) H. Zhu, J. Fan, B. Wang and X. Peng, *Chem. Soc. Rev.*, 2015, **44**, 4337–4366; (b) Z. Liu, W. He and Z. Guo, *Chem. Soc. Rev.*, 2013, **42**, 1568–1600; (c) H. N. Kim, W. X. Ren, J. S. Kim and J. Yoon, *Chem. Soc. Rev.*, 2012, **41**, 3210–3244; (d) J. H. Jung, J. H. Lee and S. Shinkai, *Chem. Soc. Rev.*, 2011, **40**, 4464–4474; (e) D. T. Quang and J. S. Kim, *Chem. Rev.*, 2010, **110**, 6280–6301; (f) Q. Zhao, F. Li and C. Huang, *Chem. Soc. Rev.*, 2010, **39**, 3007–3030.
2. (a) H. Zhu, J. Fan, B. Wang and X. Peng, *Chem. Soc. Rev.*, 2015, **44**, 4337–4366; (b) K. P. Carter, A. M. Young and A. E. Palmer, *Chem. Rev.*, 2014, **114**, 4564–4601; (c) Z. Liu, W. He and Z. Guo, *Chem. Soc. Rev.*, 2013, **42**, 1568–1600; (d) H. N. Kim, W. X. Ren, J. S. Kim and J. Yoon, *Chem. Soc. Rev.*, 2012, **41**, *Chem. Soc. Rev.*, 2012, **41**, 3210–3244.
3. D. S. McClure, *J. Chem. Phys.*, 1952, **20**, 682–686.
4. A. W. Varnes, R. B. Dodson and E. L. Wehry, *J. Am. Chem. Soc.*, 1972, **94**, 946–950.
5. (a) G. Sivaraman, T. Anand and D. Chellappa, *RSC Advances*, 2012, **2**, 10605–10609; (b) R. Martínez, F. Zapata, A. Caballero, A. Espinosa, A. Tárraga and P. Molina, *Org. Lett.*, 2006, **8**, 3235–3238; (c) K. Rurack, M. Kollmannsberger, U. Resch-Genger and J. Daub, *J. Am. Chem. Soc.*, 2000, **122**, 968–969; (d) K. Rurack, U. Resch-Genger and W. Rettig, *J. Photochem. Photobiol. A*, 1998, **118**, 143–216.
6. (a) K. Rurack, *Spectrochim. Acta. Part A*, 2001, **57**, 2161–2195; (b) L. Fabbrizzi, M. Licchelli, P. Pallavicini, A. Perotti and D. Sacchi, *Angew. Chem., Int. Ed.*, 1994, **33**, 1975–1977; (c) H. Masuhara, H. Shioyama, T. Saito, K. Hamada, S. Yasoshima and N.

- Mataga, *J. Phys. Chem.*, 1984, **88**, 5868–5873; (d) P. Svejda, A. H. Maki and R. R. Anderson, *J. Am. Chem. Soc.*, 1978, **100**, 7138–7145.
7. (a) Z. Xu, S. J. Han, C. Lee, J. Yoon and D. R. Spring, *Chem. Commun.*, 2010, **46**, 1679–1681; (b) Z. Xu, J. Yoon and D. R. Spring, *Chem. Commun.*, 2010, **46**, 2563–2565.
8. X. L. Ni, Y. Wu, C. Redshaw and T. Yamato, *Dalton Trans.*, 2014, **43**, 12633–12638.
9. X. L. Ni, J. Tahara, S. Rahman, X. Zeng, D. L. Hughes, C. Redshaw and T. Yamato, *Chem. Asian J.*, 2012, **7**, 519–527.
10. (a) D. Udhayakumari, S. Velmathi, Y. M. Sung and S. P. Wu, *Sens. Actuators B.* 2014, **198**, 285–293; (b) E. Manandhar and K. J. Wallace, *Inorg. Chim. Acta.* 2012, **381**, 15; (c) P. K. Lekha and E. Prasad, *Chem. Eur. J.*, 2011, **17**, 8609–8617.
11. (a) S. Hussain, A. H. Malik, M. A. Afroz and P. K. Iyer, *Chem. Commun.*, 2015, **51**, 7207–7210; (b) C. Zhang, K. Ji, X. Wang, H. Wu and C. Liu, *Chem. Commun.*, 2015, **51**, 8173–8176.
12. (a) K. Boonkitpatarakul, J. Wang, N. Niamnont, B. Liu, L. McDonald, Y. Pang and M. Sukwattanasinitt, *ACS Sens.*, 2016, **1**, 144–150; (b) V. Béreau, C. Duhayon and J. P. Sutter, *Chem. Commun.*, 2014, **50**, 12061–12064.
13. (a) N. J. Wang, C. M. Sun and W. S. Chung, *Sens. Actuators B.*, 2014, **171**, 984–993; (b) F. Miao, J. Zhan, Z. Zou, D. Tian and H. Li, *Tetrahedron*, 2012, **68**, 2409–2413; (c) X. L. Ni, S. Wang, X. Zeng, Z. Tao and T. Yamato, *Org. Lett.*, 2010, **13**, 552–555; (d) S. Y. Park, J. H. Yoon, C. S. Hong, R. Souane, J. S. Kim, S. E. Matthews and J. Vicens, *J. Org. Chem.*, 2008, **73**, 8212–8218.
14. (a) A. Ikeda, H. Udzu, Z. Zhong, S. Shinkai, S. Sakamoto and K. Yamaguchi, *J. Am. Chem. Soc.*, 2001, **123**, 3872–3877; (b) A. Ikeda, Y. Suzuki, M. Yoshimura and S. Shinkai, *Tetrahedron.*, 1998, **54**, 2497; (c) K. Araki, N. Hashimoto, H. Otsuka and S. Shinkai, *J. Org. Chem.*, 1993, **58**, 5958–5963.
15. C. Wu, Y. Ikejiri, J. L. Zhao, X. K. Jiang, X. L. Ni, X. Zeng, C. Redshaw and T. Yamato, *Sens. Actuators B.*, 2016, **228**, 480–485.
16. (a) S. R. Tamang, J. H. Son and J. D. Hoefelmeyer, *Dalton Trans.*, 2014, **43**, 7139–7145; (b) C. N. Burrell, M. I. Bodine, O. Elbjeirami, J. H. Reibenspies, M. A. Omary and F. P. Gabbaï, *Inorg. Chem.*, 2007, **46**, 1388–1395.
17. B. Valeur and I. Leray, *Coord. Chem. Rev.*, 2000, **205**, 3–40.

18. Selected references on tetrahedral  $\text{Hg}^{2+}$ -ligand coordination geometry: (a) A. K. Mandal, M. Suresh, P. Das, E. Suresh, M. Baidya, S. K. Ghosh and A. Das, *Org. Lett.*, 2012, **14**, 2980–2983; (b) M. Suresh, A. K. Mandal, S. Saha, E. Suresh, A. Mandoli, R. D. Liddo, P. P. Parnigotto and A. Das, *Org. Lett.*, 2010, **12**, 5406–5409; (c) Y. Liu, X. Wan and F. Xu, *Organometallics*, 2009, **28**, 5590–5592; (d) X. F. Wang, Y. Lv, T. Okamura, H. Kawaguchi, G. Wu, W. Y. Sun and N. Ueyama, *Crystal Growth & Design*, 2007, **7**, 1125–1133; (e) J. Wang, X. Qian and J. Cui, *J. Org. Chem.*, 2006, **71**, 4308–4311; (f) C. Y. Su, A. M. Goforth, M. D. Smith and H. C. Loye, *Inorg. Chem.*, 2003, **42**, 5685–5692.
19. K. W. Huang, Y. R. Wu, K. U. Jeong and S. W. Kuo, *Macromolecular Rapid Communications*, 2013, **34**, 1530–1536.

## Chapter 4

# **Click-modified Hexahomotrioxacalix[3]arenes as Fluorometric and Colorimetric Dual-modal Chemosensors for 2,4,6-Trinitrophenol**

*This chapter described a new type of chemosensor-based approach to the detection of 2,4,6-trinitrophenol (TNP). Two hexahomotrioxacalix[3]arene-based chemosensors were synthesized through click chemistry, which exhibited high binding affinity and selectivity toward TNP as evidenced by UV-vis and fluorescence spectroscopy studies.*



## 4.1 Introduction

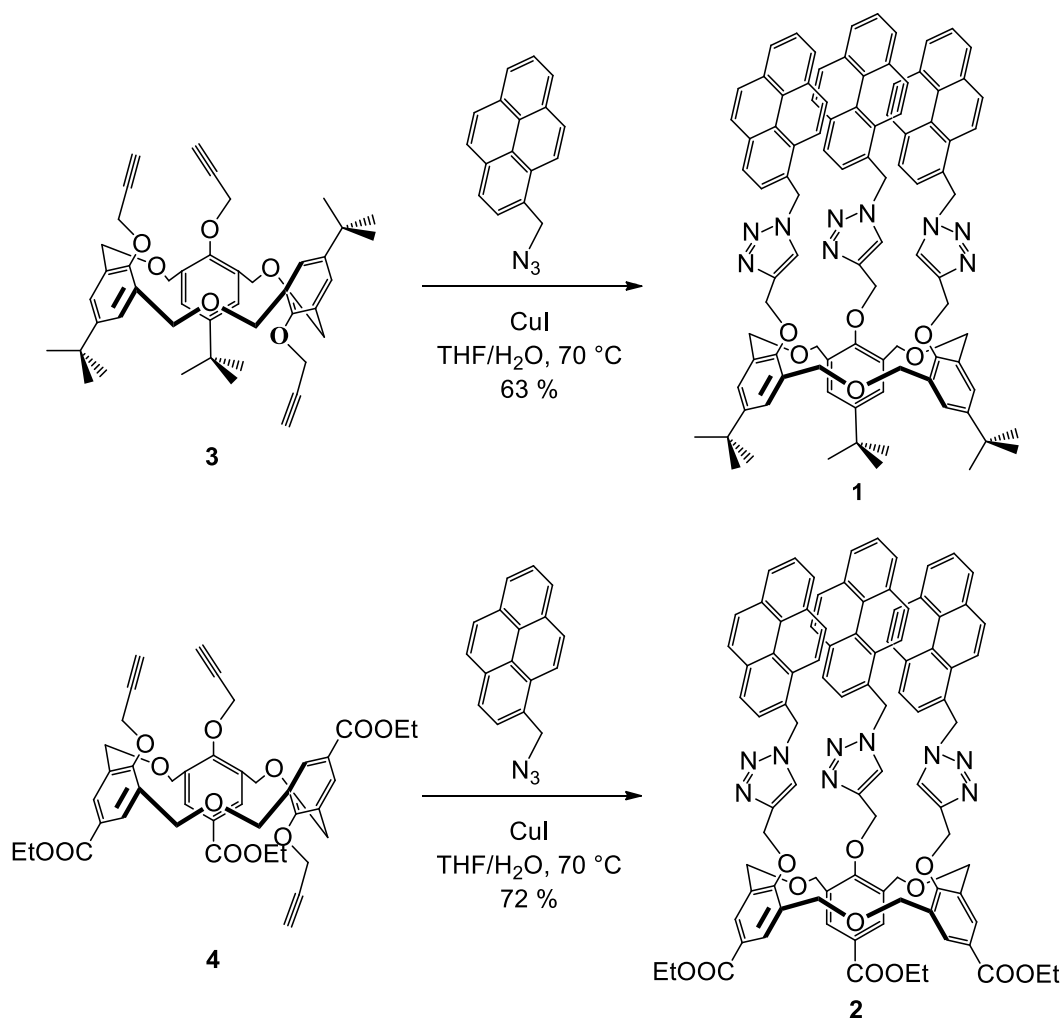
The design of chemosensors that are able to selectively recognize and sense specific analytes is an attractive research area in supramolecular chemistry.<sup>1</sup> In particular, the rapid and accurate detection of nitro-containing explosives is a high priority for security and health/environmental issues.<sup>2</sup> Various analytical techniques such as gas chromatography coupled with different detectors,<sup>3</sup> high performance liquid chromatography,<sup>4</sup> ion-mobility spectroscopy,<sup>5</sup> Raman or surface enhanced Raman spectroscopy,<sup>6</sup> electrochemical methods<sup>7</sup> and fluorescence spectroscopy<sup>8</sup> have been used for the detection of nitro-containing explosives. Among these techniques, fluorescence-based detection offers several advantages over other analytical methods with respect to high sensitivity, specificity, and real-time monitoring with fast response times.<sup>9</sup> To date, considerable effort has been devoted to the development of fluorescence sensing materials to detect nitro-containing explosives.<sup>10</sup> Even though several  $\pi$ -conjugated polymers<sup>11</sup> and metal-organic frameworks<sup>12</sup> have been employed to detect nitro-containing explosives, the development of reliable and efficient organic chemosensors possessing high selectivity for nitro-containing explosives remains a very challenging task.<sup>13</sup>

Calixarenes are ideal frameworks for the development of chemosensors in the molecular recognition of chemical and biological targets of interest since the incorporation of a suitable sensory group into the calixarene results in a tailored chromogenic receptor.<sup>14</sup> In particular, since Sharpless et al. developed click chemistry as a new coupling strategy in 2001,<sup>15</sup> numerous calixarene derivatives incorporating click-derived triazoles have been reported, which can be used as metal ions chemosensors via coordination at nitrogen atom.<sup>16</sup> However, these fluorescence systems have scarcely been exploited for the sensing of nitro-containing explosives. As a matter of fact, given the strong dipolar character of the triazole ring, the C–H bond of the heterocycle makes a surprisingly good hydrogen bond donor.<sup>17</sup> On the other hand, nitro-containing explosives often act as good electron acceptors due to the presence of electron withdrawing nitro ( $-\text{NO}_2$ ) group/s.<sup>18</sup> Considering these two opposite properties of triazole and nitro-containing explosives, one might consider if noncovalent interactions exist between them?

In molecular recognition processes, noncovalent interactions such as hydrogen bonding, aromatic  $\pi$ -stacking and weak intermolecular interactions play a crucial role. With this in mind, can we utilize the click-derived triazole to design chemosensors for nitro-containing explosive sensing? Herein, we report two triazole-modified hexahomotrioxacalix[3]arenes **1** and **2** as a new type of chemosensor for the selective detection of 2,4,6-trinitrophenol (TNP) explosive. To the best of our knowledge, this is the first report where a triazole-modified hexahomotrioxacalix[3]arene serves as a selective chemosensor for TNP.

## 4.2 Results and Discussion

### 4.2.1 Syntheses of Fluorescent Chemosensor **1** and **2**



**Scheme 1.** The synthetic route of fluorescent chemosensor **1** and **2**.

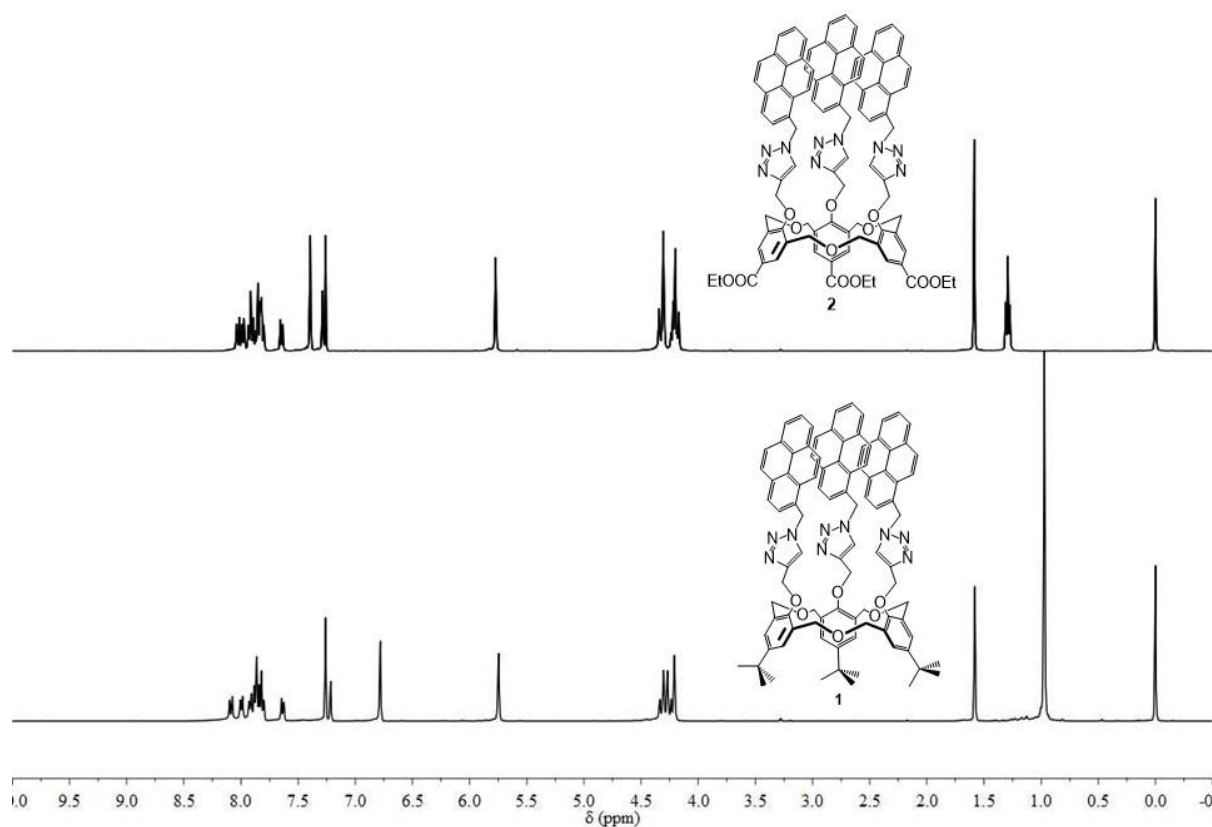


**Figure 1.** The  $^1\text{H}$  NMR spectra of chemosensors **1** and **2**.

The synthetic route for chemosensor **1** and **2** is described in Scheme 1. The Cu(I)-catalyzed 1,3-dipolar cycloaddition reaction of compound **3** or **4** with 1-azidomethylpyrene under Click conditions afforded the desired chemosensor **1** and **2** in the yield of 63 % and 72 %, respectively.  $^1\text{H}$  NMR spectra (Figure 1) of **1** showed the disappearance of the three terminal alkyne protons, whereas the new singlet appearing around  $\delta = 7.21$  ppm was attributed to the protons of the newly formed triazole groups. Moreover, the other peaks were observed as three singlets assignable to the protons in the  $\text{ArOCH}_2$ , triazole- $\text{CH}_2$ , and aromatic protons, and a AB quartet for the  $\text{ArCH}_2\text{OCH}_2\text{Ar}$  methylene protons. These findings supported the conclusion that the hexahomotrioxacalix[3]arene skeleton was immobilized in the *cone* conformation. These spectral properties also indicated that **1** possesses a  $C_3$  symmetry, which was further corroborated by the  $^{13}\text{C}$  NMR spectrum. **1** should theoretically show a *partial-cone* conformation, but interestingly the conformation converted from the

*partial-cone* **3** to *cone* **1** during the ‘click’ reaction. In this process, the Cu(I) might be employed as a metal template, which can hold the alkyne groups on the same side of the hexahomotrioxacalix[3]arene and the conformation was immobilized to the *cone*.<sup>19</sup> The Cu(I) not only catalyzed the cycloaddition of alkynes and azides, but also produced a metal template effect. It is worth highlighting that this synthesis approach opens up a new strategy to synthesize the *cone* conformational hexahomotrioxacalix[3]arene derivatives.

#### 4.2.2 Fluorescence and UV-vis Spectroscopy Studies

Sensors **1** and **2** exhibited almost identical spectral features (UV-vis and fluorescence). The UV-vis absorption spectra displayed absorption bands characteristic of pyrene with absorption maximum at 328 and 343 nm, while their emission spectra exhibited strong bands with excimer emission maximum at 484 nm upon excitation at 343 nm. To explore the potential application of compounds **1** and **2** as chemosensors for the detection of nitro-containing explosives, several analytes were used for fluorescence titration experiments. The fluorescence titration of **1** and **2** with TNP revealed that the fluorescence emission intensity rapidly died down upon addition of increasing amounts of TNP (Figure 2); the decrease in fluorescence emission could be readily observed under illumination at 365 nm (Figure 2a, insert). These results implied that there are strong interactions between the sensors and TNP, and that the quenching of fluorescence emission might occur due to the formation of a possible non-fluorescent complex. Based on the fluorescence titration results, the Stern–Volmer plot was found to be linear at lower concentrations (up to 100  $\mu\text{M}$ , Figure 3a), which indicates that fluorescence quenching involves a static quenching mechanism at lower concentrations of TNP. The Stern–Volmer constants were calculated to be  $K_{sv} = 2.23 \times 10^4 \text{ M}^{-1}$  (**1**) and  $K_{sv} = 1.04 \times 10^4 \text{ M}^{-1}$  (**2**), respectively. In particular, at higher concentrations, the plot was found to be a hyperbolic curve (Figure 3b), which may be attributed to a combination of both static and dynamic (collision) quenching.<sup>20</sup>

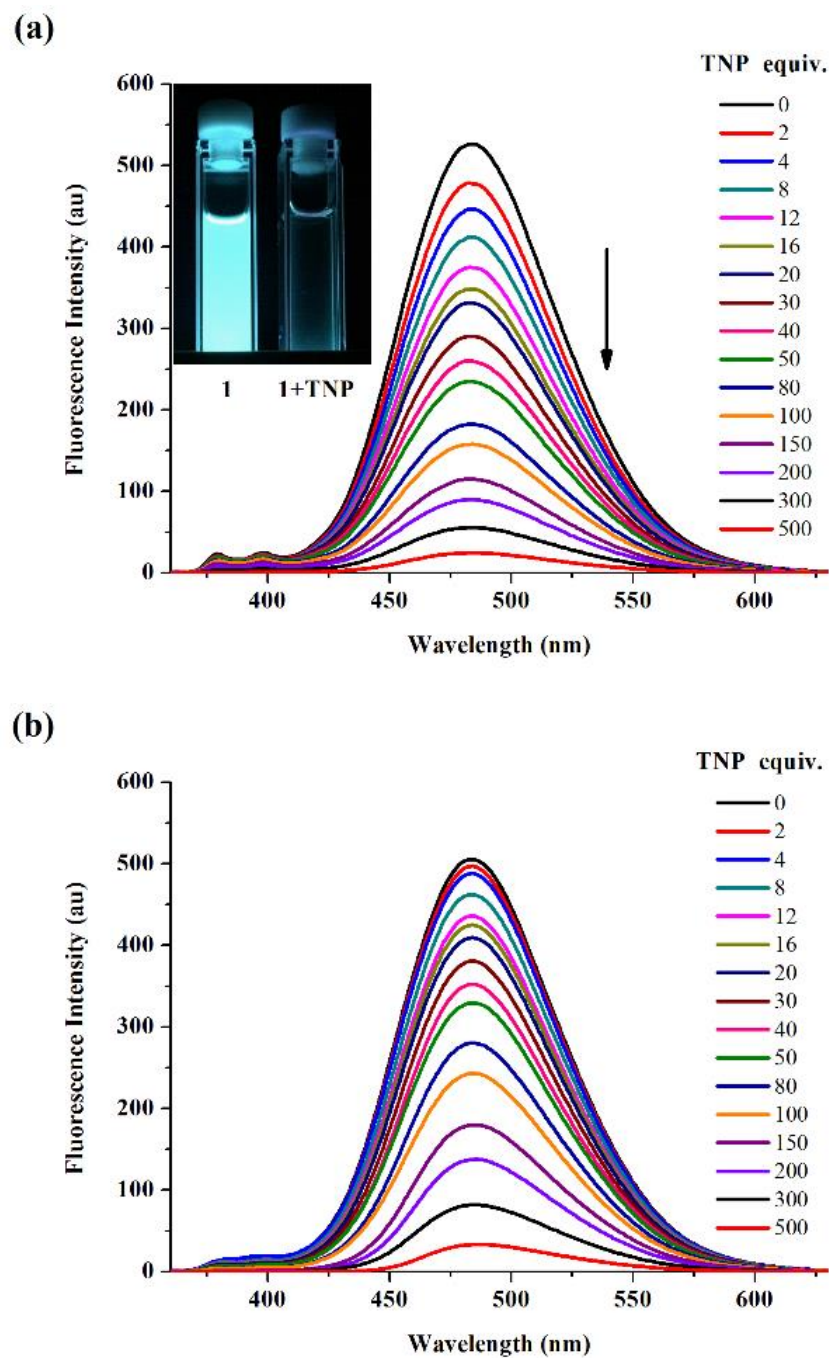


**Figure 2.** Fluorescence emission spectra of (a) **1** and (b) **2** upon the addition of increasing concentrations of TNP in  $\text{CH}_3\text{CN}$ .  $\lambda_{\text{ex}} = 343 \text{ nm}$ . The inset shows the fluorescence color of chemosensor **1** before and after the addition of TNP.

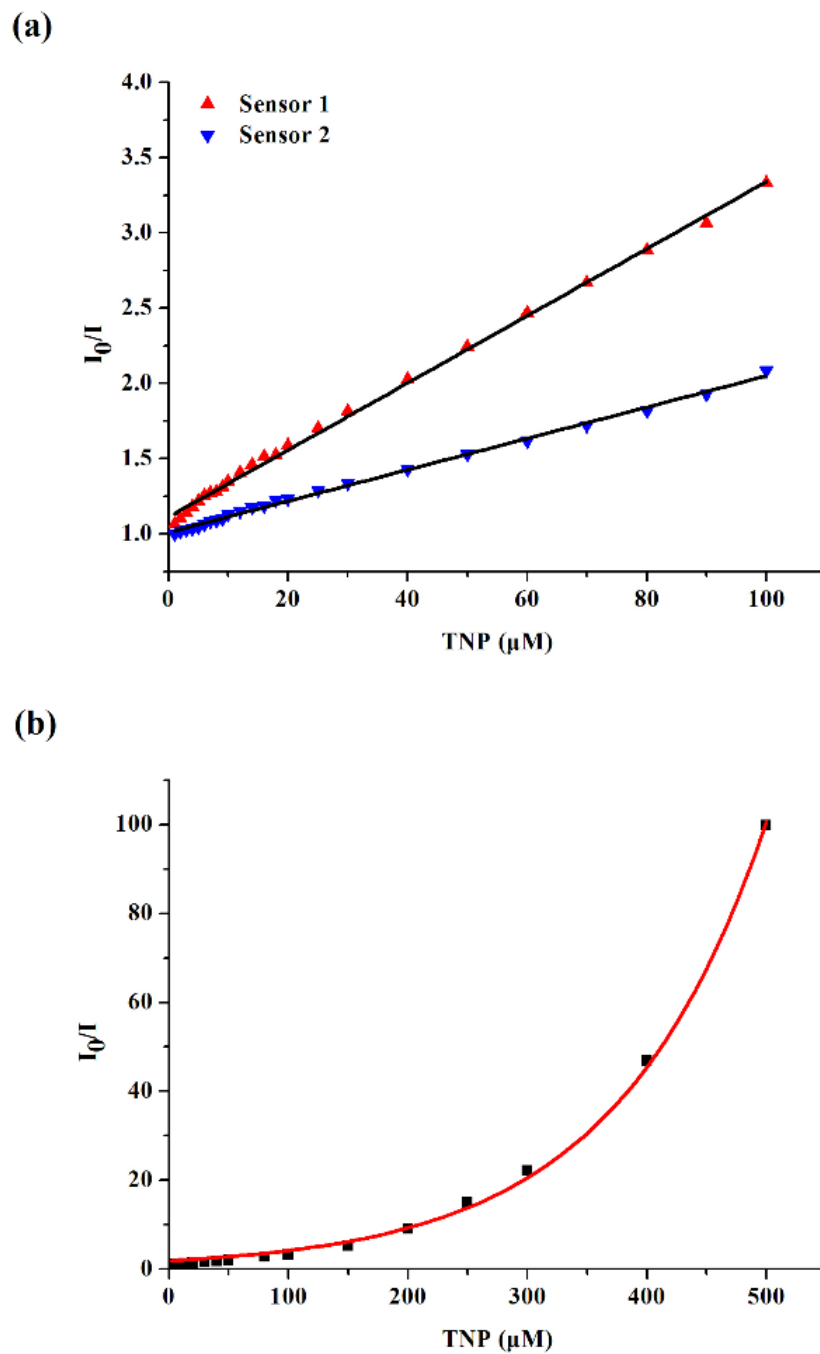


**Figure 3.** (a) Stern–Volmer plots for the titration of sensors **1** and **2** with TNP at lower concentrations (up to 100  $\mu\text{M}$ ); (b) The Stern–Volmer plot of sensor **1** with varied concentrations of TNP.

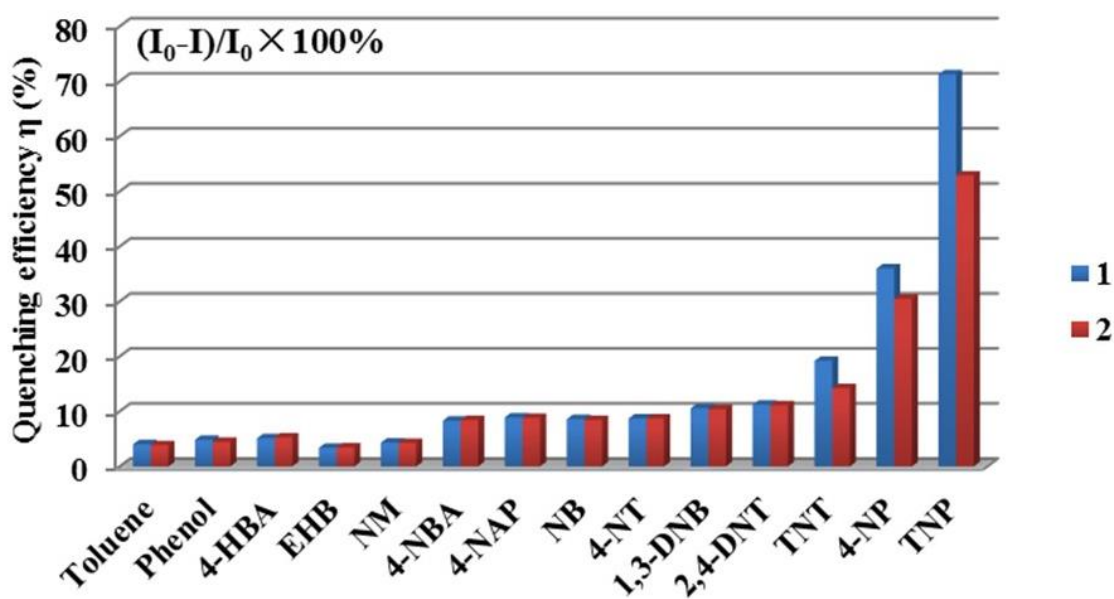


**Figure 4.** Reduction in fluorescence intensity (plotted as quenching efficiency) seen upon the addition of 100 equiv. of analytes. 4-HBA = 4-hydroxybenzoic acid, EHB = ethyl 4-hydroxybenzoate, NM = nitromethane, 4-NBA = 4-nitrobenzoic acid, 4-NAP = 4-nitroacetophenone, NB = nitrobenzene, 4-NT = 4-nitrotoluene, 1,3-DNB = 1,3-dinitrobenzene, 2,4-DNT = 2,4-dinitrotoluene, TNT = 2,4,6-trinitrotoluene, 4-NP = 4-nitrophenol and TNP = 2,4,6-trinitrophenol.

The relative fluorescence quenching efficiencies of various analytes towards sensors **1** and **2** are summarized in the bar diagram (Figure 4). The quenching efficiency was high for the electron deficient nitroaromatic compounds having an acidic -OH group. The order of the quenching efficiency was found to be TNP > NP, which is in complete agreement with the order of acidity of these analytes (TNP > NP). This may explain the unprecedented selectivity for TNP, as other nitro-compounds do not have a hydroxyl group and so they cannot interact strongly with the chemosensor and so result in a very low quenching effect. TNP, with its highly acidic hydroxyl group, interacts strongly with the chemosensor and results in very high fluorescence quenching. These results demonstrate that both chemosensors **1** and **2** have high selectivity for TNP compared to other nitro-compounds. Importantly, the detection limit for TNP lies in the ppb range (70 ppb for sensor **1**) (Figure 5) and the response time is very fast (seconds). Moreover, the extent of emission quenching of **1** in the presence of 100 equiv. of TNP after 10 seconds was practically

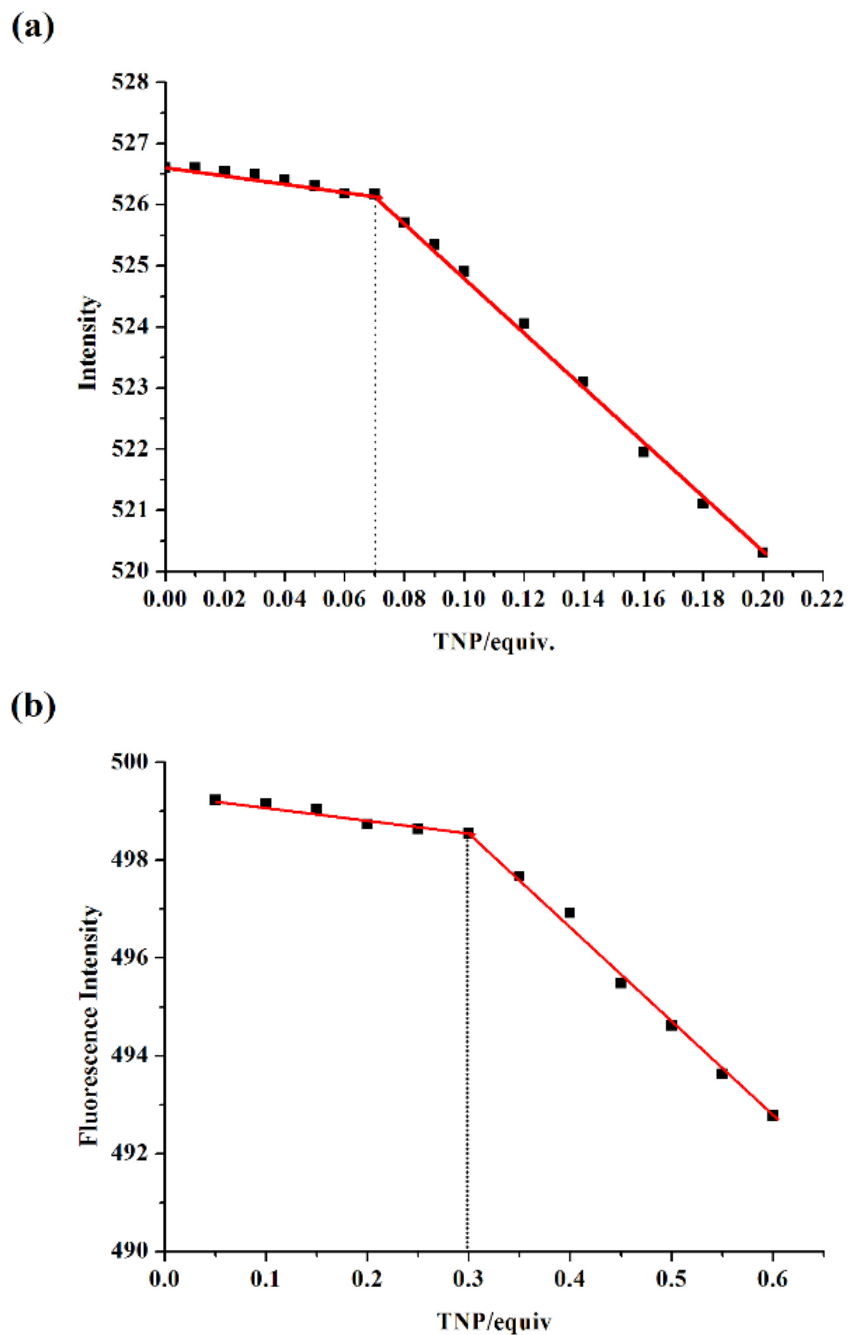


**Figure 5.** Plot for the detection limit of sensor (a) **1** and (b) **2** with TNP. Detection limit (DL) was calculated using the formula:  $DL = CL \times ET$ . (CL = Concentration of Ligand; ET = Equiv. of Titrant at which change observed).

identical to that after 2 hours (Figure 6). These experimental results demonstrate that compounds **1** and **2** can be used as fluorescent sensor for TNP detection. Furthermore, **1** and



**2** behave as better TNP sensor compared with many previous sensors reported in terms of selectivity, sensitivity and detection limit. This analyte-induced reduction in emission intensity is ascribed to the formation of charge-transfer complexes between the electron donor (chemosensor) and the electron acceptor (analyte).<sup>21</sup> Such a mechanistic rationale is consistent with previous reports in which it was suggested that thermodynamically favourable exciplex formation between a fluorophore and a quencher involves strong coupling of the respective  $\pi$  electrons, which in turn leads to deactivation of the fluorophore excited singlet state.<sup>22</sup>

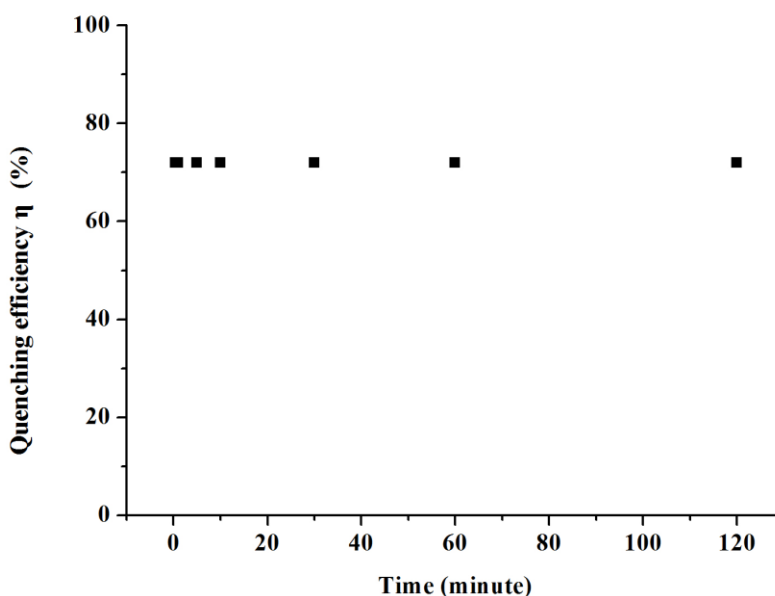


**Figure 6.** Plot of the quenching efficiency of **1** as a function of time in the presence of 100 equiv. of TNP.

The high sensitivity of sensor **1** towards TNP and the non-linear nature of the Stern–Volmer plot for TNP suggested that an energy transfer process might also be involved in the quenching process. As a matter of fact, when the absorption band of the non-emissive analyte display overlaps with the emission spectra of the fluorophore, resonance energy transfer can effectively occur.<sup>23</sup> As shown in Figure 7, a distinct spectral overlap of the absorption spectrum of TNP and the emission spectrum of sensor **1** over the range 375–475 nm was observed. In particular, there is a larger spectral overlap when TNP exists as picrate in the presence of the amine. Resonance energy transfer from sensor to picrate could make an additional contribution to the fluorescence quenching process.<sup>24</sup> Therefore, in

solution both charge-transfer and resonance energy transfer contributed to the amplified quenching of fluorescence of the present systems.

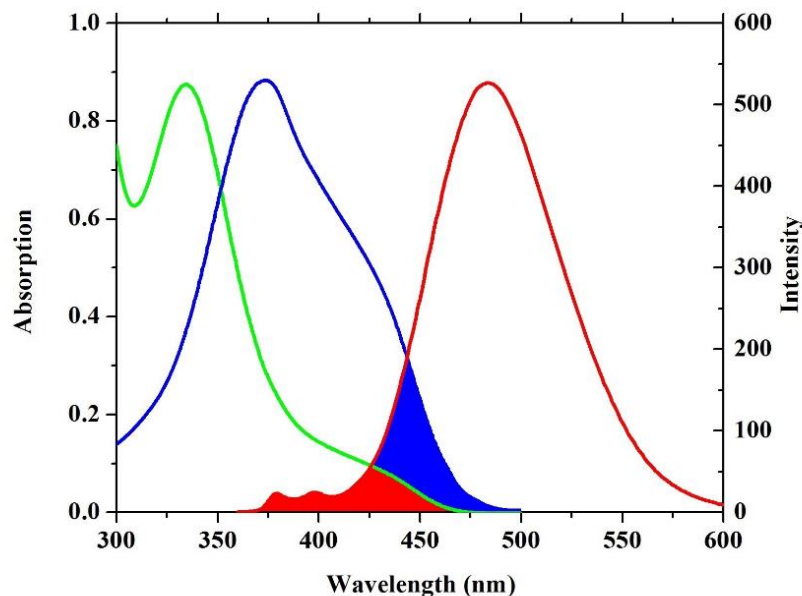


**Figure 7.** Spectral overlaps between absorption spectra of TNP (green line), TNP in the presence of amine (blue line) and the emission spectrum of **1** (red line).

Efforts were also made to determine whether sensor **1** could be used as a naked-eye detectable colorimetric chemosensor for TNP. As shown in Figure 8 (insert), on addition of TNP to solutions of **1**, a remarkable and easily visible color change was observed from pale yellow to reddish orange, which indicated the formation of the **1**•TNP complex. This color change is characterized by corresponding changes in the UV-Vis absorption spectrum. UV-Vis absorption titrations of **1** and **2** with TNP showed a steady increase in the peak intensity on increasing the concentration of TNP (Figure 8). It thus provides further support for the proposed charge-transfer interaction between the electron-rich receptor and the electron deficient analyte and is consistent with the proposed charge-transfer based fluorescence quenching. According to the titration results, a linear relationship between the absorption intensity (at 343 nm) and concentration of TNP was observed (Figure 9), which indicates that chemosensor **1** and **2** can be used for colorimetric detection of TNP.

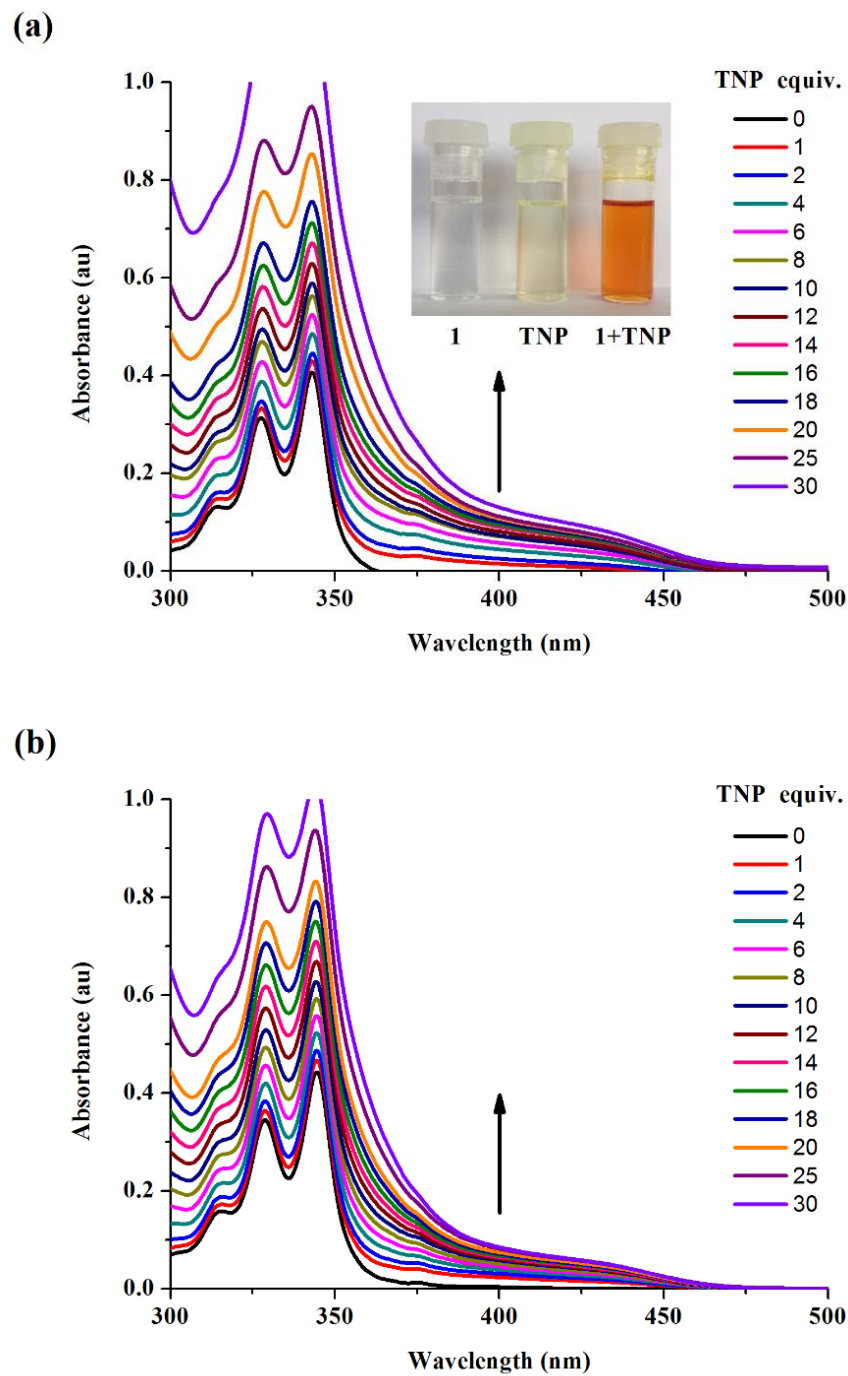
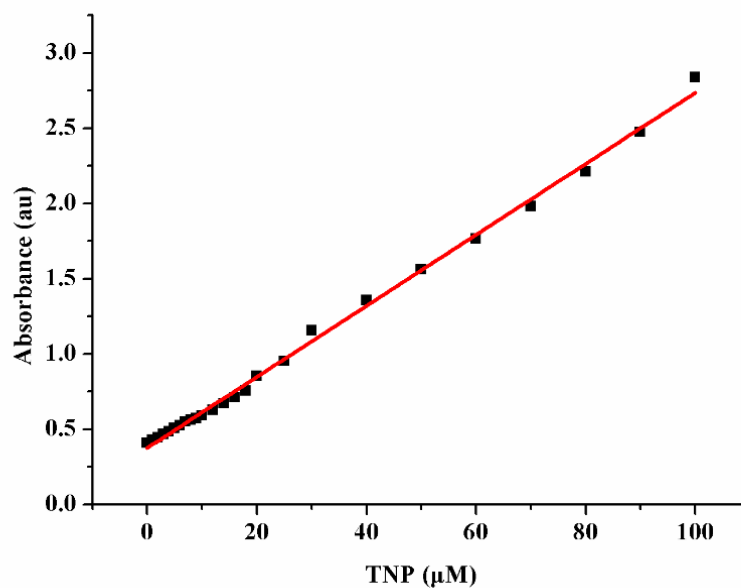


**Figure 8.** Change in absorption spectra of sensor (a) **1** and (b) **2** with the addition of TNP in  $\text{CH}_3\text{CN}$ . Inset: visual colour change due to the formation **1**•TNP complex.

(a)



(b)

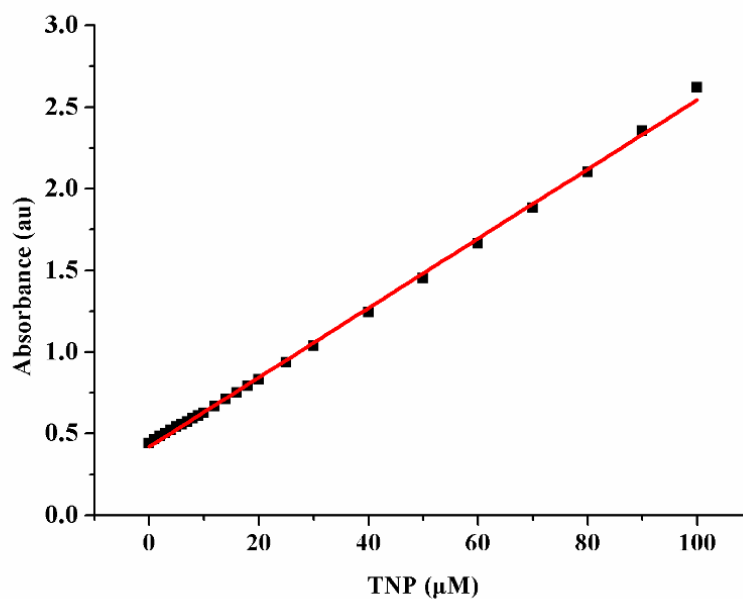


**Figure 9.** The relative absorption intensity change (343 nm) of sensor (a) **1** and (b) **2** to the different concentration of TNP.

In order to employ the detection in a feasible method, a test strip was conveniently prepared by dip coating a solution of **1** onto a filter paper and then subsequently drying in air. As shown in Figure 10, with the increase of TNP, there was an obvious difference of

quenching. When the concentration of TNP reached the 0.5 mM level, the fluorescence was completely quenched.

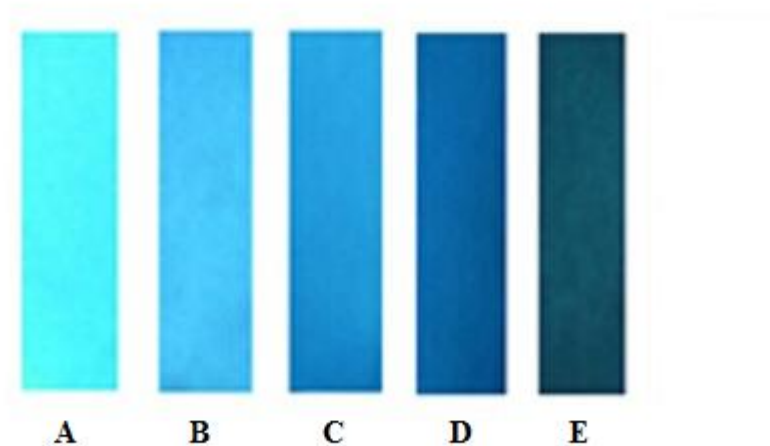


**Figure 10.** Photographs (under 365 nm UV light) of the fluorescence response of **1** on test strips after contact with various concentrations of TNP: (A) 0.0  $\mu\text{M}$ , (B) 5.0  $\mu\text{M}$ , (C) 10.0  $\mu\text{M}$ , (D) 100.0  $\mu\text{M}$  and (E) 0.5 mM.

#### 4.2.3 Proton NMR Titration Analysis

To explore the mechanism and to identify the actual binding position of TNP,  $^1\text{H}$  NMR titrations involving TNP and sensors **1** and **2** were performed. As shown in Figure 11, the signals of  $H_a$ ,  $H_b$  and  $H_c$  were clearly shifted downfield upon the addition of 15 equiv. of TNP into the solution of sensor **1** ( $\Delta\delta = 0.17$ , 0.47 and 0.14 ppm, respectively). In the case of sensor **2**, upon addition of 30 equiv. of TNP to the solution of **2**, the peaks for  $H_a$ ,  $H_b$  and  $H_c$  exhibited a similar but smaller downfield shift by  $\Delta\delta = 0.17$ , 0.33 and 0.13 ppm, respectively (Figure 12). From the spectral shifts, it was observed that proton  $H_b$  underwent the maximum chemical shift, whereas protons  $H_a$  and  $H_c$  proximal to the triazole rings underwent a smaller chemical shift. These downfield shifts were ascribed to TNP withdrawing electron density from the sensor. The significant change in the chemical shift of proton  $H_b$  suggested that the C–H bond of the triazole group acts as the receptor site. It is possible that  $\text{CH}\cdots\text{O}$  hydrogen bonding between  $H_b$  and TNP was formed, thus a plausible binding mode between **1** and TNP is presented (Figure 13). Hence, these results clearly

indicate that intermolecular charge transfer takes place between the sensor and TNP. Based on the differences in the induced fluorescence quenching response, greater changes in the chemical shift for sensor **1** were seen upon the addition of TNP than for sensor **2** (for the same number of molar equivalents). It suggests that sensor **1** is more effective and sensitive for the detection of TNP in comparison to sensor **2**.

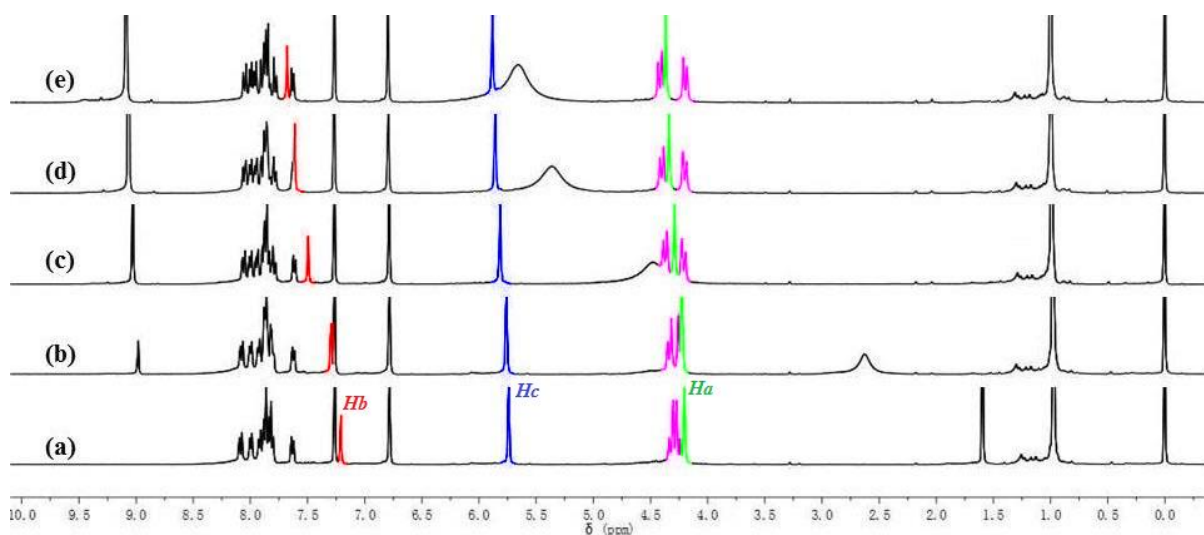


**Figure 11.** The  $^1\text{H}$  NMR spectra of **1** (5.0 mM) upon titration with TNP in  $\text{CDCl}_3$ . (a) **1** only, (b c d and e) in the presence of 1.0, 5.0, 10.0 and 15.0 equiv. of TNP, respectively.

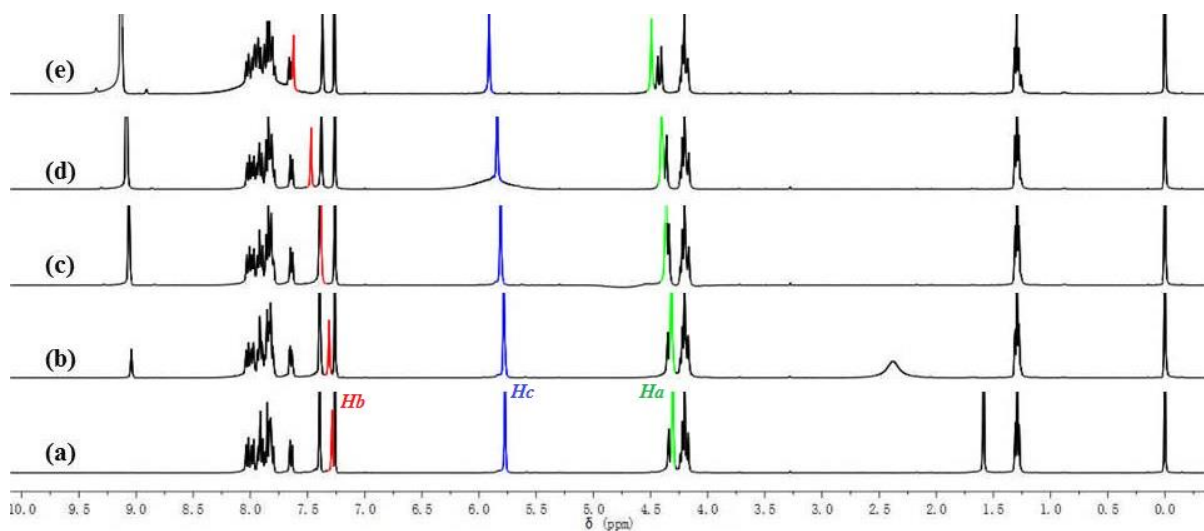


**Figure 12.** The  $^1\text{H}$  NMR spectrum of **2** (5.0 mM) upon titration with TNP in  $\text{CDCl}_3$ . (a) **2** only, (b c d and e) in the presence of 1.0, 5.0, 10.0 and 30.0 equiv. of TNP, respectively.

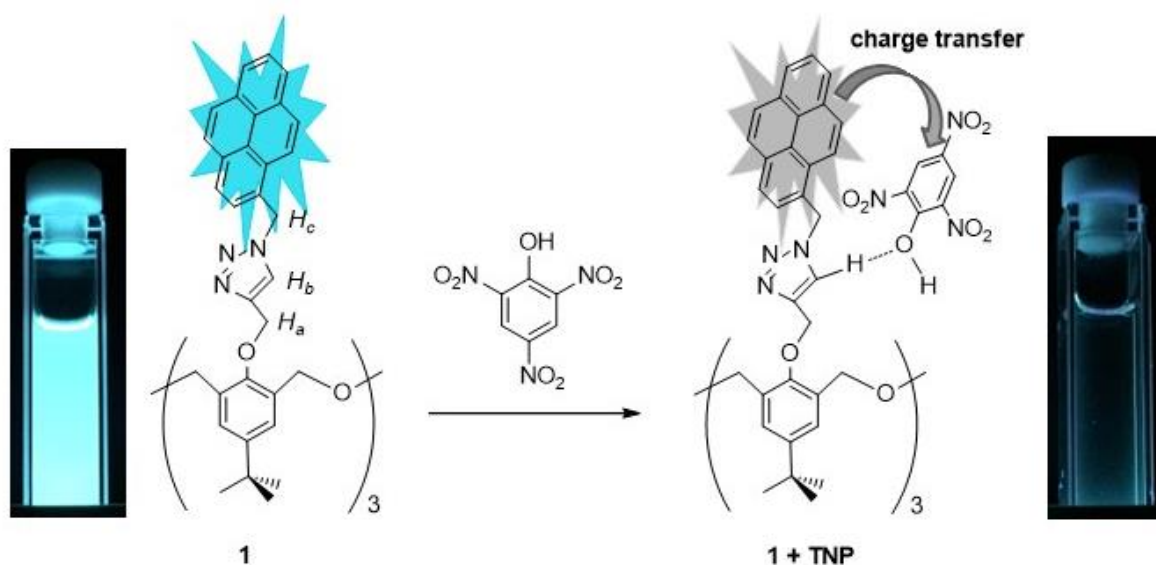


**Figure 13.** Plausible binding mode between **1** and TNP.

### 4.3 Conclusions

In summary, we have designed and synthesized two click-modified hexahomotrioxacalix[3]arenes **1** and **2**, each of which can be utilized as fluorometric and colorimetric chemosensor for 2,4,6-trinitrophenol. Chemosensor **1** and **2** exhibited high binding affinity and selectivity toward 2,4,6-trinitrophenol as evidenced by UV-vis and fluorescence studies.  $^1\text{H}$  NMR spectroscopic titrations revealed **1**•TNP complex formed via  $\text{CH}\cdots\text{O}$  hydrogen bonding interaction. As a general design strategy, structural modifications by click chemistry may allow us to develop further chemosensor candidates for the future detection of nitro-containing explosives.

## 4.4 Experimental Section

### 4.4.1 General

Unless otherwise stated, all reagents were purchased from commercial sources and used without further purification. All solvents were dried and distilled by the usual procedures before use. Melting points were determined using a Yanagimoto MP-S1.  $^1\text{H}$  NMR and  $^{13}\text{C}$  NMR spectra were recorded on a Nippon Denshi JEOL FT-300

NMR spectrometer and a Varian-400MRvnmrs400 with SiMe<sub>4</sub> as an internal reference: *J*-values are given in Hz. IR spectra were measured as KBr pellets or as liquid films on NaCl plates in a Nippon Denshi JIR-AQ2OM spectrophotometer. UV spectra were measured by a Shimadzu UV-3150UV-vis-NIR spectrophotometer. Fluorescence spectroscopic studies of compounds in solution were performed in a semi-micro fluorescence cell (Hellma®, 104F-QS, 10 × 4 mm, 1400 µL) with a Varian Cary Eclipse spectrophotometer. Mass spectra were obtained on a Nippon Denshi JMS-01SG-2 mass spectrometer at an ionization energy of 70 eV using a direct inlet system through GLC. Elemental analyses were performed by a Yanaco MT-5.

#### 4.4.2 General Procedure for Synthesis of Chemosensor 1 and 2

Compound **3**<sup>25</sup> and **4**<sup>26</sup> were prepared following the reported procedures. A solution of 1-azidomethylpyrene (230 mg, 0.89 mmol) and copper iodide (10 mg) was added to **3** (185 mg, 0.27 mmol) or **4** (200 mg, 0.27 mmol) in THF/H<sub>2</sub>O (v/v, 5:1, 30 mL), respectively, and the heterogeneous mixture was stirred at 70 °C for 24 h. The resulting solution was cooled and extracted twice with CH<sub>2</sub>Cl<sub>2</sub>. The organic extracts were combined, dried over MgSO<sub>4</sub>, and then evaporated to give the solid crude products. Column chromatography on silica gel eluting with 1:1 hexane/chloroform gave white solid compounds **1** and **2** in 63 % and 72 % yield, respectively.

*Compound 1.* Mp. 139–141 °C. <sup>1</sup>H NMR (400 MHz, CDCl<sub>3</sub>): δ = 0.97 (s, 27H, *t*Bu), 4.21 (s, 6H, ArO–CH<sub>2</sub>–triazole), 4.23–4.34 (AB q, 12H, ether bridge, *J* = 10.8 Hz), 5.75 (s, 6H, triazole–CH<sub>2</sub>–pyrene), 6.78 (s, 6H, ArH), 7.21 (s, 3H, triazole–H), 7.62–7.64 (d, 3H, pyrene–H, *J* = 7.6 Hz), 7.80–7.93 (m, 18H, pyrene–H), 7.99–8.00 (d, 3H, pyrene–H, *J* = 7.6 Hz), 8.07–8.10 (d, 3H, pyrene–H, *J* = 9.2 Hz). <sup>13</sup>C NMR (100 MHz, CDCl<sub>3</sub>) δ = 31.4, 34.1, 51.7, 66.8, 69.5, 121.9, 123.4, 124.1, 124.5, 124.7, 125.4, 125.5, 125.9, 126.0, 127.0, 127.2, 127.3, 127.9, 128.6, 128.7, 130.2, 130.8, 130.9, 131.6, 144.2, 146.2, 152.1. MS: *m/z* 1462.68 (M<sup>+</sup>). Anal. Calcd for C<sub>96</sub>H<sub>87</sub>N<sub>9</sub>O<sub>12</sub> (1462.77): C 78.82, H 5.99, N 8.62. Found: C 78.99, H 6.14, N 8.47.

*Compound 2.* Mp. 214–216 °C. <sup>1</sup>H NMR (400 MHz, CDCl<sub>3</sub>): δ = 1.27–1.31 (t, 9H,



COOCH<sub>2</sub>CH<sub>3</sub>,  $J = 6.8$  Hz), 4.17–4.20 (d, 6H, ArCH<sub>2</sub>(*eq*)O,  $J = 13.2$  Hz), 4.19–4.24 (q, 6H, COOCH<sub>2</sub>CH<sub>3</sub>,  $J = 6.8$  Hz), 4.31 (s, 6H, ArO–CH<sub>2</sub>–triazole), 4.31–4.34 (d, 6H, ArCH<sub>2</sub>(*ax*)O,  $J = 13.2$  Hz), 5.78 (s, 6H, triazole–CH<sub>2</sub>–pyrene), 7.29 (s, 3H, triazole–H), 7.39 (s, 6H, ArH), 7.64–7.66 (d, 3H, pyrene–H,  $J = 8.0$  Hz), 7.80–7.88 (m, 12H, pyrene–H), 7.90–7.94 (t, 6H, pyrene–H,  $J = 8.0$  Hz), 7.98–8.00 (d, 3H, pyrene–H,  $J = 8.0$  Hz), 8.02–8.04 (d, 3H, pyrene–H,  $J = 8.0$  Hz). <sup>13</sup>C NMR (100 MHz, CDCl<sub>3</sub>)  $\delta = 14.3, 51.8, 60.6, 66.9, 68.9, 121.7, 123.4, 124.1, 124.6, 124.7, 125.5, 125.6, 126.1, 126.1, 126.9, 127.0, 127.3, 127.9, 128.6, 128.7, 130.2, 130.8, 131.1, 131.7, 131.8, 143.6, 158.2, 165.4$ . FABMS:  $m/z$  1510.56 (M<sup>+</sup>), 1511.57(M+H<sup>+</sup>). Anal. calcd for C<sub>93</sub>H<sub>75</sub>N<sub>9</sub>O<sub>12</sub> (1510.64): C 73.94, H 5.00, N 8.34. found: C 73.89, H 5.04, N 8.36.

#### 4.4.3 General Procedure for the UV-vis and Fluorescence Titrations

For absorption or fluorescence measurements, compounds were dissolved in acetonitrile to obtain stock solutions (1 mM). The stock solutions were diluted with acetonitrile to the desired concentration. In titration experiments, typically, aliquots of freshly prepared standard solutions (10<sup>−3</sup> M to 10<sup>−6</sup> M) of various analytes in acetonitrile were added to record the UV-vis and fluorescence spectra.

#### 4.5 References

1. (a) X. Zhou, S. Lee, Z. Xu and J. Yoon, *Chem. Rev.*, 2015, **115**, 7944–8000; (b) Y. Zhou, J. F. Zhang and J. Yoon, *Chem. Rev.*, 2014, **114**, 5511–5571; (c) Y. Zhou and J. Yoon, *Chem. Soc. Rev.*, 2012, **41**, 52–67; (d) H. N. Kim, W. X. Ren, J. S. Kim and J. Yoon, *Chem. Soc. Rev.*, 2012, **41**, 3210–3244; (e) J. F. Zhang, Y. Zhou, J. Yoon and J. S. Kim, *Chem. Soc. Rev.*, 2011, **40**, 3416–3429; (f) J. Wu, W. Liu, J. Ge, H. Zhang and P. Wang, *Chem. Soc. Rev.*, 2011, **40**, 3483–3495.
2. (a) F. Akhgari, H. Fattahi and Y. M. Oskoei, *Sens. Actuators B*, 2015, **221**, 867–878; (b) J. S. Caygill, F. Davis and S. P. J. Higson, *Talanta*, 2012, **88**, 14–29.
3. (a) E. Holmgren, S. Ek and A. Colmsjö, *J Chromatogr. A*, 2012, **1222**, 109–115; (b) C. Cortada, L. Vidal and A. Canals, *Talanta*, 2011, **85**, 2546–2552.

4. (a) S. Schramm, D. Vailhen and M. C. Bridoux, *J. Chromatogr. A*, 2016, **1433**, 24–33; (b) S. Babaei and A. Beiraghi, *Anal. Chim. Acta*, 2010, **662**, 9–13.
5. (a) J. Lee, S. Park, S. G. Cho, E. M. Goh, S. Lee, S.-S. Koh and J. Kim, *Talanta*, 2014, **120**, 64–70; (b) M. Tabrizchi and V. Ilbeigi, *J. Hazard. Mater.*, 2010, **176**, 692–696.
6. (a) K. L. Gares, K. T. Hufziger, S. V. Bykov and S. A. Asher, *J. Raman Spectrosc.*, 2016, **47**, 124–141; (b) A. Hakonen, P. O. Andersson, M. S. Schmidt, T. Rindzevicius and M. Käll, *Anal. Chim. Acta*, 2015, **893**, 1–13.
7. (a) J. Riedel, M. Berthold and U. Guth, *Electrochimica Acta*, 2014, **128**, 85–90; (b) J. Zang, C. X. Guo, F. Hu, L. Yu and C. M. Li, *Anal. Chim. Acta*, 2011, **683**, 187–191.
8. (a) M. S. Meaney and V. L. McGuffin, *Anal. Chim. Acta*, 2008, **610**, 57–67; (b) R. Tu, B. Liu, Z. Wang, D. Gao, F. Wang, Q. Fang and Z. Zhang, *Anal. Chem.*, 2008, **80**, 3458–3465.
9. M. E. Germain and M. J. Knapp, *Chem. Soc. Rev.*, 2009, **38**, 2543–2555.
10. (a) X. Sun, Y. Wang and Y. Lei, *Chem. Soc. Rev.*, 2015, **44**, 8019–8061; (b) R. L. Woodfin, *Trace chemical sensing of explosives*, John Wiley & Sons, Inc., Hoboken, NJ, USA, 2006, pp. 193–209 (Chapter 9).
11. S. J. Toal and W. C. Trogler, *J. Mater. Chem.*, 2006, **16**, 2871–2883.
12. Z. Hu, B. J. Deibert and J. Li, *Chem. Soc. Rev.*, 2014, **43**, 5815–5840.
13. (a) S. Shanmugaraju and P. S. Mukherjee, *Chem. Commun.*, 2015, **51**, 16014–16032; (b) M. Rong, L. Lin, X. Song, T. Zhao, Y. Zhong, J. Yan, Y. Wang and X. Chen, *Anal. Chem.*, 2015, **87**, 1288–1296; (c) S. Sandhu, R. Kumar, P. Singh, A. Mahajan, M. Kaur and S. Kumar, *ACS Appl. Mater. Interfaces*, 2015, **7**, 10491–10500; (d) N. Niamnont, N. Kimpitak, K. Wongravee, P. Rashatasakhon, K. K. Baldrige, J. S. Siegel and M. Sukwattanasinitt, *Chem. Commun.*, 2013, **49**, 780–782; (e) Y. Salinas, R. Martínez-Máñez, M. D. Marcos, F. Sancenón, A. M. Costero, M. Parra and S. Gil, *Chem. Soc. Rev.*, 2012, **41**, 1261–1296.
14. (a) P. M. Marcos, *In Calixarenes and Beyond*; P. Neri, J. L. Sessler, M.-X. Wang, Eds.; Springer International Publishing: Switzerland, 2016; Chapter 17, pp 445–466. (b) R. Joseph and C. P. Rao, *Chem. Rev.*, 2011, **111**, 4658–4702; (c) J. S. Kim and D. T. Quang, *Chem. Rev.*, 2007, **107**, 3780–3799.

15. H. C. Kolb, M. G. Finn and K. B. Sharpless, *Angew. Chem. Int. Ed.*, 2001, **40**, 2004–2021.
16. (a) J. J. Bryant and U. H. F. Bunz, *Chem. Asian J.*, 2013, **8**, 1354–1367; (b) M. Watkinson, *Top Heterocycl. Chem.*, 2012, **28**, 109–136; (c) Y. H. Lau, P. J. Rutledge, M. Watkinson and M. H. Todd, *Chem. Soc. Rev.*, 2011, **40**, 2848–2866; (d) M. Song, Z. Sun, C. Han, D. Tian, H. Li and J. S. Kim, *Chem. Asian J.*, 2014, **9**, 2344–2357; (e) Y. Hua and A. H. Flood, *Chem. Soc. Rev.*, 2010, **39**, 1262–1271.
17. (a) D. Schweinfurth, S. Strobel and B. Sarkar, *Inorg. Chim. Acta*, 2011, **374**, 253–260; (b) D. Urankar, A. Pevec, I. Turel and J. Košmrlj, *Cryst. Growth Des.*, 2010, **10**, 4920–4927; (c) H. Zheng, W. Zhou, J. Lv, X. Yin, Y. Li, H. Liu and Y. Li, *Chem. Eur. J.*, 2009, **15**, 13253–13262; (d) V. D. Bock, H. Hiemstra and J. H. van Maarseveen, *Eur. J. Org. Chem.*, 2006, 51–68.
18. B. Gole, S. Shanmugaraju, A. K. Bara and P. S. Mukherjee, *Chem. Commun.*, 2011, **47**, 10046–10048.
19. (a) M. Ashram, S. Mizyed and P. E. Georghiou, *Org. Biomol. Chem.*, 2003, **1**, 599–603; (b) K. Araki, N. Hashimoto, H. Otsuka and S. Shinkai, *J. Org. Chem.*, 1993, **58**, 5958–5963.
20. (a) M. K. Chahal and M. Sankar, *Anal. Methods*, 2015, **7**, 10272–10279; (b) S.S. Nagarkar, A. V. Desai and S. K. Ghosh, *Chem. Commun.*, 2014, **50**, 8915–8918; (c) V. Bhalla, H. Arora, H. Singh and M. Kumar, *Dalton Trans.*, 2013, **42**, 969–974.
21. S. Shanmugaraju and P. S. Mukherjee, *Chem. Eur. J.*, 2015, **21**, 6656–6666.
22. Y. H. Lee, H. Liu, J. Y. Lee, S. H. Kim, S. K. Kim, J. L. Sessler, Y. Kim and J. S. Kim, *Chem. Eur. J.*, 2010, **16**, 5895–5901.
23. (a) B. Joarder, A. V. Desai, P. Samanta, S. Mukherjee and S. K. Ghosh, *Chem. Eur. J.*, 2015, **21**, 965–969; (b) S. S. Nagarkar, B. Joarder, A. K. Chaudhari, S. Mukherjee and S. K. Ghosh, *Angew. Chem. Int. Ed.*, 2013, **52**, 2881–2885.
24. (a) R. Chopra, P. Kaur and K. Singh, *Anal. Chim. Acta*, 2015, **864**, 55–63; (b) S. Hussain, A. H. Malik, M. A. Afroz and P. K. Iyer, *Chem. Commun.*, 2015, **51**, 7207–7210.
25. (a) Y. Wu, X. L. Ni, L. Mou, C. C. Jin, C. Redshaw and T. Yamato, *Supramol. Chem.*, 2015, **27**, 501–507; (b) C. Wu, Y. Ikejiri, J.-L. Zhao, X.-K. Jiang, X.-L. Ni, X. Zeng, C. Redshaw and T. Yamato, *Sens. Actuators B*, 2016, **228**, 480–485

26. (a) X. L. Ni, S. Wang, X. Zeng, Z. Tao and T. Yamato, *Org. Lett.*, 2011, **13**, 552–555; (b) C.-C. Jin, T. Kinoshita, H. Cong, X.-L. Ni, X. Zeng, D. L. Hughes, C. Redshaw and T. Yamato, *New J. Chem.*, 2012, **36**, 2580–2586.

## Summary

Fluorescent chemosensors are widely used as powerful tools to detect neutral and ionic species owing to their high sensitivity, selectivity, versatility, and relatively simple handling. On the other hand, calixarenes have been extensively used as molecular platforms for the design and construction of different kinds of excellent receptors in molecular recognition by easy chemical modifications. Compared to other molecular systems, calixarenes have some advantages such as a hydrophobic cavity and easy functionalization at the upper or lower rims; moreover, the flexible core can be modified for well-defined substrate binding. As a new generation of calixarenes, hexahomotrioxacalix[3]arenes are related to both calixarenes and crown ethers, and possess a three-dimensional cavity with a  $C_3$  symmetric structure. This last feature can provide a suitable binding environment for species that require trigonal-planar, tetrahedral or octahedral coordination. Furthermore, the flexibility of the macrocycles can allow them to establish ideal bond distances and angles to bind such species. In other words, use of the hexahomotrioxacalix[3]arene as the platform has potential application in the development of novel fluorescence chemosensors.

The Cu(I)-catalyzed 1,3-dipolar cycloaddition of alkynes and azides ('Click' reaction) has provided a straightforward molecular linking strategy adopted in a wide range of synthetic applications. The resulting 1,2,3-triazole group served not only as an efficient covalent linker, but also a binding site for specific metal cations and anions. Thus, various calixarene-based fluorescent sensors have been designed and synthesized by using click chemistry. Fluorophores such as anthracene, pyrene, pyridine, Schiff base, naphthalene, and quinoline have been efficiently coupled to the upper and lower rims of calixarenes by means of click reactions and showed good performance as fluorescent chemosensors.

Thus, against this background, a series of hexahomotrioxacalix[3]arene-based fluorescent chemosensors were designed and synthesized in this dissertation. The sensitivity and selectivity properties of these chemosensors to the target analyte were carefully evaluated.

In chapter 1 a shortly review focus on the development of fluorescence chemosensors based on calixarene derivatives. Calixarenes have been shown to be useful molecular scaffold in the development of fluorescent chemosensors especially for metal ion recognition. Most calixarene-based fluorescent chemosensors have been designed based on photophysical

changes upon metal ion binding and their mechanisms include photoinduced electron transfer (PET), photoinduced charge transfer (PCT), formation of monomer/excimer, and fluorescence resonance energy transfer (FRET). In recent years, researchers have found that click chemistry can easily couple photoelectric groups to calixarenes. Taking advantage of the easily-synthesized triazole binding site and the highly selective nature of the alkyne-azide cycloaddition, the click reaction is a general method to introduce various functional groups/moieties to the upper or lower rim of calixarenes. However, Click chemistry has been scarcely exploited for the functionalization of the hexahomotrioxacalix[3]arene scaffold.

In chapter 2, we designed and synthesized a quinoline-functionalized homooxacalix[3]arene via Click chemistry. The chemosensor exhibited a high selectivity and anti-disturbance for  $\text{Fe}^{3+}$  amongst environmentally and biologically relevant metal ions, leading to a prominent ‘off-on’ type fluorescent signalling behaviour. Before coordinating with  $\text{Fe}^{3+}$ , free sensor exhibited weak fluorescence because of the lone electron pairs of the nitrogen atom in the triazole moieties being located adjacent to the quinoline fluorophores, which resulted in an intramolecular photo-induced electron transfer (PET). When the sensor was coordinated with  $\text{Fe}^{3+}$ , the non-radiative channel was inhibited simultaneously, and thus the  $\text{Fe}^{3+}$ -complex exhibited the enhanced fluorescence. Thus, the chemosensor could be serve as a high selective and sensitive fluorescent chemosensor for  $\text{Fe}^{3+}$ .

Following the same interest, in chapter 3, upper rim pyrene-functionalized hexahomotrioxacalix[3]arene L and a non-calixarene analogue M were further obtained. Chemosensor L exhibited a significant fluorescence quenching response to  $\text{Hg}^{2+}$  in  $\text{CH}_3\text{CN}$  solution, which was unaffected by the coexistence of other competitive metal cations. Interestingly, the quenched fluorescence emission can be successfully revived upon the addition of water. In this process, the heavy atom effect of  $\text{Hg}^{2+}$  can be blocked by further coordination of water molecule and resulted in the revival of the fluorescence emission of L/ $\text{Hg}^{2+}$  complex. The heavy atom effect and blocking thereof were demonstrated within the same system by the use of a  $C_3$ -symmetric homooxacalix[3]arene scaffold.

In particular, nitroaromatics often act as good electron acceptors due to the presence of electron withdrawing nitro ( $-\text{NO}_2$ ) group/s. On the other hand, given the strong dipolar character of the triazole ring, the C–H bond of the heterocycle makes a surprisingly good

hydrogen bond donor. The opposite properties of triazole and nitroaromatics promoted us to design chemosensors for nitroaromatics sensing via the Click chemistry.

In chapter 4, we have designed and synthesized two click-modified hexahomotrioxacalix[3]arene chemosensors, each of which can be utilized as fluorometric and colorimetric chemosensor for 2,4,6-trinitrophenol. They exhibited high binding affinity and selectivity toward 2,4,6-trinitrophenol as evidenced by UV-vis and fluorescence spectroscopy studies.  $^1\text{H}$  NMR titration analysis verified that  $\text{CH}\cdots\text{O}$  hydrogen bonding is demonstrated as the mode of interaction, which possibly facilitates effective charge-transfer. As a general design strategy, structural modifications by click chemistry may allow us to develop further chemosensor candidates for the future detection of nitro-containing explosives.

In summary, several hexahomotrioxacalix[3]arene-based fluorescent chemosensors were designed and synthesized via Click chemistry. These chemosensors exhibited excellent selective recognition towards specific guest molecules. Hexahomotrioxacalix[3]arene with its unique  $C_3$  symmetry is beneficial to the design and synthesis of highly selective chemosensors. We expect that the present design strategy and the remarkable photophysical properties of these chemosensors will help to extend applications of homotrioxacalix[3]arene-based fluorescent chemosensors for heavy metal ions and nitroaromatics detection.

## Publications

1. Click-modified hexahomotrioxacalix[3]arenes as fluorometric and colorimetric dual-modal chemosensors for 2,4,6-trinitrophenol

**Chong Wu**, Jiang-Lin Zhao, Xue-Kai Jiang, Xin-Long Ni, Xi Zeng, Carl Redshaw, Takehiko Yamato

*Analytica Chimica Acta*, **2016**, 936, 216–221.

2. A novel fluorescence “on–off–on” chemosensor for  $\text{Hg}^{2+}$  via a water-assistant blocking heavy atom effect

**Chong Wu**, Jiang-Lin Zhao, Xue-Kai Jiang, Chuan-Zeng Wang, Xin-Long Ni, Xi Zeng, Carl Redshaw, Takehiko Yamato

*Dalton Transactions*, **2016**, 45, 14948–14953.

3. A pyrene-functionalized triazole-linked hexahomotrioxacalix[3]arene as a fluorescent chemosensor for  $\text{Zn}^{2+}$  ions

**Chong Wu**, Yusuke Ikejiri, Jiang-Lin Zhao, Xue-Kai Jiang, Xin-Long Ni, Xi Zeng, Carl Redshaw, Takehiko Yamato

*Sensors and Actuators B*, **2016**, 228, 480–485.

4. Synthesis of mono-O-alkylated homooxacalix[3]arene and a protection-deprotection strategy for homooxacalix[3]arene

**Chong Wu**, Yusuke Ikejiri, Xi Zeng, Mark R. J. Elsegood, Carl Redshaw, Takehiko Yamato

*Organic Letters*, **2017**, 19, 66–69.

5. Click synthesis of a quinoline-functionalized hexahomotrioxacalix[3]arene: a turn-on fluorescence chemosensor for  $\text{Fe}^{3+}$

**Chong Wu**, Chuan-Zeng Wang, Qin Zhu, Xi Zeng, Carl Redshaw and Takehiko Yamato

*Sensors and Actuators B*, **2018**, 254, 52–58.